KEK Internal 82- 5
July 1982
B

KENS REPORT- III

Edited by

Y. ISHIKAWA
N. NIIMURA
S. IKEDA

NATIONAL LABORATORY FOR
HIGH ENERGY PHYSICS

National Laboratory for High Energy Physics, 1982

KEK Reports are available from:

Technical Information Office
National Laboratory for High Energy Physics
Oho-machi, Tsukuba-gun
Ibaraki-ken, 305
JAPAN

Phone: 0298-64-1171
Telex: 3652-534 (Domestic)
(0)3652-534 (International)
Cable: KEKOHO

PREFACE

The present report follows a previous issue, KENS Report II published in March 1981 as Proceedings of Meeting of International Collaboration on Advanced Neutron Sources (ICANS-IV). This volume collects the summaries of the works performed at KENS during the 1981 fiscal year.

The KENS facility has been operative since October 1980. After a half year's test performance, five spectrometers, HIT, MAX, LAM, SAN, and TOP were started to be used for the academic researches from April 1981. Therefore, this issue is the first volume where the results of the academic works are reported. The total machine time allocated to the neutron scattering facility this year was 1,300 hrs. The neutron sources including the refregerator for the cold neutron source were operated without trouble.

The total number of people using this facility was 100, and the report contains 50 papers, the most of which are concerning with the works with the above mentioned five spectrometers as collected in Section III. Another five spectrometers were also constructed this year. They are: FOX, LAM', CAT, RAT, and PRE-PEN, and the results of the preliminary tests of the spectrometers are reported in IV. Note that CAT and LAM' were already used for the academic works.

We have also started a new project of increasing the neutron intensity one order of magnitude (KENS-I' Project) by improving several factors as increasing the proton beam current, improving the moderator configuration, etc. The paper of II is the first step to this activity, where we report that the grooved moderator doubles the cold neutron intensity.

The details of each paper will be published in original journals. Any one who has an interest in the details is asked to make a direct contact with the authors.

June 1982

Editors: Y. Ishikawa
N. Niimura
S. Ikeda

CONTENTS

Present Status of BSF Operation

Hiroshi Sasaki, Yoshiro Irie, Toshikazu Adachi,
Yoshiharu Yano and Masayuki Miki

Booster Synchrotron Utilization Facility, National Laboratory for High Energy Physics, Oho-machi, Tsukuba-gun, Ibaraki, 305 Japan

BSF operation for the Fy '81 was made since 14 May 1981 through 6 March 1982. The total machine time during this period was 2883 hours which corresponds to 88 % of the accelerator operation time. The operation was performed so efficiently that the actual experimental beam time was 93 % of the total machine time including the users' beam reject time, accelerator and beam line down time. The machine time for neutron experiments was 1,422 hours with parasitic experiment of 26 hours for meson experiments. For meson, total machine time was 1,413 hours during which neutron experiments and the proton beam irradiation on calcium 48 was made parasitically for 104 hours. The extracted beam from the booster synchrotron was transported to the neutron or meson target with a little loss. The beam transmission was measured by comparing the beam intensity near the target points to that in the synchrotron. The results are 0.93 ± 0.06 in the neutron machine time and 0.89 ± 0.10 for the meson. Table 1 summarizes the BSF operation.

There existed some points indicating high radioactivity along the beam line especially near the pulsed switching magnet (PHB2). To reduce the beam amplitude at the hot points, the excitation current of the quadrupole magnet (QDO) was modified. For calculating the amplitude, twiss parameters and beam emittances were measured. Consequently the vertical amplitudes at the hot points were reduced to about 80 %, and the area where residual activity exceeded 10 rem/h has disappeared.

Improvement of the beam steering system is also effective for reducing the residual activity. Five steering magnets and one profile monitor were newly installed in the beam line. Especially four of the magnets were also intended for the beam centering at the proton irradiation experiment in the beam dump room.

The construction of the information system of BSF status is in progress. The system will cover the users' beam request status, beam pulse number, beam intensity and profile. The information will be available on CATV.

Table 1 Summary of BSF Operation since May 1981 through March 1982

	NEUTRON EXPERIMENT	MESON EXPERIMENT	BEAM LINE TUNING and STUDY
BEAM ON	1325.87 hours	1307.18 hours	48.15 hours
REJECT	8.67	41.96	
BEAM LINE TROUBLE	3.48	15.37	
ACCELERATOR TROUBLE	77.42	41.47	
OTHERS	6.85	6.60	
TOTAL	1422.29	1412.58	48.15
BEAM TRANSMISSION FROM SYNCHROTRON TO TARGET	0.93 ± 0.06	0.89 ± 0.10	

Cold methane grooved moderator experiment for KENS-I'

Kazuhiko Inoue*, Noboru Watanabe**, Yoshikazu Ishikawa+, J. M. Carpenter++, Yoshiaki Kiyanagi*, Susumu Ikeda** and Hirokatsu Iwasa*

* Department of Nuclear Engineering, Hokkaido University, Sapporo, Hokkaido 060

** National Laboratory for High Energy Physics, Oho-machi, Ibaraki 305

\+ Physics Department, Tohoku University, Sendai, Miyagi 980

++ Intense Pulsed Neutron Source Program, Argonne National Laboratory, Argonne, Illinois 60439

Based on the results of our experiments and laboratory experiences over a period of several years, we have concluded that the accelerator-based cold neutron source using a 20 K methane moderator is a safe, reliable and highly efficient device which can be applied to both a photo neutron source and a spallation neutron source[1~3]. We have installed a spallation cold neutron source within the KENS source at the National Laboratory for High Energy Physics (KEK), and current operations have proved it to be satisfactory[3].

We are now planning to increase the intensity of the KENS source. Of course, this endeavor will require the testing of several sophisticated techniques, among them the adoption of a grooved moderator to increase the cold neutron beam. Current plans call for the installation of the new chamber in the present fast neutron reflector under its limited space and restricted

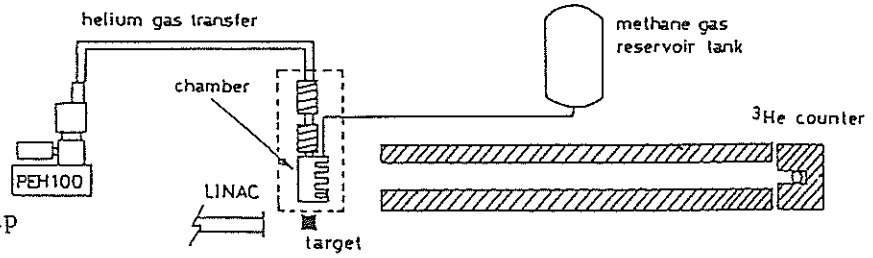

Fig. 1 Illustration of experimental set-up and chambers.

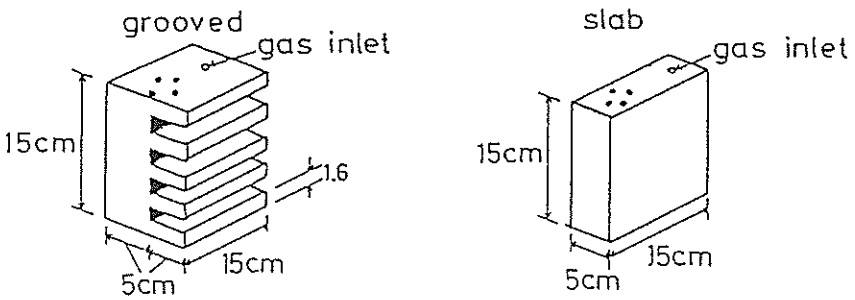

design conditions. Thus we decided to conduct a certain mockup measurement of the cold methane grooved moderator by using the cold source facility at Hokkaido University. In this short note, some of the results of the preliminary experiments are reported.

We purchased both a grooved chamber and a slab one made of aluminum, as shown in Fig. 1, and attached them to the bottom of the heat exchanger of the cold source facility instead of to the actual moderator chamber. Because of clogging of the methane at the entrance of the gas inlet tube, we had to replace the inlet tube with a wider one to overcome the problem.

Fig. 2 shows the experimental spectra obtained from the grooved and slab moderators. These data were normalized at a higher energy region. These results provided sufficient proof that the grooved moderator could enhance the performance of our cold moderator. Before sufficient data can be accumulated for the optimum design of the KENS-I' cold moderator chamber, we need to take many measurements concerning the spatial distribution of the emanated neutron beam, the pulse shape of the neutrons as a function of the emission time, and so on, as well as the optimum size and shape of the grooves.

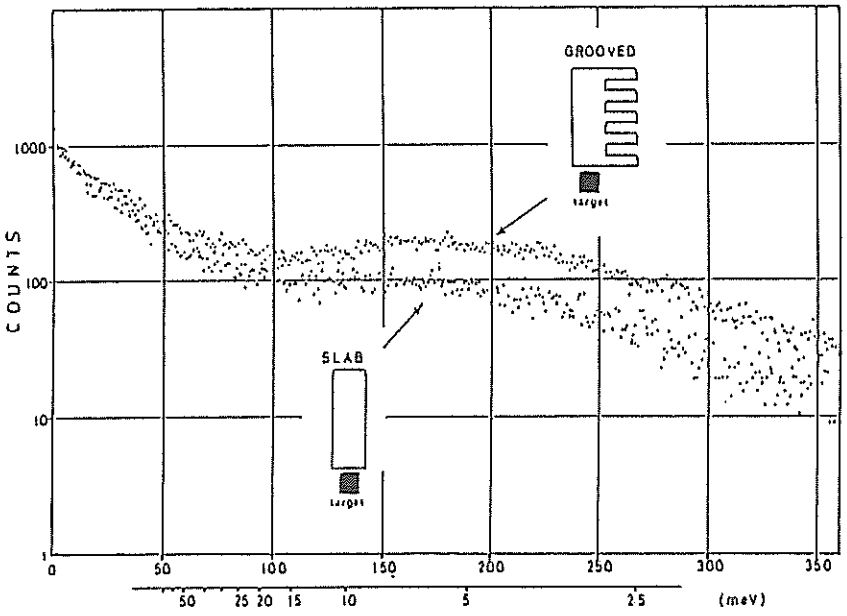

Fig. 2 Time-of-flight spectra from solid methane grooved and slab moderators.

References

1) K. Inoue et al.: J. Nucl. Sci. Tech., 13(1976)389

2) K. Inoue et al.: Nucl. Instr. Meth., 192(1982)129

3) Y. Ishikawa: Proc. 4th Int. Collaboration on Advanced Neutron Source(ICANS), Tsukuba, Japan(Oct.1980)

Structure of Ni-B Alloy Glass Having Two Glass Forming Ranges

Toshiharu Fukunaga, Fumitake Itoh, Noriyuki Hayashi,
Noboru Watanabe* and Kenji Suzuki

The Research Institute for Iron, Steel and Other Metals,
Tohoku University, Sendai 980, Japan.

* National Laboratory for High Energy Physics, Oho-machi,
Tsukuba-gun, Ibaraki-ken 305, Japan.

The chemical short-range structure of the archetypical metal-metalloid alloy glass with the composition close to 20at% metalloid atom is known to be characterized by a trigonal prismatic configulation analogous to that found in Fe_3C cementite crystal structure[1]. On the other hand, it has been shown recently that Co-B, Fe-B and Ni-B binary alloy glasses could be easily vitrified in wide glass forming range[2]. The Ni-B alloy glasses used in this study were found to be vitrified in two composition regions, 18-20at%B and 30-40at%B.

The aim of this study is to examine how the chemical short-range structure of Ni-B alloy glasses is related between low and high B concentration ranges, based on the observation of the high resolution radial distribution

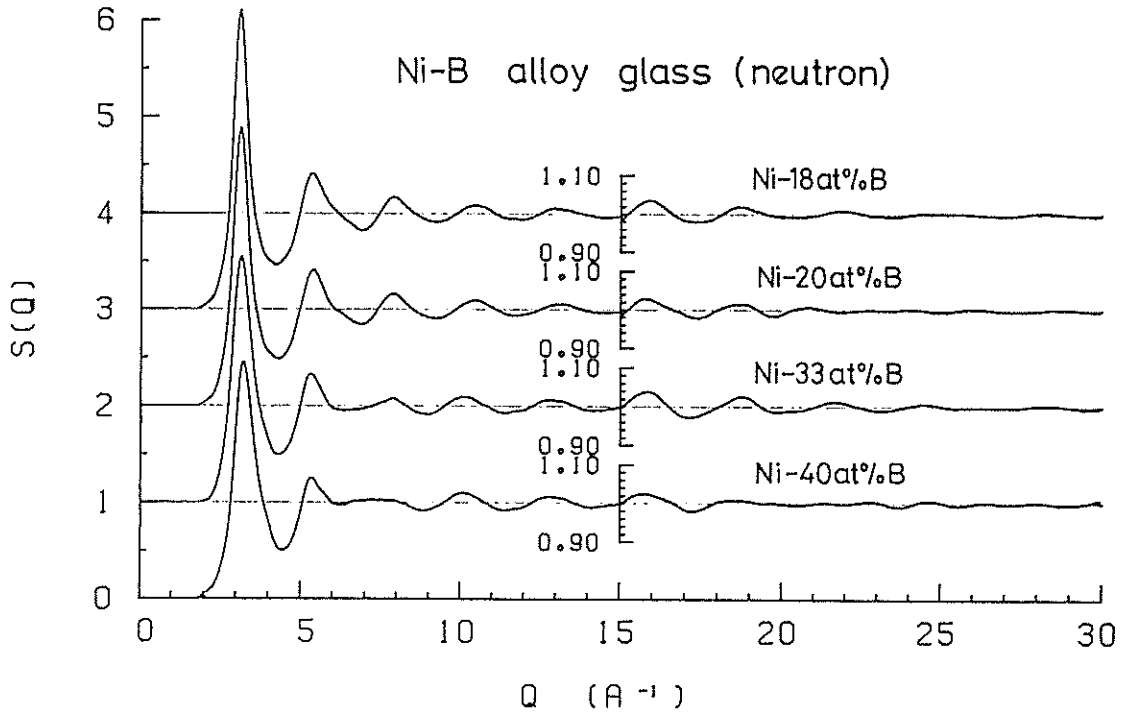

Fig. 1. Total structure factors of Ni-B alloy glasses.

function obtained as the Fourier transform of the S(Q) truncated at high Q values.

Figure 1 shows the total structure factors S(Q)'s of Ni-18at%B, Ni-20at %B, Ni-33at%B and Ni-40at%B alloy glasses. A comparison of S(Q) between the two groups of Ni-B alloy glasses with the low and high B concentrations shows clearly a remarkable difference. The famous shoulder on the high Q side of the second peak of S(Q) found in Ni-18at%B and Ni-20at%B alloy glasses, which has been observed in the archetypical metal-metalloid alloy glass with the low metalloid concentration, is not observed in S(Q)'s of Ni-33at%B and Ni-40at%B alloy glasses.

Figure 2 shows the pair distribution functions g(r)'s obtained by the Fourier transformation of the S(Q)'s of Ni-20at%B, Ni-33at%B and Ni-40at%B alloy glasses. The first peak of g(r) is split into two peaks. From the comparison of the atomic distribution between Ni-B alloy glasses and the crystalline compounds(Ni_3B, Ni_2B and Ni_4B_3), the sub-peak located at the low r side in the first peak is found to correspond to the Ni-B pair correlation. The coordination number of Ni atoms around a B atom estimated from the area under this sub-peak is almostly constant at 5.5 Ni atoms. This means that the chemical short-range structure in Ni-B alloy glasses with all B concentrations is analogous to the trigonal prism which has 6 Ni atoms at 6 vertices

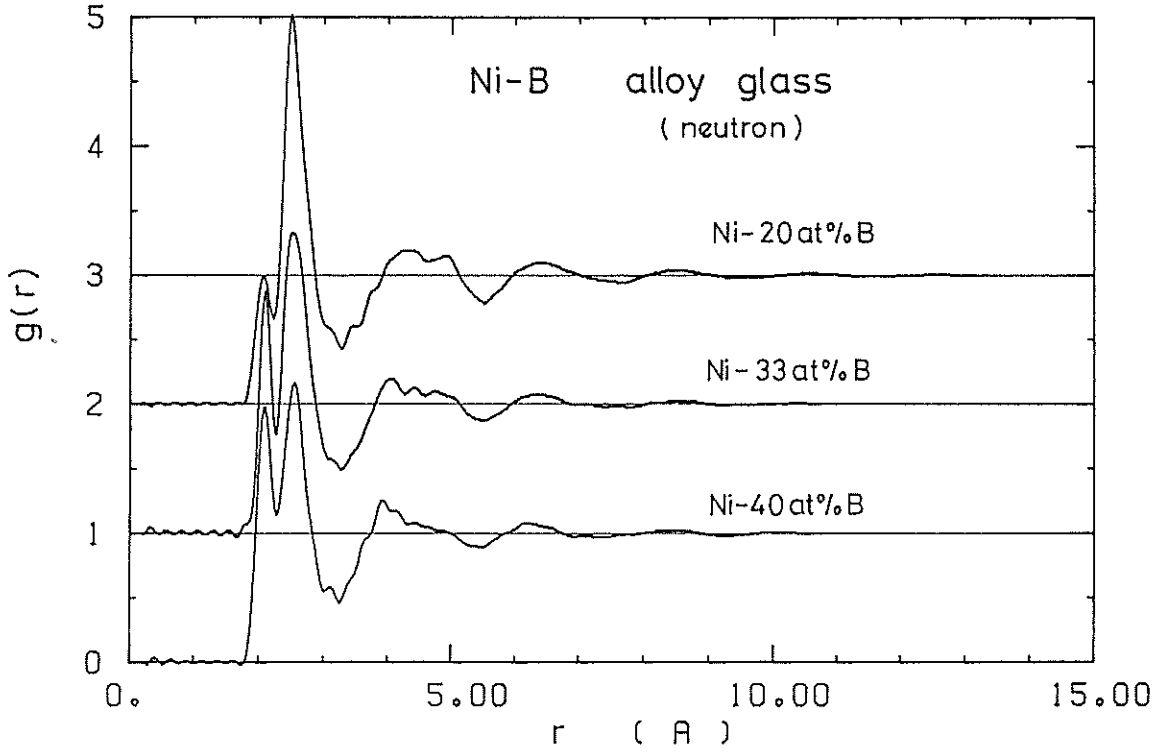

Fig. 2. Total pair distribution functions of Ni-B alloy glasses.

and a B atom in the central hole as shown in Fig. 3(a). Therefore, the absence of the characteristic second peak shoulder in the S(Q) of high B content alloy glasses is due to the variation in the atomic arrangement located at the main peak of the first peak of g(r). This means that a part of Ni atoms existing in the second nearest neighbor from a B atom located at the center of the trigonal prism is substituted with B atoms as shown in Fig. 3(b).

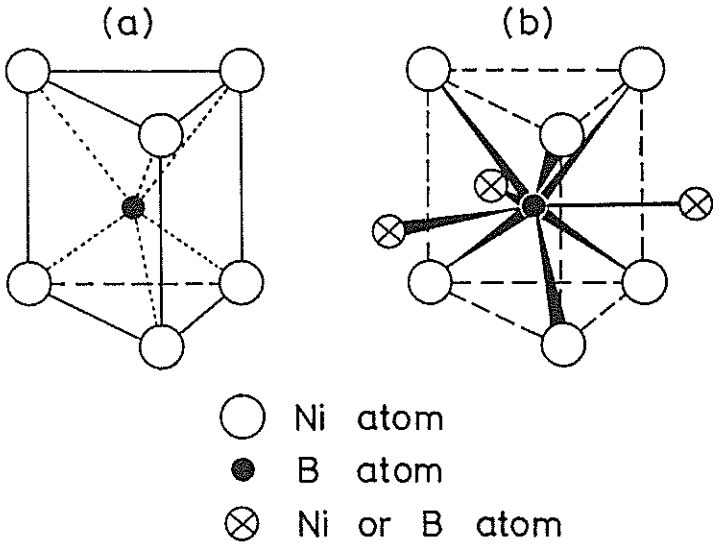

Fig. 3. Environment around a B atom in Ni-B alloy glasses.
(a) trigonal prism with Ni atoms at 6 vertices and a B atom in central hole.
(b) second nearest neighboring Ni or B atoms(⊗) from a B atom.

References

1) T. Fukunaga and K. Suzuki, Sci. Rep. Res. Inst. Tohoku Univ.,A-29(1981) 153.

2) A. Inoue, A. Kitamura and T. Masumoto, J. Mater. Sci.,16(1981)1895.

Structural Anisotropy of Sputter-deposited Mo-32at%Si Amorphous Alloy

Toshiharu Fukunaga, Noriyuki Hayashi, Susumu Ikeda*,
Noboru Watanabe* and Kenji Suzuki

The Research Institute for Iron, Steel and Other Metals, Tohoku University, Sendai 980, Japan.

* National Laboratory for High Energy Physics, Oho-machi, Tsukuba-gun, Ibaraki-ken 305, Japan.

Although atomic arrangements in amorphous solids have commonly been assumed to be macroscopically isotropic and uniform, some amorphous alloys have been reported to have remarkable anisotropies in their magnetic and mechanical properties. For example, sputter-deposited Gd-Co amorphous alloys show a large magnetic field perpendicular to the deposition plane[1].

These anisotropic characters in amorphous alloys are thought to originally come from the anisotropies in the atomic scale structure. The time-of-flight total neutron scattering technique using a spallation pulsed neutrons installed at KEK is powerfull to get the information of the structural anisotropy in amorphous alloys, because we can simultaneously measure the structure factor $S(\vec{Q})$ with the scattering vector parallel$(\vec{Q})$ to the sample plane$(\vec{a})$ ($\vec{Q} /\!/ \vec{a}$) and with the scattering vector perpendicular to the sample plane ($\vec{Q} \perp \vec{a}$) locating ^{3}He-counters at symmetric positions on the both sides of an incident neutron beam with the scattering angle $2\theta=\pm 90°$.

As shown in Fig. 1, a plate specimen(0.5mm thick × 10mm long × 10mm wide) of DC sputter-deposited Mo-32at%Si amorphous alloy is mounted at 45° to the incident beam so that the counter on the left hand side at $2\theta=+90°$ records the $S(\vec{Q})$ with $\vec{Q} /\!/ \vec{a}$ and that at $2\theta=-90°$ with $\vec{Q} \perp \vec{a}$. The result of this measurement reveals a significant anisotropy in the S(Q)'s around the first peak region but there are little anisotropies in high Q region. This suggests that the degree of the long range periodicity in the atomic spacing is not isotropic in Mo-32at%Si amorphous alloy, while the short-range structure may be isotropic. The Mo-32at%Si amorphous alloy supplied to this measurement has the columnar structure of $3 \sim 5$ μm in diameter which grows perpendicular to the sample plane[2]. We need further measurements of the S(Q)'s over high Q region with a reasonable statistical accuracy in order to find the

correlation between the experimental condition of sputter-deposition and the anisotropic arrangement of atoms in Mo-32at%Si amorphous alloy.

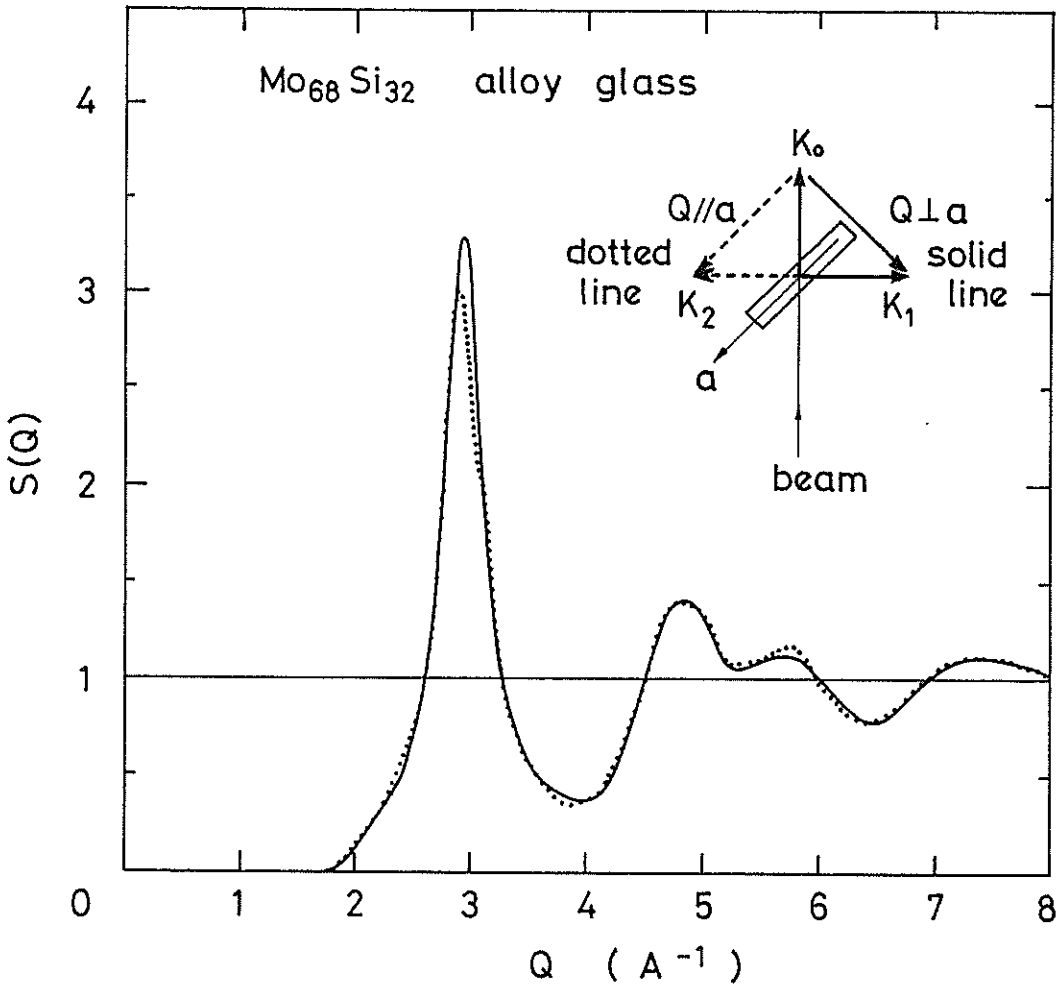

Fig. 1. Anisotropy in neutron structure factor of Mo-32at%Si amorphous alloy with $\vec{Q} // \vec{a}$ and $\vec{Q} \perp \vec{a}$, where $\vec{Q}$ is the scattering vector and $\vec{a}$ is the direction parallel to the sample plane.

References

1) P. Chaudhari, J. J. Cuomo and R. J. Gambina, IBM J. Res. Dev. 17(1973)66.

2) S. Ikeda, H. Fujimori, M. Ikebe, Y. Muto and K. Suzuki, Proc. RQ-4 (1981)1252.

Chemical Short-Range Structure of Cu-Ti and Ni-Ti Alloy Glasses

Toshiharu Fukunaga, Kenzo Kai, Noriyuki Hayashi, Noboru Watanabe* and Kenji Suzuki

The Research Institute for Iron, Steel and Other Metals, Tohoku University, sendai 980, Japan.

* National Laboratory for High Energy Physics, Oho-machi, Tsukuba-gun, Ibaraki-ken 305, Japan.

The aim of this study is to characterize the topological and chemical short-range order of the atomic arrangement in metal-metal alloy glasses through the high resolution observation of the radial pair correlation function using an epithermal energy pulsed neutron total scattering technique. It is advantageous to express S(Q) in terms of Bhatia-Thornton's partial structure factors[1] $S_{NN}(Q)$, $S_{NC}(Q)$ and $S_{CC}(Q)$, where $S_{NN}(Q)$ and $S_{CC}(Q)$ represent the density and composition fluctuations respectively and $S_{NC}(Q)$ represents its cross term, because a neutron zero-alloy(<b>=0) can provide the direct observation of pure $S_{CC}(Q)$.

Experimental S(Q)'s of Ni-Ti and Cu-Ti alloy glasses are shown in Fig.1,

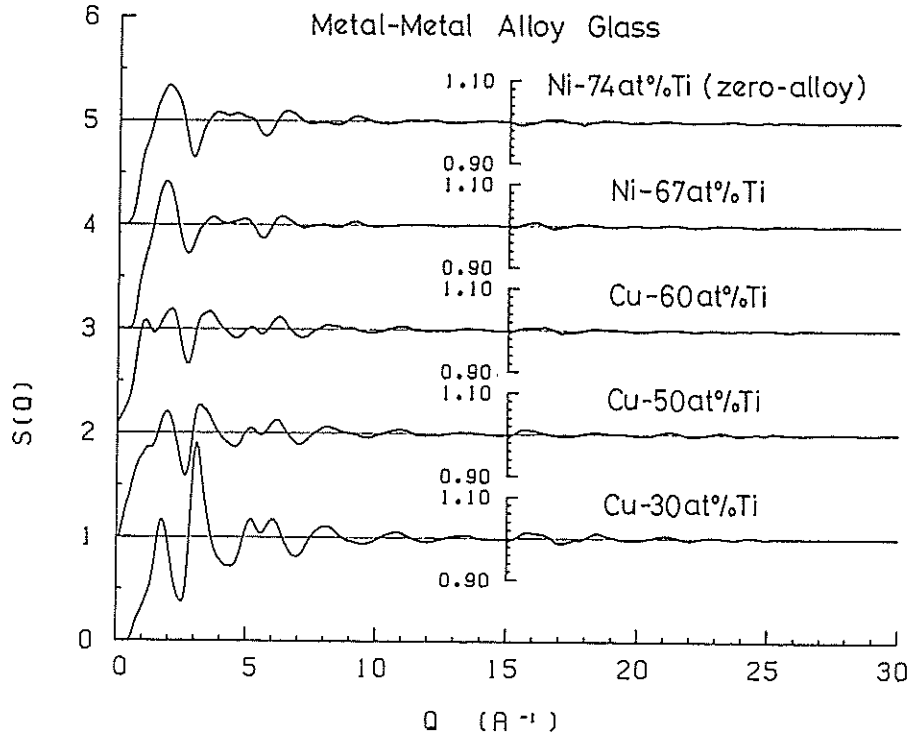

Fig. 1. Total structure factors of Ni-Ti and Cu-Ti alloy glasses. The S(Q) for Ni-74at%Ti zero-alloy glass is equal to the $S_{CC}(Q)/C_{Ni}C_{Ti}$ due to <b>=0.

where the S(Q) is defined as $(d\sigma_{coh}/d\Omega)_{total}=N<b^2>S(Q)$. The S(Q) of Ni-74at%Ti alloy glass describes directly the concentration-concentration structure factor $S_{CC}(Q)/C_{Ni}C_{Ti}$, since this alloy glass is a so-called neutron zero-alloy.

Figure 2 shows the reduced atomic distribution functions G(r)'s obtained as the Fourier transform of S(Q)'s of Ni-74at%Ti and Cu-60at%Ti alloy glasses. The G(r) of Ni-74at%Ti alloy glass is exactly equal to the reduced concentration-concentration function $G_{CC}(r)=4\pi r\rho_{CC}(r)$. By comparison between the crystal structure of $NiTi_2$ compound(Fe_3W_3C-type) and the $G_{CC}(r)$ of Ni-74at%Ti alloy glass the negative peak at r=2.564 A in the $G_{CC}(r)$ is found to correspond to the Ni-Ti unlike atom pair correlation in $NiTi_2$ crystalline compound. On the contrary, the positive peak in $G_{CC}(r)$ of Cu-60at%Ti alloy glass appearing at r=2.50 A corresponds to Cu-Cu like atom neighbors as shown in comparison between the G(r) of Cu-60at%Ti alloy glass and the crystal structure of CuTi crystalline compound(γ-CuTi type). Therefore, Ni-Ti unlike atom pairs in Ni-Ti alloy glasses prefer existing in the first nearest neighbor, while Cu-Cu like atom pairs prefer to exist in the first nearest neighbor in Cu-Ti alloy glasses. These results show clearly that the chemical short-range order is essentially different between Ni-Ti and Cu-Ti alloy glasses and this difference is charactaristically found between the crystal structures of both compounds.

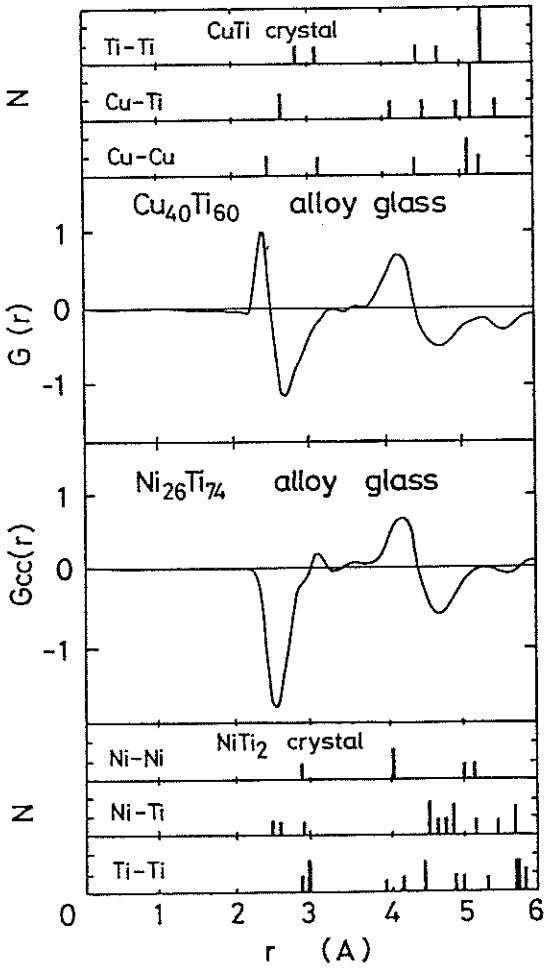

Fig. 2. $G_{CC}(r)$ of Ni-74at%Ti alloy glass, $G(r)_{CC}$ of Cu-60at%Ti alloy glass and crystal structures of $NiTi_2$ and CuTi compounds.

Reference

1) A. B. Bhatia and D. E. Thornton, Phys. Rev. B2(1970)3004.

A Total Scattering Experiment of Silicate Glasses by Using HIT Spectrometer at KENS

Norimasa Umesaki, Hiroaki Hidaka, Toshiharu Fukunaga*,
Noriyuki Hayashi*, Nobuya Iwamoto, Noboru Watanabe**
and Kenji Suzuki*

Welding Research Institute, Osaka University, Mihogaoka,
Ibaraki, Osaka 567, Japan.

* The Research Institute for Iron,Steel and Other Metals, Tohoku University, sendai 980, Japan.

** National Laboratory for High Energy Physics, Oho-machi, Tsukuba-gun, Ibaraki-ken 305, Japan.

Silica and silicate glasses are important as fundamental materials not only in glass technology but also in metallurgical processes. Based on the advantage of a high flux of epithermal energy neutrons in KENS spallation neutron source, this study aimes at finding the local atomic arrangement in complicated silicate glasses with a high resolution in real space.

The silicate glass specimens measured in this study are classified into two categories. One is the elucidation of the chemical short-range structure around a Ti atom in Na_2O-SiO_2-TiO_2 glasses, while the other is to find the effect of substituting Na_2O with MO(M=Ca, Sr and Ba) on the glass structure.

All the silicate glass specimens were prepared by casting, with a reasonable cooling rate, their melts into a cylindrical form of 8 mm in diameter and 50 mm in length. The total structure factors S(Q) of these glass specimens were measured at room temperature in vacuo by using a High Intensity Total(HIT) scattering spectrometer. Details of experimental performances and data processing will be described elsewhere.

Figure 1 shows the S(Q)'s of $(Na_2O)_{0.1}(SiO_2)_{0.9}$ and $(Na_2O)_{0.1}(SiO_2)_{0.7}(TiO_2)_{0.2}$ glasses. The relative height of peaks in S(Q) is drastically modified in both the regions of $Q \leq 4$ A^{-1} and $Q \geq 25$ A^{-1} by substituting SiO_2 with TiO_2.

The radial distribution functions(RDF) defined as the Fourier transform of the S(Q) are illustrated in Figs. 2 and 3, together with the effect of truncating the Fourier transformation at Q_{max} on the peak profiles. Even at the range of $Q_{max}=30 \sim 50$ A^{-1}, there is still found a narrowing of the first

peak(~1.6 A) corresponding to the Si-O bond. The small peak(~1.8 A) appearing at higher r side of the first peak may represent the $Si-O^-$ bond. The two negative peaks located at about 2.1 and 2.4 A are expected to the Ti-O correlations around a Ti atom coordinated tetrahedrally and octahedrally with O atoms respectively.

The discussions described above need the more confirmation assisted by further careful data analysis.

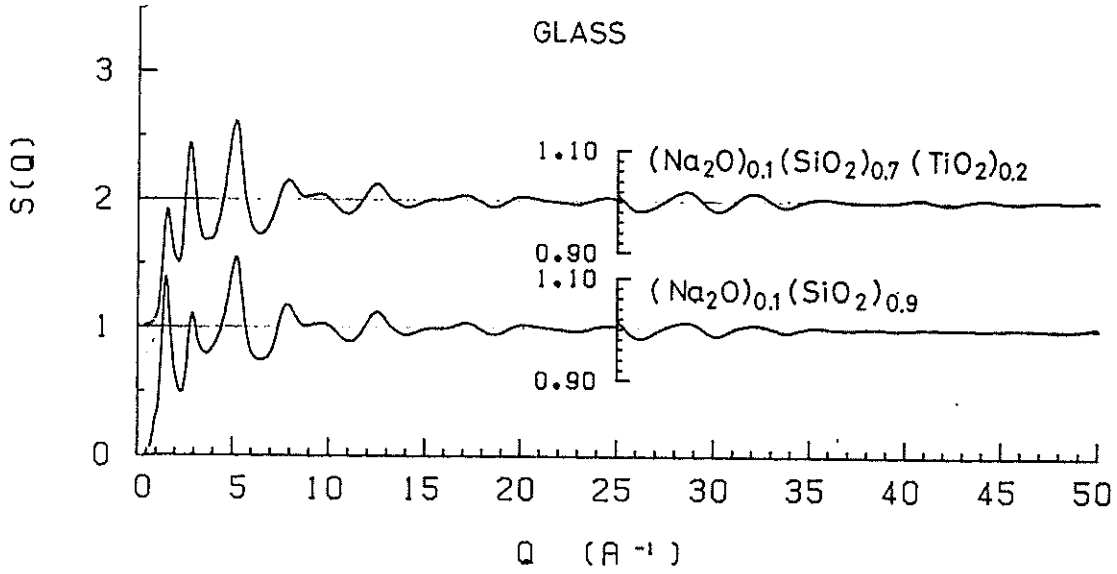

Fig. 1. Neutron total structure factors of $(Na_2O)_{0.1}(SiO_2)_{0.9}$ and $(Na_2O)_{0.1}(SiO_2)_{0.7}(TiO_2)_{0.2}$ glasses.

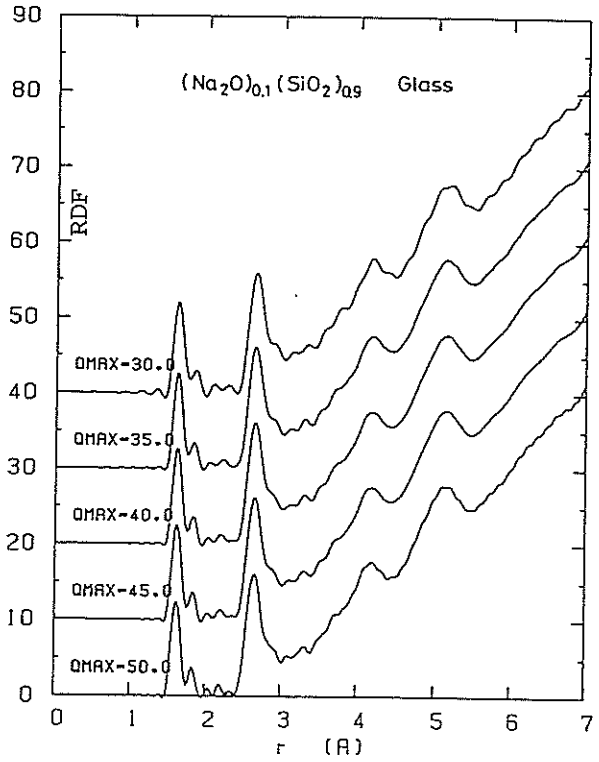

Fig. 2. Neutron radial distribution of $(Na_2O)_{0.1}(SiO_2)_{0.9}$ glass.

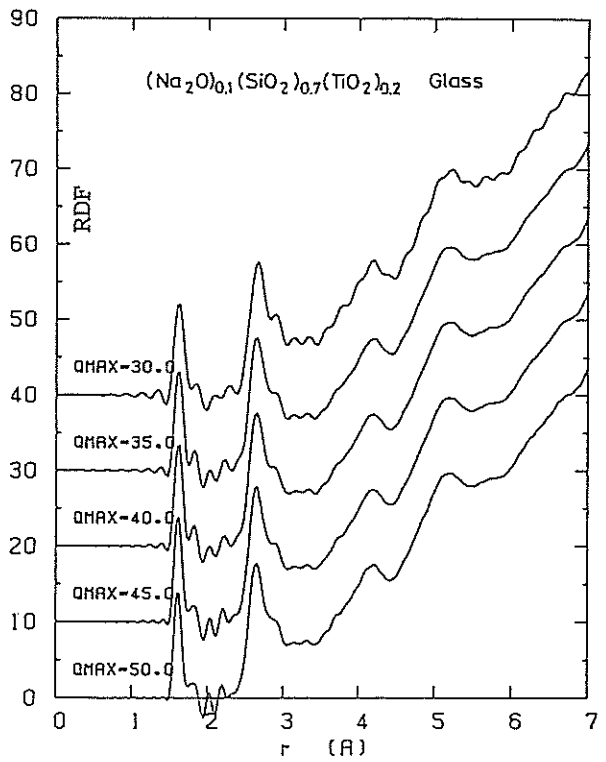

Fig. 3. Neutron radial distribution of $(Na_2O)_{0.1}(SiO_2)_{0.7}(TiO_2)_{0.2}$ glass.

Local Environment Around Hydrogen Atoms in $Pd_{.35}Zr_{.65}D_X$ Alloy Glasses

Kenzo Kai, Toshiharu Fukunaga, Noboru Watanabe* and Kenji Suzuki

The Research Institute for Iron, Steel and Other Metals,
Tohoku University, Sendai 980, Japan.

* National Laboratory for High Energy Physics, Oho-machi,
Tsukuba-gun, Ibaraki-ken 305, Japan.

The aim of this work is to examine what kind of atomic sites in $Pd_{.35}Zr_{.65}$ alloy glass are occupied by hydrogen atoms. The measurement of S(Q) for $Pd_{.35}Zr_{.65}D_X$(X=0.0, 0.17, 0.34, 0.42, 0.85 and 1.25) alloy glasses [1] was carried out by a high intensity total scattering spectrometer(HIT) installed at a spallation neutron source of KEK.

Thin ribbons of about 30 μm in thickness and 2 mm in width were fabricated in a controlled Ar-gas atomosphere by rapid quenching from the melts using a single roll. Deuterium atoms were charged into the glass ribbons under 20 Kg/cm^2 pressure at 300 °C, but the deuterium charge for $Pd_{.35}Zr_{.65}D_{1.25}$ alloy glass were carried out at 130 °C.

The experimental S(Q) of $Pd_{.35}Zr_{.65}D_X$(X=0.$\sim$1.25) alloy glasses obtained are shown in Fig. 1. The first and second peak profiles in S(Q) are completely modified with higher D concentration beyond X=0.42, while the distortion of S(Q) is relatively small in a low D concentration alloy of X=0.17. Figure 2 shows the atomic radial distribution function(RDF) obtained as the Fourier transforms of S(Q) truncated at Q_{max}=30 A^{-1}. The first peak around r$\sim$2 A in the deutrized alloy glasses corresponds to the nearest neighbour correlation of D-M(M=Pd, Zr) pairs. The splitting of the first peak in the RDF of $Pd_{.35}Zr_{.65}D_X$(X=0.17$\sim$1.25) alloy glasses was numerically simulated by two Gaussian fitting. The positions of the two Gaussian peaks fitted are shown in Fig. 3 and the coordination numbers of M atoms around a D atom are shown in Fig. 4. At the low D concentration of X$\leq$0.17, a D atom is surrounded by about 1.7 Pd atoms with the bond length of $r^1_{DM}\sim$2.0 A and 2.8 Zr atoms with $r^1_{DM}\sim$2.2 A. This configuration suggests that a D atom is likely to occupy the central hole surrounded by four M atoms consisting of Pd and Zr atoms with the ratio of 0.35 to 0.65 in the low D concentration limit. However, the topological arrangement of M atoms around a D atom is drastically modified with increasing D concentration. Near X=0.42, a D atom

is located at an octahedral-like site where the other new atomic distance r^2_{DM} of D-Zr atomic pair appears. The further increase in the D concentration approaching X=1.25 leads to the average local atomic arrangement of a five-atoms coordination.

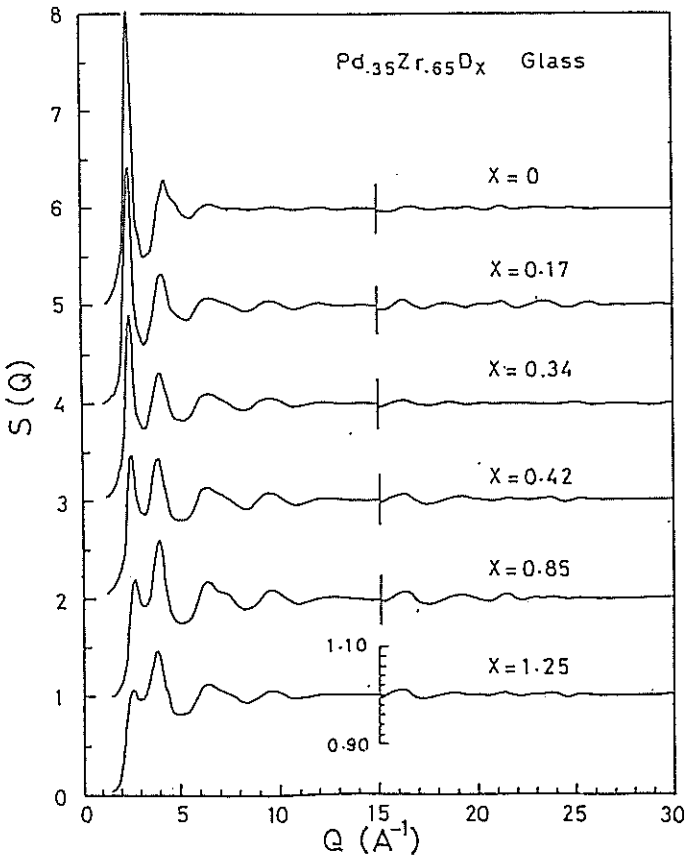

Fig. 1. Structure factors of $Pd_{.35}Zr_{.65}D_X$ alloy glasses.

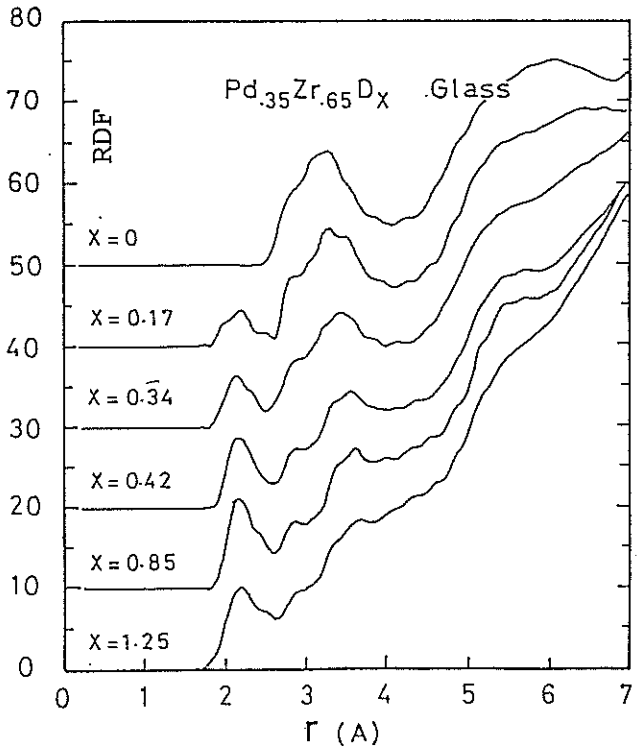

Fig. 2. Radial distribution functions of $Pd_{.35}Zr_{.65}D_X$ alloy glasses obtained by Fourier transforming the S(Q) shown in Fig. 1.

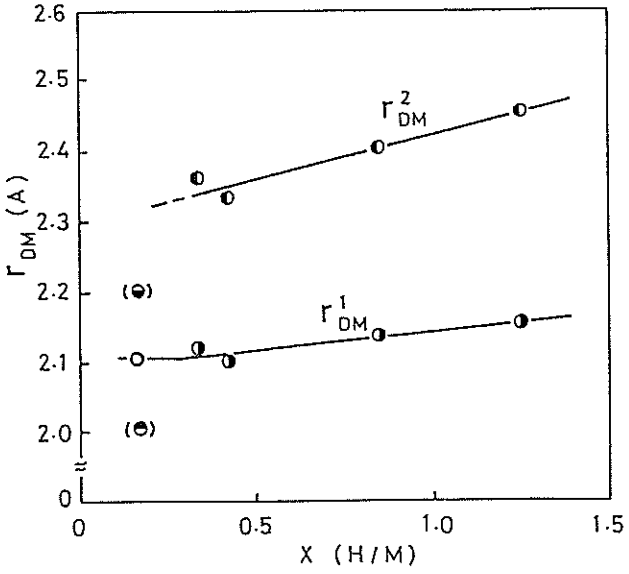

Fig. 3. Positions of M atoms around a D atom obtained by two Gaussian curves-fitting in RDF r^1_{DM} means the average of D-Pd and D-Zr atomic distances and r^2_{DM} is the other D-Zr atomic distance. D-Pd and D-Zr atomic distances of r^1_{DM} are separated in the D concentration of X=0.17 (shown as (◓) and (◒), respectively).

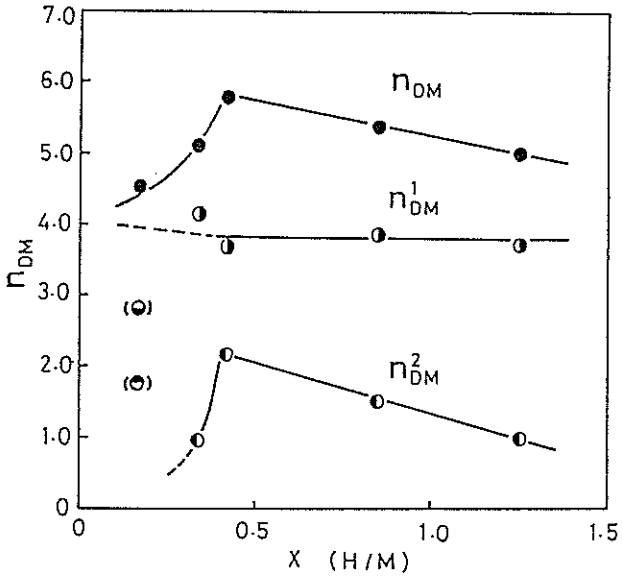

Fig. 4. Nearest neighbour coordination numbers around a D atom. n^1_{DM} and n^2_{DM} are the coordination numbers corresponding to the atomic distances r^1_{DM} and r^2_{DM}, respectively. (◓) and (◒) are the coordination numbers of Pd and Zr atoms around a D atom in the glass alloy of X=0.17, respectively.

References

1) K. Kai, T. Fukunaga, T. Nomoto, N. Watanabe and K. Suzuki, Proc. 4th Int. Conf. on Rapidly Quenched Metals(Sendai, 1981) ed. T. Masumoto and K. Suzuki (The Japan Institute of Metals, 1982)p.1609.

K. Suzuki, K. Kai, T. Fukunaga and N. Watanabe, presented at Int. Symp. on Properties & Applications of Metal Hydrides-II , Toba, Japan, May-June 1982 and published from J. Less. Comm. Metals.

Structure Change of Pd-17at%Si Alloy Glass by Cold Rolling

Noriyuki Hayashi, Toshiharu Fukunaga, Noboru Watanabe* and Kenji Suzuki

The Research Institute for Iron, Steel and Other Metals,
Tohoku University, Sendai 980, Japan.

* National Laboratory for High Energy Physics, Oho-machi,
Tsukuba-gun, Ibaraki-ken 305, Japan.

Physical and mechanical properties of metal-metalloid alloy glasses change with external forces. For example, annealing just below the Curie temperature under a magnetic field increases the magnetic anisotropy in Co-Fe-B-Si alloy glass[1] and the anisotropy of Young's modulus of Pd-Si alloy glass is enhanced by cold rolling[2]. These changes of magnetic and mechanical properties due to external forces may be attributed to the rearrangement of the atomic structure in metal-metalloid alloy glasses. The aim of this study is to observe the structure change of Pd-17at%Si alloy glass which is induced by cold rolling at room temperature and to explore the atomic scale mechanism of the mechanical structure relaxation of metallic glass.

The sample of Pd-17at%Si alloy glass was prepared in a form of thin ribbon with about 3 mm in width and 35 μm in thickness by rapid quenching from the molten state using a single roll technique. The sample was rolled to reduce 52 % in thickness. The density of the sample was measured using Archimedes' method. The density decreases by about 1.2 % after cold rolling. The structure factors S(Q) of as-quenched and cold-rolled Pd-17at%Si alloy glasses were measured by using a High Intensity Total scattering spectrometer (HIT) in vacuo at room temperature.

Figure 1 shows S(Q)'s of as-quenched and cold-rolled Pd-17at%Si alloy glasses and their difference ΔS(Q). The behavior of ΔS(Q) indicates that the height of the first peak in S(Q) slightly and its shape becomes broader after cold rolling. From comparison of the radial distribution functions (RDF) between as-quenched and cold-rolled Pd-17at%Si alloy glasses, defined as the Fourier transforms of S(Q)'s truncated at Q_{max}=30 A^{-1}, it can be found that there is no significant change in the subpeak located at low r side of the first peak in RDF but there is a little change in the profile of the first main peak at high r side as shown in Fig. 2. These results mean that there is no change of the atomic distribution in the Pd-Si nearest neighbor region, while some rearrengements of the Pd-Pd nearest neighbors take place

due to the plastic deformation of the alloy glass by cold rolling.

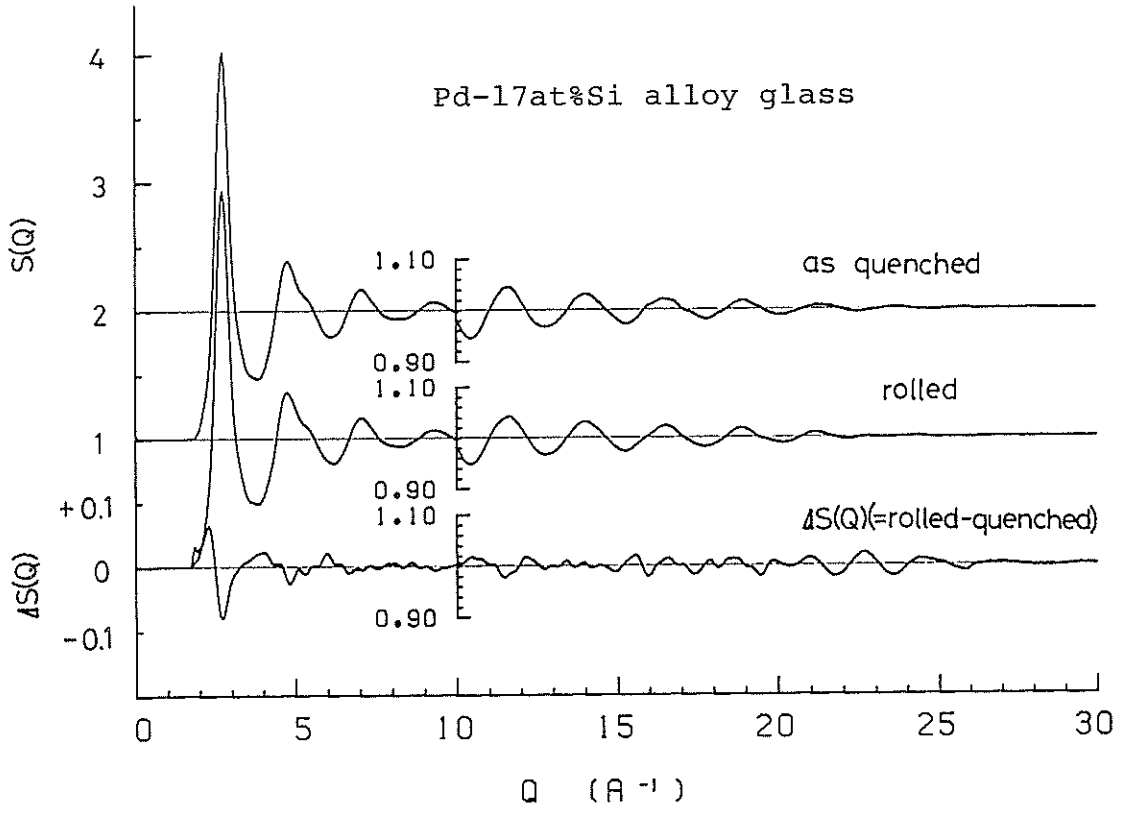

Fig. 1. Total structure factors S(Q) of as-quenched and cold-rolled Pd-17 at%Si alloy glasses and their difference ΔS(Q) (=rolled - quenched).

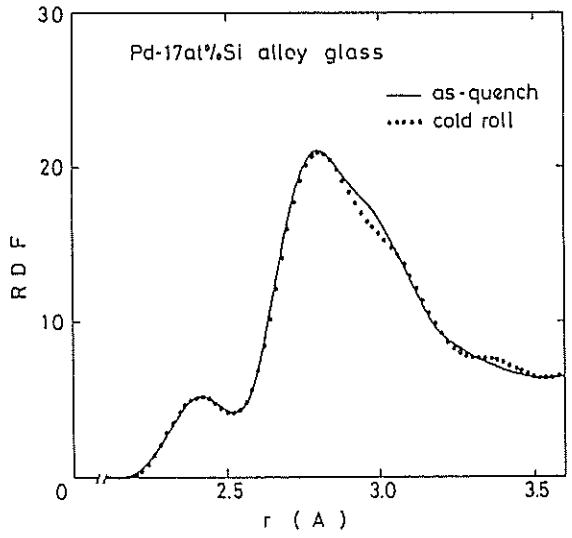

Fig. 2. Total radial distribution functions of as-quenched and cold-rolled Pd-17at%Si alloy glasses.

References

1) H. Fujimori, H. Morita, Y. Obi and S. Ohta, Amorphous Magnetism II (ed. R. A. Levy and R. Hasegawa, 1977)p.393.

2) K. Fukamichi, M. Kikuchi, H. M. Kimura and T. Masumoto, The Autumn Meeting of the Japan Institute of Metals(tokyo, 1981) to be submitted.

TOF neutron Diffraction Study of Binary Amorphous Alloys

T. Mizoguchi, S. Yamada, J. Nishioka,
T. Suemasa, N. Akutsu, S. Yoda and H. Narumi
Faculty of Science, Gakushuin University

and

N. Watanabe
Laboratory for High Energy Physics

For structural studies of binary amorphous alloys, TOF Neutron diffraction experiments were carried out at room temperature using the HIT (High Intensity Total Scattering) spectrometer with pulse neutron source at KENS in Laboratory for High Energy Physics.

The amorphous alloys were prepared by rapid quenching from the melt with a single roll in argon atmosphere. The chemical composition of alloys so far studied were $Fe_{.90}Zr_{.10}$, $Co_{.36}Zr_{.64}$, Ni_xZr_{1-x}(x=0.18, 0.24, 0.34, 0.36, 0.64, 0.90) $Cu_{.36}Zr_{.64}$, Cu_xTi_{1-x}(x=0.4, 0.5, 0.6), $Mg_{.30}Zn_{.70}$. In order to investigate the partial structure of binary amorphous alloy, isotope ^{60}Ni and ^{65}Cu were substituted in Ni_xZr_{1-x}(x=0.36, 0.64) and Cu_xTi_{1-x}(x=0.4, 0.5, 0.6), respectively.

For neutron scattering experiment amorphous alloy ribbons of about 30 ~ 50um thick were cut into small pieces and packed into a cylindrical sample cell of 8mm in diameter made of thin vanadum foil. The amount of samples was usually 2 ~ 4g and effective sample hight in the cell was roughly 2 ~ 4cm.

Scattered neutrons were detected with 0.5"ϕ ^3He counters located in the time focussing configuration in each counter bank at the scattering angle of $2\theta = 13.3^\circ$, 24.6°, 31.5°, 50°, 93° and 155°. Outputs of each detectors are amplified and shaped by fast electronic circuits and accumulated in multi-channels

time annalyzers which were synchronized with bursts of incident neutron pulses.

Scattering from the empty vanadium cell and background was measured successively. Attenuation effect of scattered neutrons in the sample and the cell was calculated neumerically. The multiple scattering in the cyrindrical sample was also calculated. The spectrum of incident neutrons was calibrated by the scattering spectrum from an incoherent scatterer, that is, a vanadium rod of same size as the sample.

After the above necessary corrections the interference function, S(Q), was obtained as the function of $Q = 4\pi \sin\theta / \lambda$. By Fourier Transform we get the pair correration function, g(r), of the binary amorphous alloys.

For example, in Fig.1 and Fig.2, S(Q) and g(r) of the amorphous $Ni_{.34}Zr_{.76}$ alloy are shown. The first peak of g(r) splits into two subpeaks for the Zr rich Ni_xZr_{1-x} alloys (x=0.18, 0.24 and 0.34). The first subpeak seems to corresponds to the combination of Ni-Ni and Ni-Zr pairs and the second one corresponds to the Zr-Zr pairs.

In order to get the partial structures of binary amorphous alloys quantitative analysis is in progress.

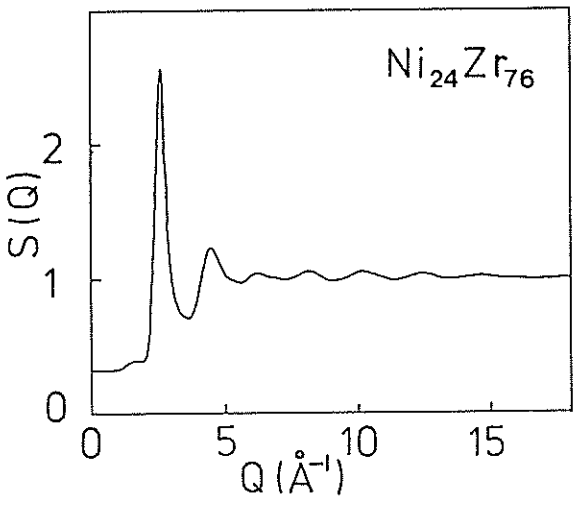

Fig. 1. S(Q) of an amorphous $Ni_{24}Zr_{76}$ alloy.

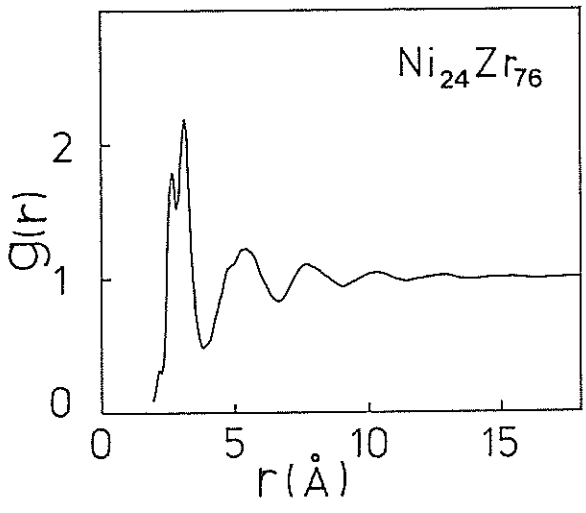

Fig. 2. g(r) of an amorphous $Ni_{24}Zr_{76}$ alloy.

Local Structures of Amorphous As-Chalcogenide Systems by Means of High Q-Neutron Scattering

T. Arai, M. Kato, T. Mori, M. Hatori, H. Yasuoka
H. Saegusa, K. Ohkawa, T. Fukunaga* and N. Watanabe**

Institute of Applied Physics, The University of Tsukuba
Sakura, Ibaraki 305, Japan
* The Research Institute for Iron, Steel and Other Metals
Tohoku University
Sendai, Miyagi 980, Japan
** National Laboratory for High Energy Physics,
Oho-machi, Ibaraki 305, Japan

In amorphous materials the short range orderings are very similar to those of the single crystals. However, the single crystals of As-chalcogenides have peculiar structures. The unit cell consists of two layers and the basic unit in a layer consists of four $As(X_{1/2})_3$ molecules, X = S or Se. The lengths of 6 As-X bonds in the basic unit differ slightly each other.[1] The radial distribution functions of amorphous systems determined from X-ray diffraction have only a broad first peak.[2] The neutron diffraction experiment up to high Q-value was carried out to get the detailed knowledge of the local structure in As-S-Se system.

The sample materials of $(As_2Se_3)_x(As_2S_3)_{1-x}$ (x = 0.0, 0.1, 0.2, 0.3, 0.5, 0.65, 0.9, 1.0) were prepared by direct synthesis from properly weighed high purity As, Se and S. The raw materials which were sealed in evacuated quartz ampoules ($1x10^{-5}$ Torr, 8 mm in diameter) were heated up at 600°C for about 24 hours while being rocked. They were then quenched in air at room temperature. The quartz ampoules were carefully broaken to take out the ingots. The each sample was then annealed for 24 hours near the glass transition temperature, 120°C.

The neutron diffraction measurements were carried out using pulse neutron up to high Q value, 35 A^{-1}, with HIT in National Laboratory for High Energy Physics. The structure factor of each sample, S(Q), is shown as a function of Q value in Fig. 1 (a) and (b). The radial distribution function obtained from it is shown in Fig. 2. A new shoulder, denoted by

an arrow in Fig. 2, was found at the longer radius side in the first main band. As this shoulder does not depend on the cut off of Fourier

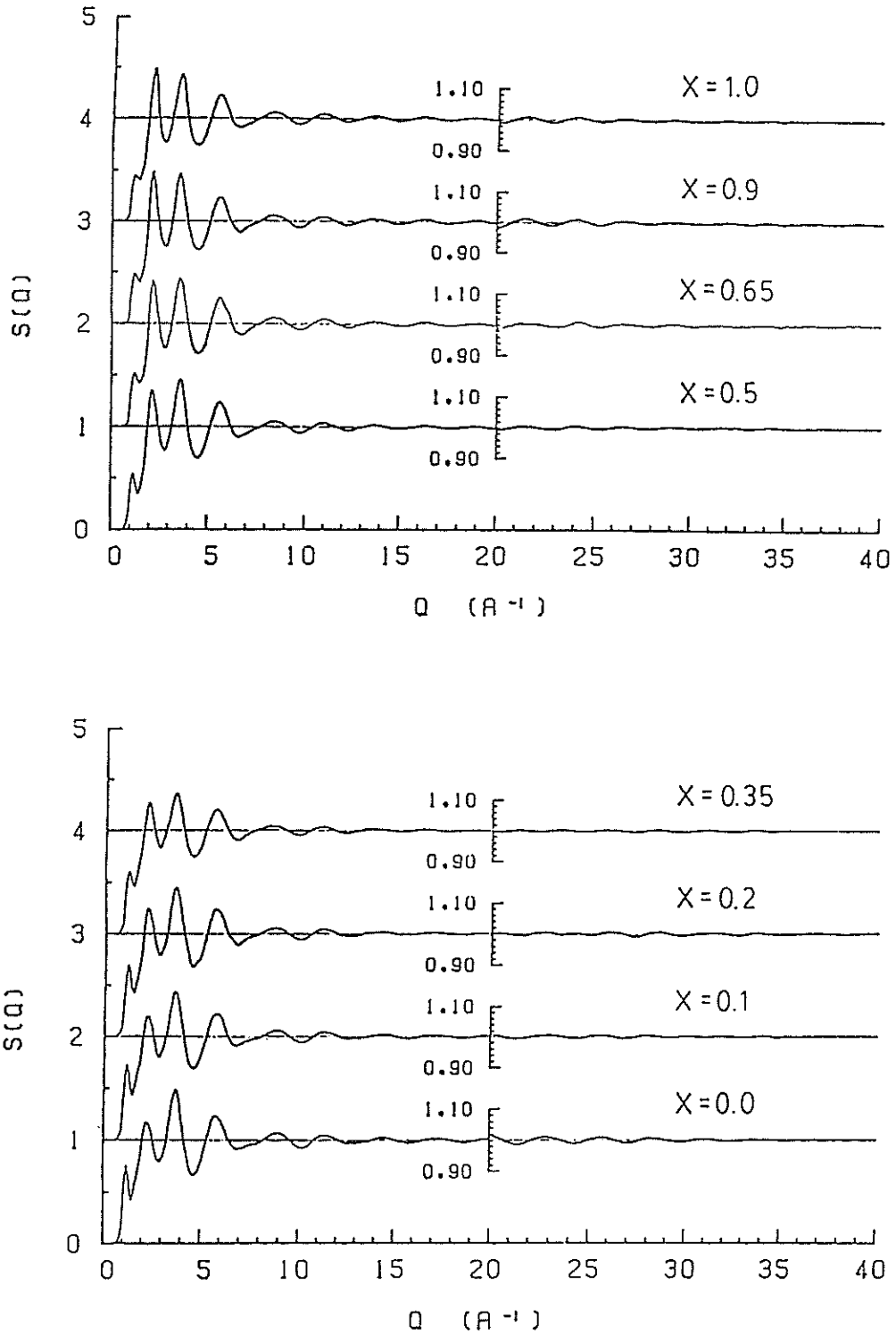

Fig. 1. The structure factor as a function of Q value.

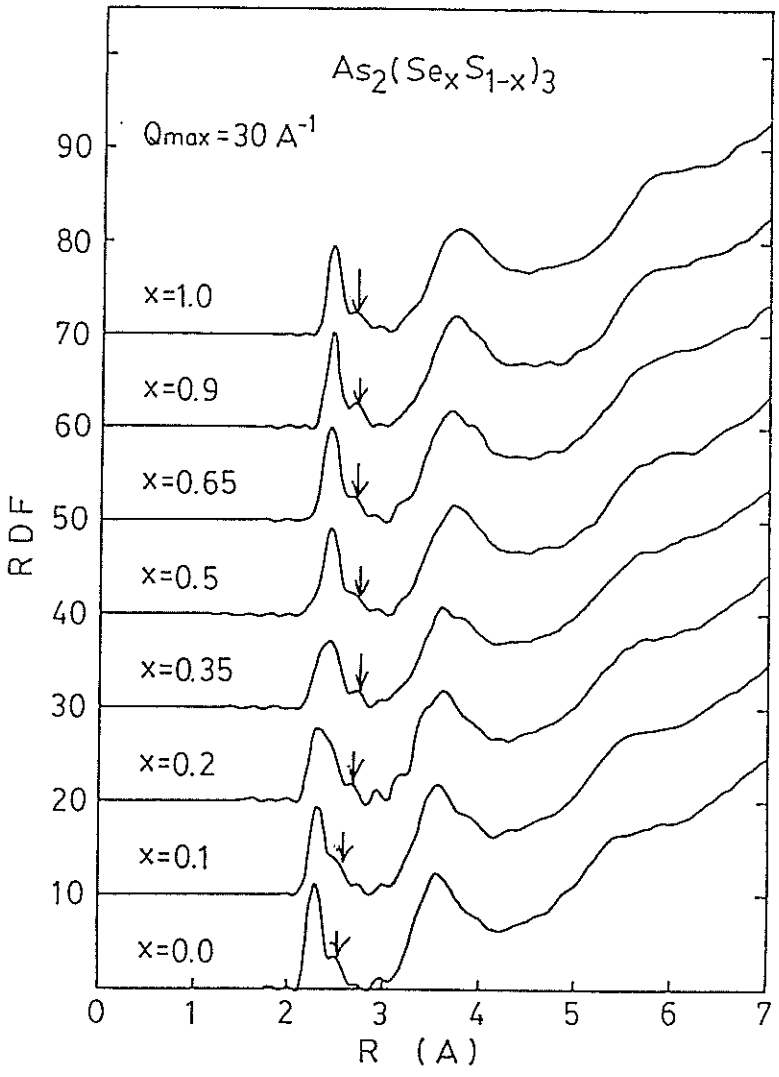

Fig. 2. The radial distribution function.

transformation, it is not a spurious peak. The intensity raito of the first main peak to the shoulder for x = 0 and 1.0 was ca. 4. The coordination number of As atom calculated from the first main band intensity with including the shoulder was 3.

Lengthes of As-X bonds in a single crystal are devided into two groups. The bond length in one group is slightly longer than that in the other group. The longer bond is the bridge bond between spiral chains in a layer. The existing ratio of the longer bonds to shorter bonds is one fifth. This ratio is nearly equal to the intensity ratio of the shoulder to the first main peak. From the things discribed above we may be able to say that the basic unit of these amorphous is constructed with four pyramidal molecules, 4 x $As(X_{1/2})_3$, and the ordering in these amorphous extends to the fourth and fifth nearest neighbour atoms, 6 $\sim$ 7 A. This ordering length agrees with that obtained from the thermal and photo-crystallization in As doped Se.[3] This interpretation is in good agreement

with the conclusion deduced from the experimental result of the compositional dependence of the vibrational frequencies.[4)]

The radial distribution function for the intermediate composition can be synthesized from that for As_2S_3 and As_2Se_3. It means that the all most of the basic units in intermediate compositions do not include S- and Se-atoms in the same basic unit. Only one glass transition temperature was determined from the thermal analysis for each sample. The phase separation has, therefore, not occurred in these materials. The results of infrared absorption experiments in these materials also did not show any evidence of the phase separation. From the things discribed above, it may be interpreted that the materials of intermediate composition is constructed with the S rich and Se rich regions and each region is not so large as it is considered by phase separation.

References

1) F. Hulliger:
"Structural Chemistry of Layer-Type Phase", ed. by F. Levy (Reidel, Boston, 1976) p. 67.

2) J. Chang and D.B. Dove:
J. Non-Cryst. Solids 16 (1974) 72.
O. Uemura, Y. Sagara, D. Muno and T. Satow:
J. Non-Cryst. Solids 30 (1978) 155.

3) 森 龍男：
"a-Se の結晶化に及ぼす As と光の効果", 筑波大物理学研究科 修士論文 1982.

4) S. Onari, O. Sugino, M. Kato and T. Arai:
Jpn. J. Appl. Phys. 21 no. 3 (418 - 423) 1982.

Structural Investigation of Fe-B Amorphous Invar Alloys

Ze Xianyu, Y. Ishikawa T. Fukunaga[+] and N watanabe[++]

Physics Department, [+]The Research Institute for Iron Steel and Other Metals, Tohoku University and [++]National Laboratories for High Energy Physics

The paper reports briefly the preliminary results of the structural studies of the amorphous $Fe_{1-x}B_x$ alloys with three different compositions x=0.14, 0.17 and 0.25 by using the total scattering spectrometer HIT at KENS. The amorphous $Fe_{1-x}B_x$ alloys are the unique system which has the stable amorphous phase in a wide range of composition x ($0.12 \leq x \leq 0.25$) and the strongly composition dependent physical properties. The magnetization at 0 K become maximum around x=0.17 and the invar effect which is quite large in $Fe_{86}B_{14}$ is significantly reduced when x approaches to 0.25. The behaviors are quite similar to those of the crystalline Fe_xNi_{1-x} alloys around x=0.5. Therefore the detailed studies of the local atomic order in the amorphous Fe-B alloys with different composition will give us an insight into the relation between the local atomic order and electronic structure, because the invar alloys are quite sensitive to the electronic structure. The structural investigations hiterto performed on this system are restricted either to neutron diffraction studies of a single composition or to x ray diffraction studies for different compositions. A $Co_{83}B_{17}$ alloy was also studied for comparison because this alloy does not exhibit the invar effect at all.

The amorphous samples were prepared by rapidly quenched method and the neutron scattering experiments were carried out on HIT in a magnetic field H of 5 K Oe applied parallel and perpendicular to the scattering vector Q in order to separate the magnetic contribution. The scattering function S(Q) obtained with $\vec{H} // \vec{Q}$ for four differnet samples are shown in Fig. 1. They were measured by three single He^3 counters with scattering angles of 29.6 31.5 and 152.5 degrees. The pair correlation functions G(r) derived by Fourier transform of S(Q) are displayed in Figs. 2. The inner most peak

found at the left hand side of the first high peak which was absent in the x ray scattering data is the n.n Fe-B corretalion function. Since the results of Fe-B alloys exhibit small composition dependence, the elaborated analysis is required to find the difference in local atomic order in the different compositions which is now in progress.

By taking the difference between the scattering functions with the magnetic field parallel and perpendicular to the scattering vector gives the scattering function of the magnetic atoms which is also in progress.

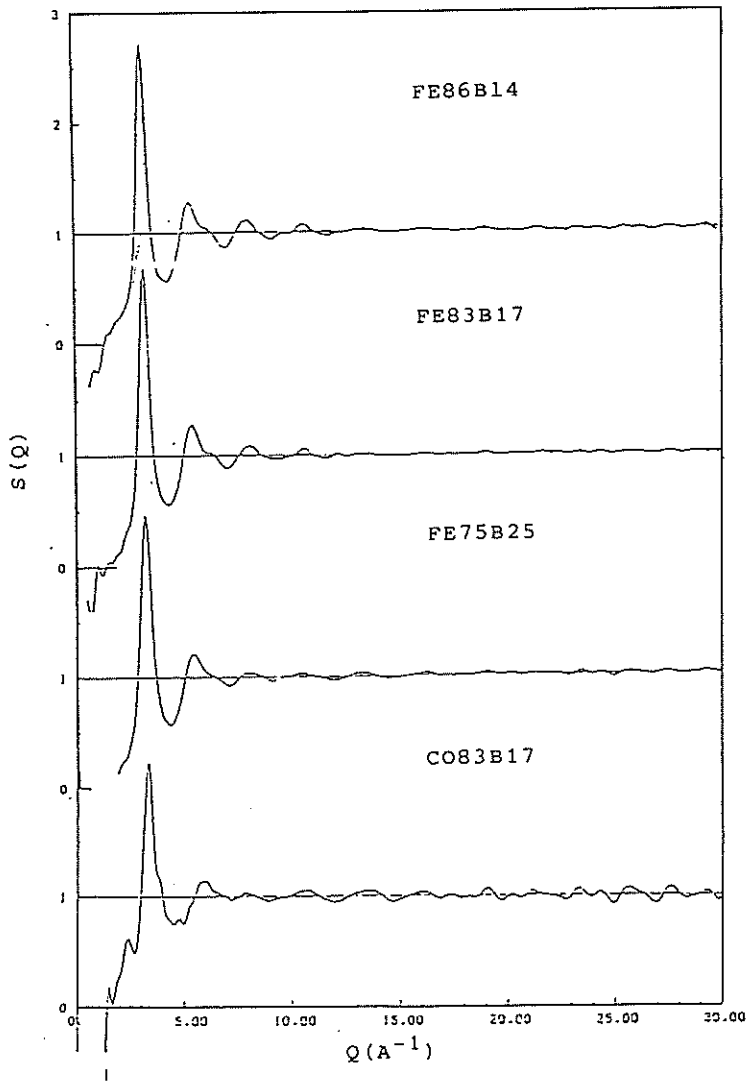

Fig. 1. S(Q) of $Fe_{1-x}B_x$ and $Co_{83}B_{17}$ alloys measured in a field parallel to scattering vector.

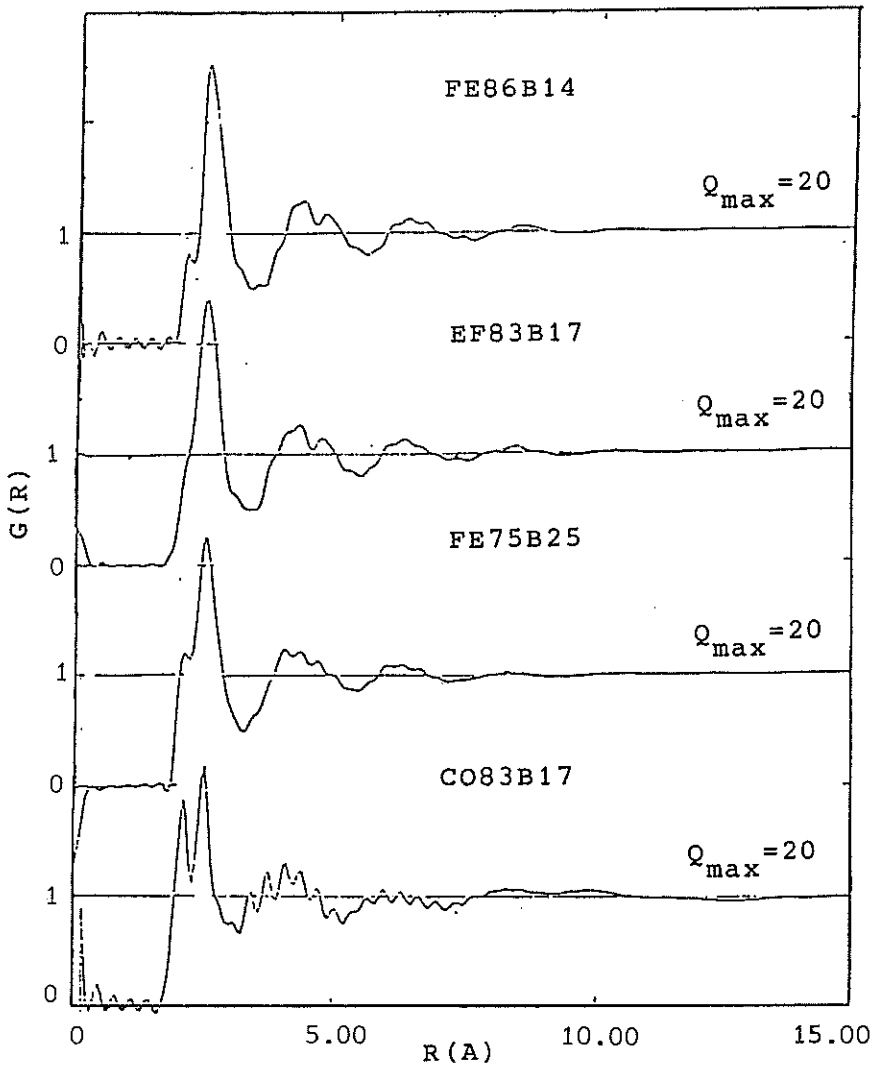

Fig. 2. Atomic pair correlation functions G(R) of $Fe_{1-x}B_x$ and $Co_{83}B_{17}$ alloys.

Neutron Diffraction Experiments of Sulfuric Acid Solutions

T. Matsumoto, K. Ichikawa*, N. Watanabe**

Nuclear Department, *Chemical Department, Hokkaido University, Sapporo 060 and **High Energy Physics Institute, Tsukuba 305

This paper reports the preliminary results of neutron diffraction experiments of sulfuric acid solutions, which were made at HIT. The sulfuric acid solutions of the various concentrations (97, 81, 61, 38, 17 mol%) and heavy water were measured at room temperature. Figure 1 shows the structure factors obtained at 6 different angles for 97, 81, 61 mol% sulfuric acid solutions and heavy water. The data were not corrected for the dynamical effect. The dynamical correction is somewhat difficult for HIT, because (1) the ratio of the scattered flight path to the total one, Υ, is fairly large and depends on the angle and (2) the efficiency of the ^3H_e detector largely deviates from the 1/v dependence due to the high pressure (10 atm). The two effects on the structure factor can be seperately discussed by the following equation which is derived from Eq. (5) of the reference 1:

$$N_T \overline{b_T^2} R(2\theta, Q_e) = \int d\omega \frac{k}{k_e} \frac{\varepsilon(E)}{\varepsilon(E_e)} S(Q,\omega) + \gamma \int d\omega \frac{k}{k_e} \frac{\varepsilon(E)}{\varepsilon(E_e)} \left\{ 1 - \left(\frac{k_e}{k}\right)^3 \right\} S(Q,\omega) + O(\gamma^2)$$

The values of Υ for HIT are shown in Tab. 1.

(1) T. Matsumoto: J. Nucl. Sci. Technol., 16(6), 401(1979).

	A	B	C	D	E	F
2θ(°)	9.7	13.3	24.6	49.9	90.2	152.5
γ (%)	12.8	12.1	10.6	9.0	6.1	6.1

Table 1. The values of γ

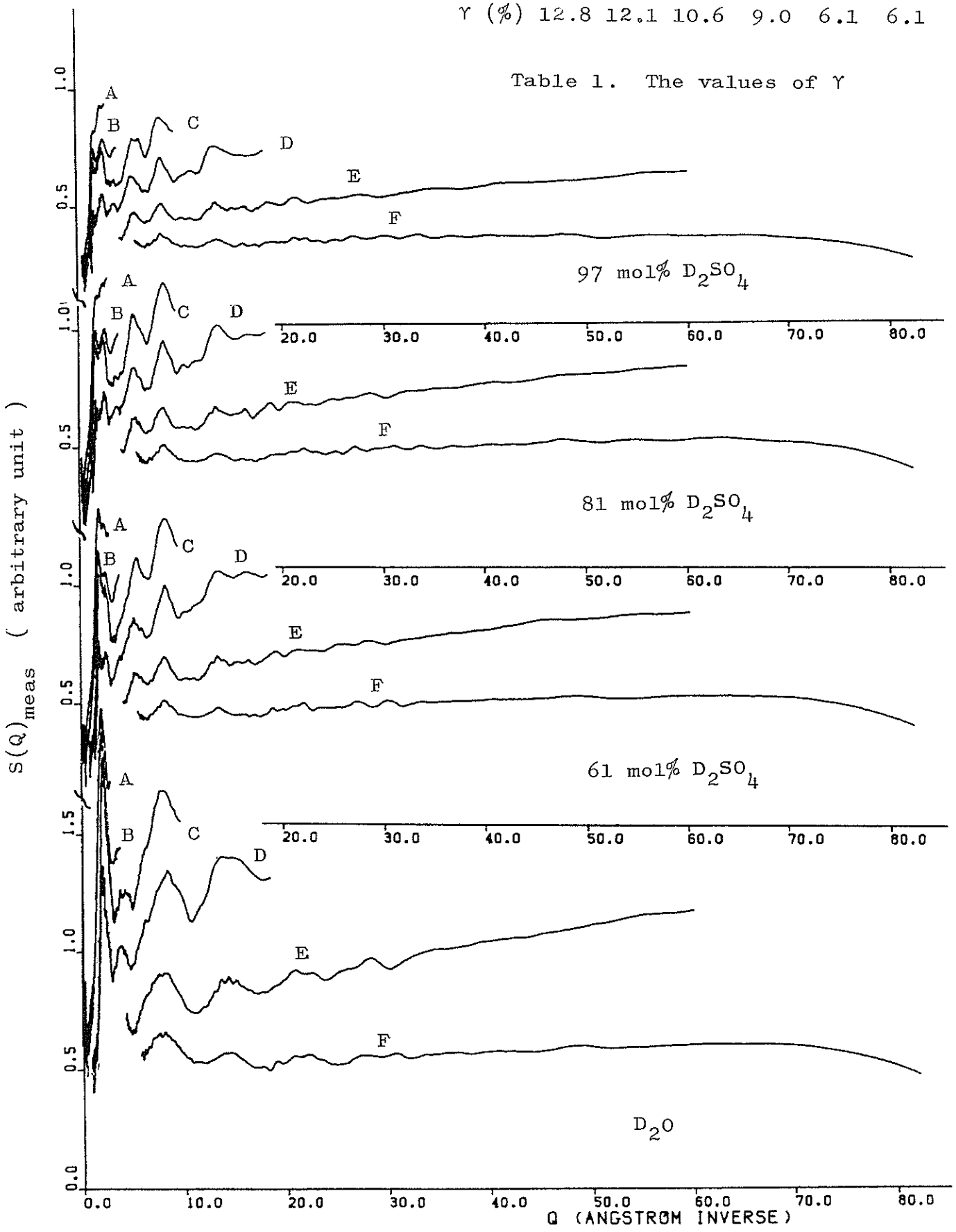

Figure 1. The structure factors of sulfuric acid solutions and heavy water

Quasielastic Scattering of Water

Kazuhiko Inoue

Department of Nuclear Engineering, Hokkaido University,
Sapporo 060

Localized diffusive motion of the water molecule has been studied by measuring the neutron quasielastic scattering from water at ambient temperature by using the LAM spectrometer. A scattering specimen was prepared in a sample container of 14 mm diameter cylinder, 0.15 mm thickness and 80 mm length. The whole apparatus was housed in an evacuated cage, and the sample container was vacuum-proofed.

Fig. 1 shows the raw data of the measured quasielastic spectra from the water at scattering angles ranging from 13° to 125°. Fig. 2 is a comparison between the present results and those of several authors who measured the full width at half maximum (FWHM) of the quasielastic peak. The agreement between them, is satisfactory except Sakamoto's data. It is commonly recognized that the central peak of the quasielastic spectrum relates to the translational jump diffusion of the hydrogen atom, and that the shoulder in the spectrum might be an inelastic background. However,

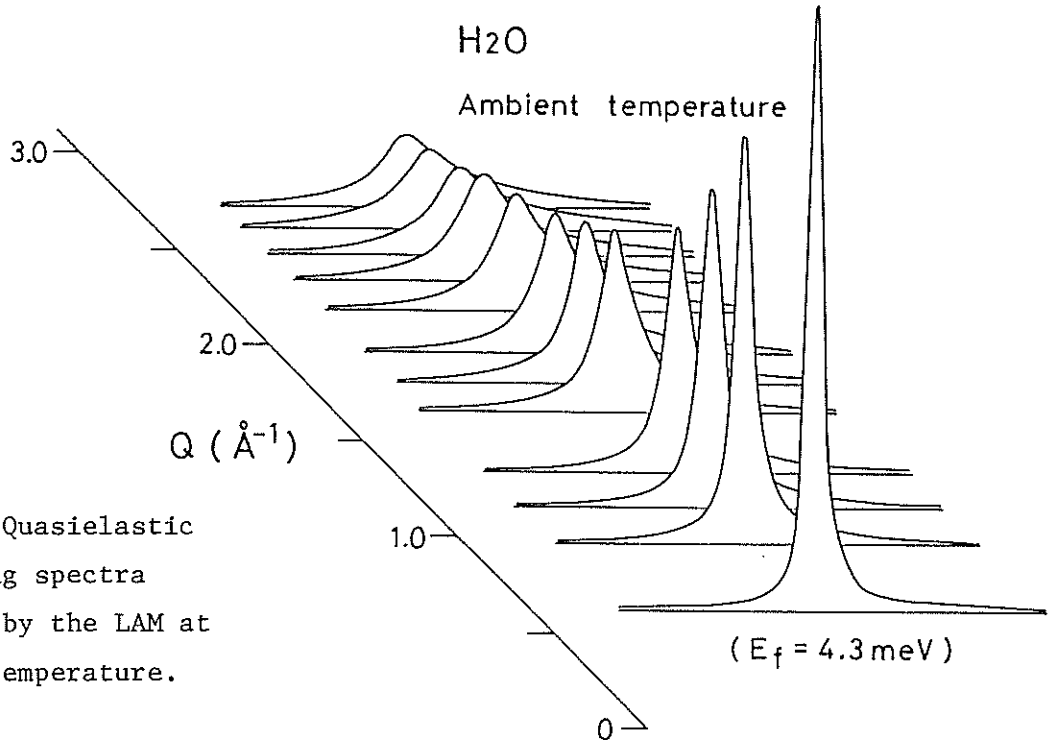

Fig. 1 Quasielastic scattering spectra measured by the LAM at ambient temperature.

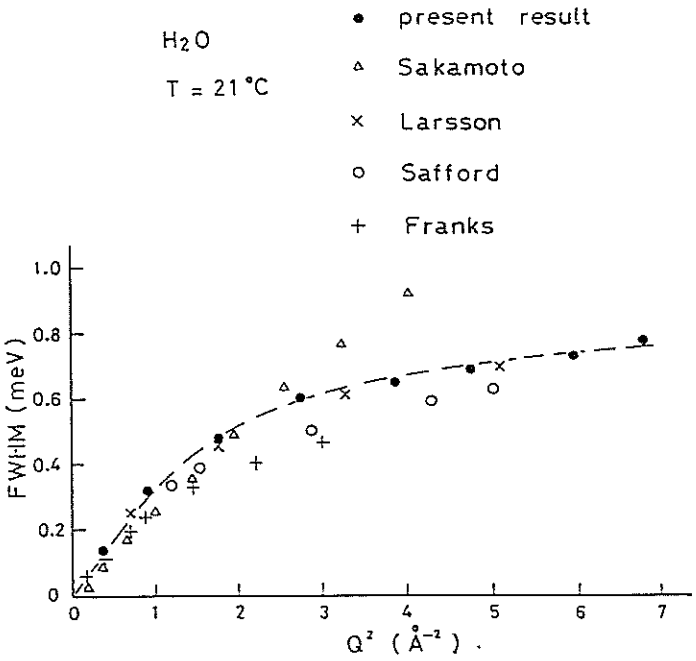

Fig. 2 Full width at half-maximum (FWHM) of central quasielastic peak vs. Q^2 for water at ambient temperature, which were measured by several authors.

we believe that the shoulder is a broad quasielastic peak and that its characteristics can give some information about the localized random motion of the water molecule.

Fig. 3 shows the experimental results of the elastic incoherent structure factor (EISF) and some theoretical curves. Further precise treatment of the data is needed to evaluate the precise characteristics of the localized diffusive motion of the water molecule.

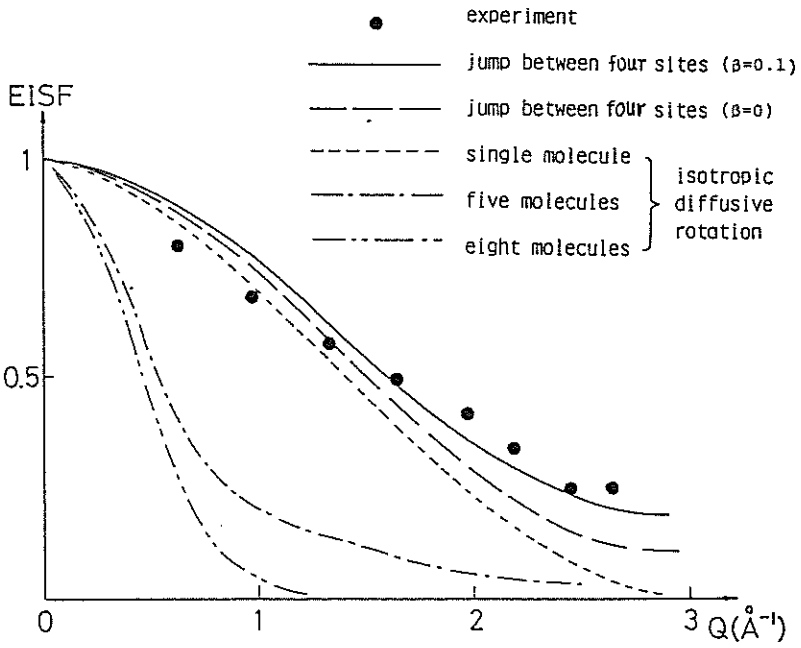

Fig. 3 Experimental data of the elastic incoherent structure factor (EISF) and theoretical curves due to various models for localized motion.

Motion of Individual Polymeric Chains

Kazuhiko Inoue*, Keisuke Kaji**, Yoshiaki Kiyanagi*,
Hirokatsu Iwasa* and Kiyoshi Jinguji*

* Department of Nuclear Engineering, Hokkaido University, Sapporo 060

** Institute for Chemical Research, Kyoto University, Uji, Kyoto-Fu 611

The motion of individual chains for polymers in the rubber state has been studied by measuring the time-of-flight spectra from chloroprene and stretched natural rubber bands. To suppress the effect of the side chain motion in the rubber, we adopted the isotopic substitution method and used chloroprene as a sample. We measured the spectra from samples by using the LAM quasielastic scattering spectrometer, energy resolution ~ 200 μeV, Q range 0.2 ~ 2.6 $Å^{-1}$, at ambient temperature. The chloroprene sheet sample of 0.25 mm in thickness was shaped into a cylinder of 14 mm in diameter and 80 mm in length.

Fig. 1 shows the time-of-flight spectra of chloroprene at lower and higher temperatures than the glass transition temperature at 77° scattering angle. At lower temperatures the motion of individual segments is suppressed, and the onset of the motion is observed for the higher temperature spectra.

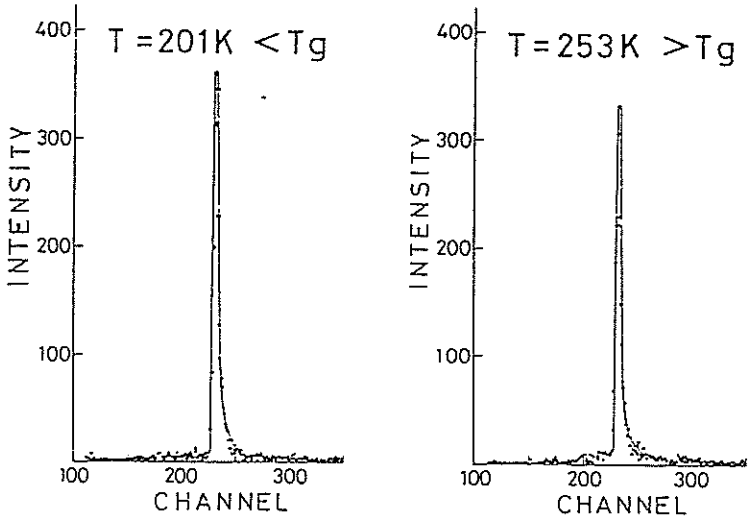

Fig. 1 Time of flight spectra of chloroprene at lower and higher temperatures than the glass transition temperature.

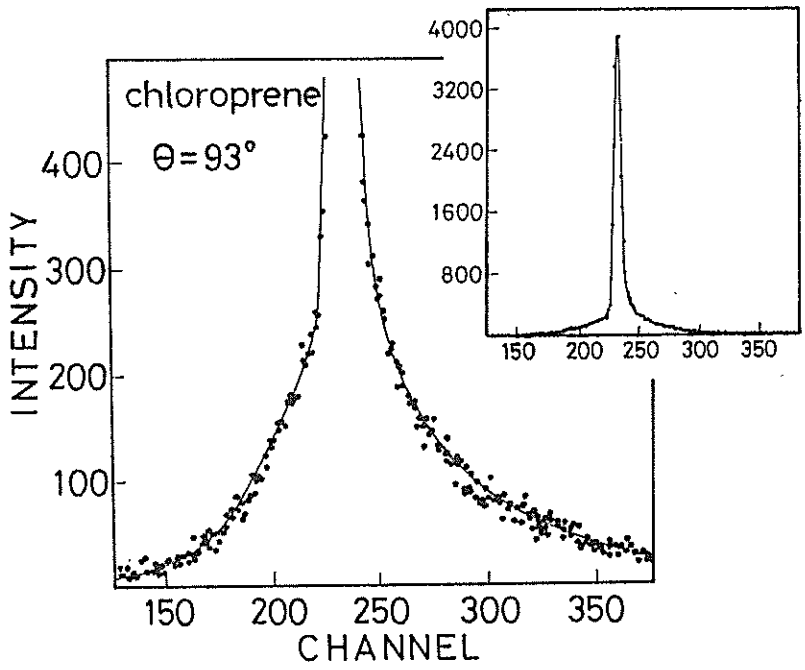

Fig. 2 Time-of-flight spectrum of chloroprene at ambient temperature.

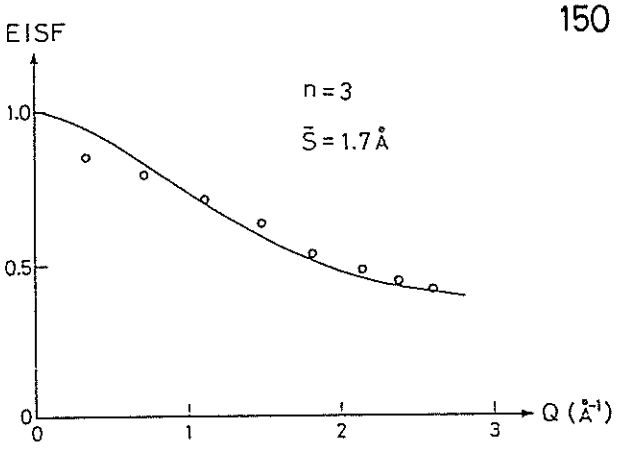

Fig. 3 Calculated and measured values of the elastic incoherent structure factor for the migration of kinks in chloroprene.

Fig. 2 shows an expanded figure of the shoulder of the spectrum at 93° scattering angle at ambient temperature. The inserted figure is the whole spectrum, which reveals a sharp elastic component and a broad underlying shoulder. Careful examination of the ratio of the integrated intensities of the elastic and quasielastic parts gives the elastic incoherent structure factor (EISF). Fig. 3 shows a comparison between the theoretical and experimental EISF. Further detailed experiments and treatment of data are now being conducted.

Diffusion of hydrogen in Ti

Yoshiaki Kiyanagi*, Kazuhiko Inoue*, Kenzo Kai** and Hirokatsu Iwasa*

* Department of Nuclear Engineering, Hokkaido University, Sapporo 060

** Institute for Iron, Steel and Other Metals, Tohoku University, Sendai, Miyagi 980

We measured the quasielastic scattering from the hydrogen in Ti with the LAM spectrometer. Specimen was $TiH_{0.24}$ which was prepared in a cylindrical aluminum sample container of 14 mm in outer diameter of cylinder, 0.75 mm in thickness and 80 mm in length, then heated with an electric heater in an evacuated cage. $TiH_{0.24}$ is in the (α+β) phase at temperatures lower than 300°C, and is in the (α+β) phase at higher temperatures, as shown in Fig. 1.

Fig. 2 shows the elastic spectra in the (α+γ) phase, and Fig. 3 shows the composite spectra of elastic and quasielastic scatterings in the (α+β) phase at 328°C. Obviously, in the (α+γ) phase, the proton does not diffuse or has a very small diffusion constant. On the other hand, in the (α+β) phase, a certain fraction of the protons can perform quick diffusive motion and the diffusion constant in that phase is of the order of 10^{-5} cm^2/sec. Analysis using the curve-fitting data treatment of the quasielastic spectra combined with observations of the localized frequency of the protons in Ti lattice might give information on the diffusion process in the (α+β) phase. We are now preparing to carry out such measurements and data processing.

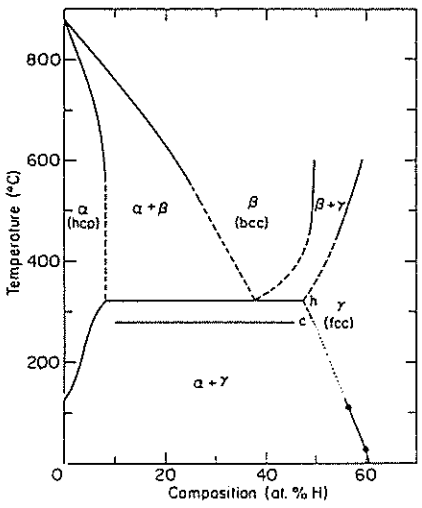

Fig. 1 Equilibrium phase diagram of titanium-hydrogen system.(1)

Refference

(1) C. Korm and D. Zamir: J. Phys. Chem. Solids, 31(1970)489.

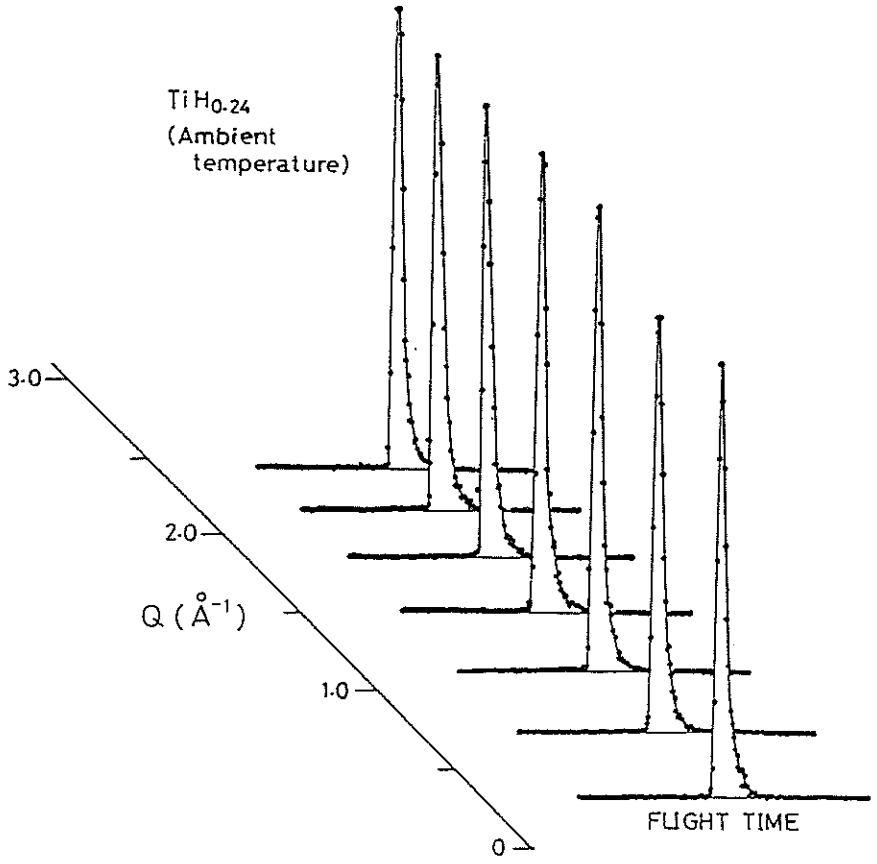

Fig. 2 Time of flight spectra of $TiH_{0.24}$ in (α+γ) phase.

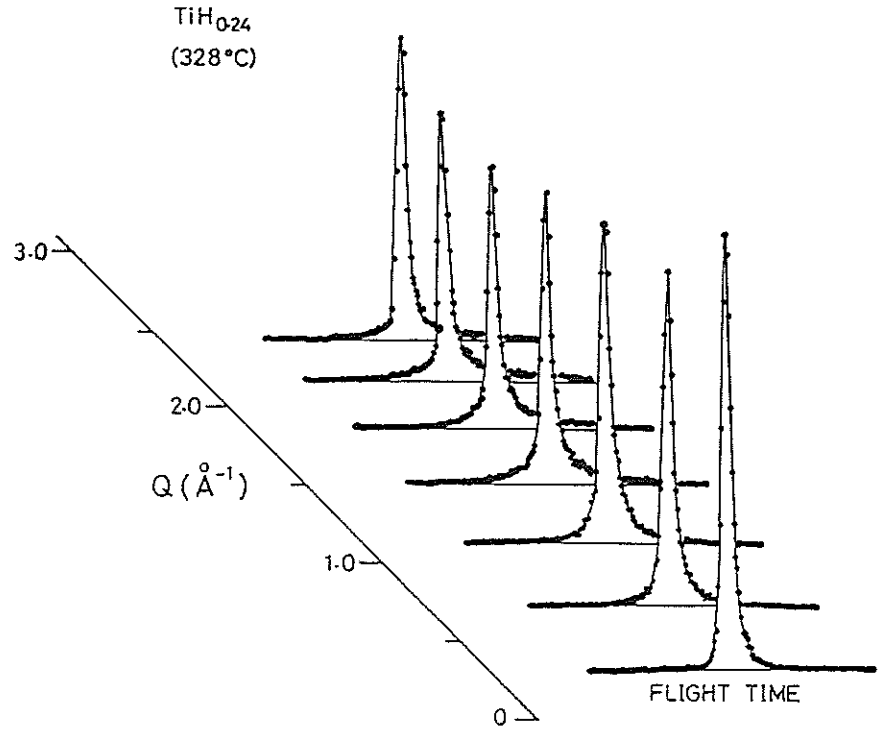

Fig. 3 Time of flight spectra of $TiH_{0.24}$ in (α+β) phase.

Low energy neutron scattering from solid benzene

Yoshiaki Kiyanagi, Kazuhiko Inoue and Hirokatsu Iwasa

Department of Nuclear Engineering, Hokkaido University,
Sapporo 060

To investigate low energy lattice vibration and diffusive motion of the benzene molecule in the solid phase, we measured the low energy neutron scattering spectra from solid benzene by using the LAM spectrometer. The melting point of benzene is 278.6 K; therefore, we made the measurements at 253 K and 200 K. The specimen was placed in cylindrical aluminum container of 14 mm diameter, 0.25 mm in thickness and 80 mm in length, and its temperature was controlled by a refregirator and an electric heater.

Fig. 1 shows the spectra at both temperatures at a scattering angle of 77°, and Fig. 2 shows the expanded figures for the shoulder of the both spectra. As shown, the one-phonon inelastic spectra were clearly distinguished in both cases, which had appreciably different spectral shape from the quasielastic one. The inelastic spectra were subtracted, and the sharp peaks were shown in Fig. 3. Obviously, the spectrum obtained at the higher temperature revealed a somewhat broder spectrum than that obtained at the lower one. These results suggest diffusive rotation and its time constant is longer than 10^{-11} sec. Further investigations are now being conducted.

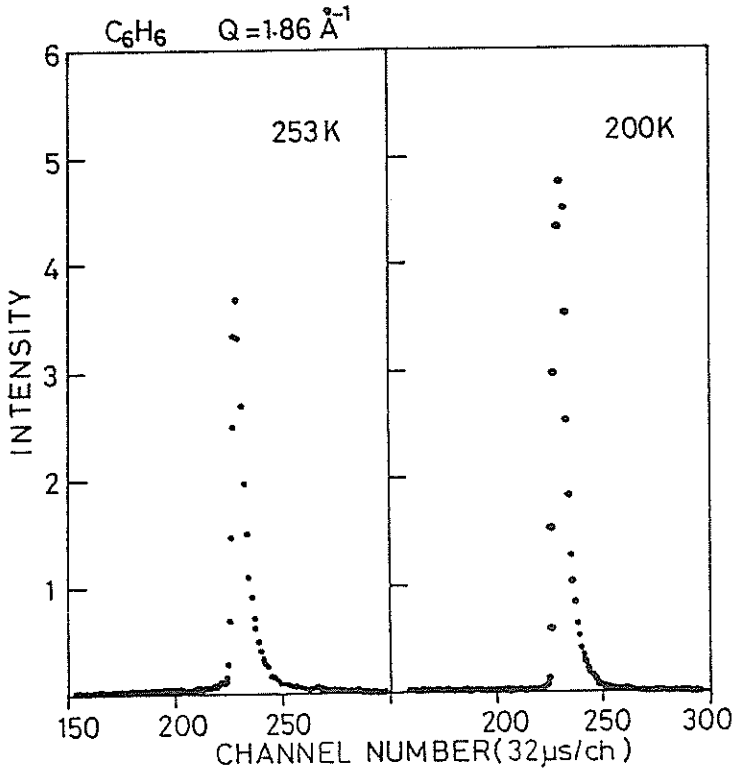

Fig. 1 Time-of-flight spectra of solid benzene.

Fig. 2 Expanded spectra for the shoulder at both temperatures.

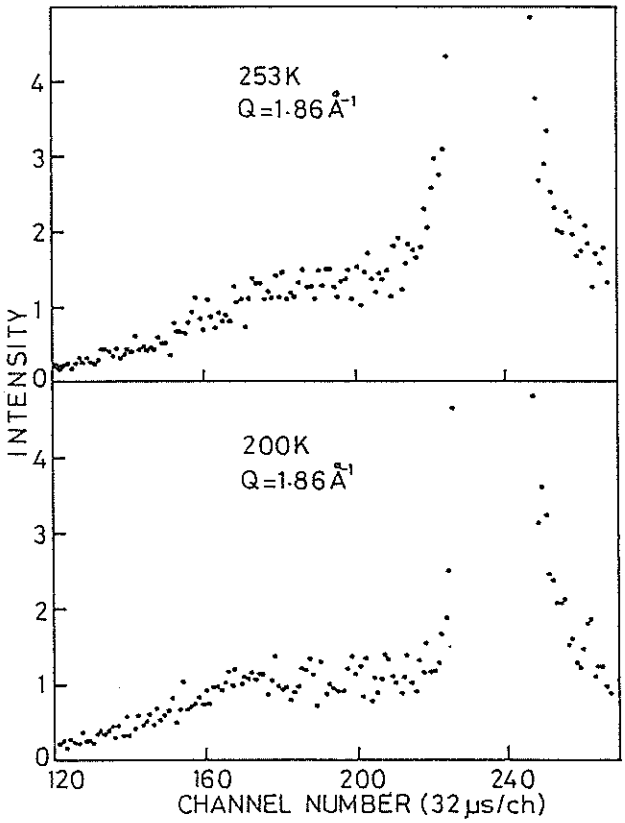

Fig. 3 Sharp peaks from solid benzene at two temperatures. The inelastic spectra were subtacted.

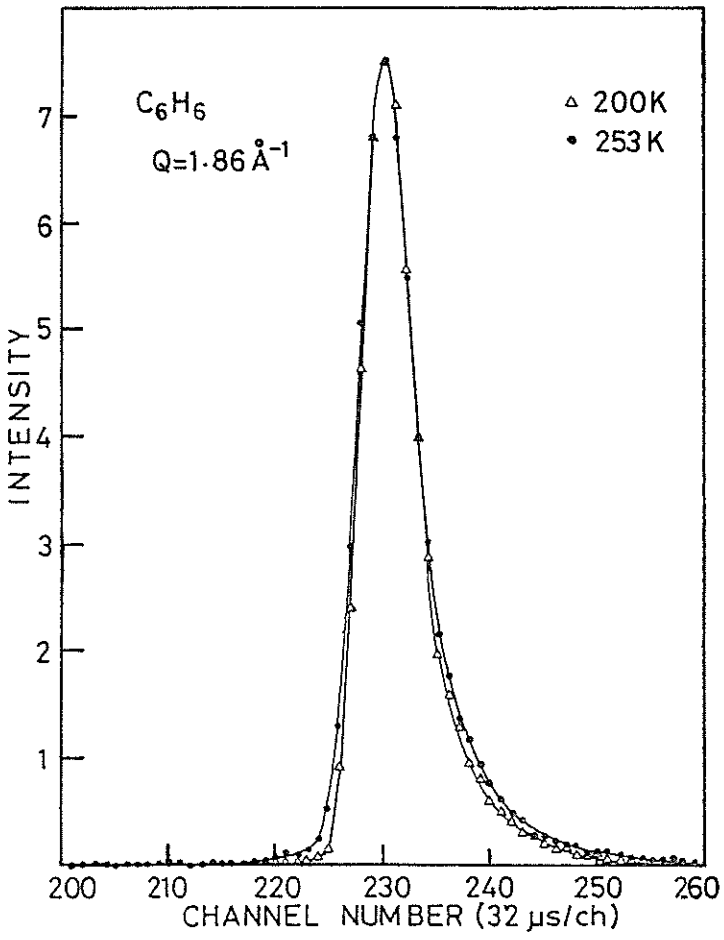

Molecular dynamics of polyisobutylene rubber

Keisuke Kaji, Hiroshi Urakawa, Ryozo Kitamaru,
Kazuhiko Inoue* and Yoshiaki Kiyanagi*

Institute for Chemical Research, Kyoto University, Uji, Kyoto-Fu 611 and *Department of Nuclear Engineering, Faculty of Engineering, Hokkaido University, Sapporo 060

The study of the intramolecular motion of polyisobutylene has been carried out by quasielastic neutron scattering (QENS). The QENS spectrum of rubber usually consists of at least two components, elastic and quasielastic parts. In this work the energy spectrum of the polyisobutylene rubber was measured for various Q-values and each spectrum was separated into the two components. The results obtained are analysed by applying a rotational jump model. The elastic incoherent structure factor (EISF) and the width of the QENS part give information of the number of jump sites and the average time between successive jumps, respectively. The sample Oppanol B-100 (M.W. 10^5) was compression-moulded into film 0.2mm thick and mounted on the outer surface of an aluminium cylinder 13mm in diameter and 100mm high. The measurements were carried out using KENS-LAM spectometer. The wavelength of the analyser mirror of this spectrometer is 4.22Å. The time-of-flight spectrum was obtained simultaneously at eight scattering angles 10°, 26°, 42°, 58°, 74°, 90°, 106° and 122°. The results are shown in Fig. 1. The Q-dependence of EISF (intensity ratio of elastic

to total scattering) suggests that the number of sites is 2 to 3, assuming the average jump distance of 1 to 2Å. The average time between successive jumps is estimated from the widths of the QENS parts to be about 1 ps. Therefore, the motion observed in this study is related to the very short range intramolecular dynamics.

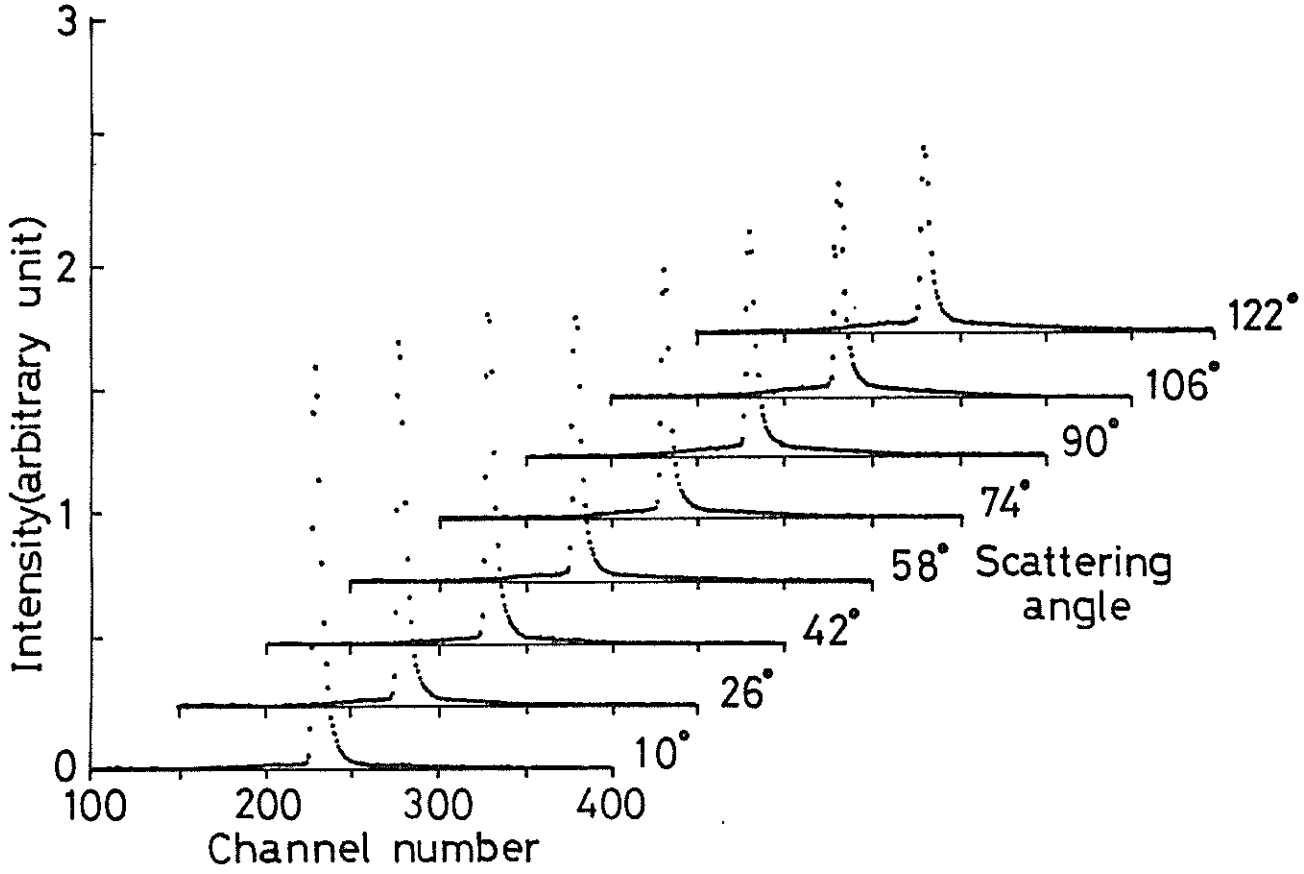

Fig. 1 Time-of-flight spectra of polyisobutylene at scattering angles from 10° to 122°. A channel width is 32 μs.

Molecular motion of amorphous chains in semicrystalline low density polyethylene film

Keisuke Kaji, Hiroshi Urakawa, Ryozo Kitamaru, Kazuhiko Inoue* and Yoshiaki Kiyanagi*

Institute for Chemical Research, Kyoto University, Uji, Kyoto-Fu 611 and *Department of Nuclear Engineering, Faculty of Engineering, Hokkaido University, Sapporo 060

In order to investigate the molecular motion in the amorphous state of polyethylene, the quasielastic neutron scattering (QENS) experiment has been carried out. Polyethylene material is usually semicrystalline and consists of crystallites and amorphous phase. To obtain sufficient intensity for analysis, a low density polyethylene (Sumikathene® G 806, Sumitomo Kagaku Kogyo Co. Ltd., a melt index of 50g/10min, 3.3 CH_3 units per 100 main-chain carbons, $\bar{M}n=2.3\cdot10^4$, and $\bar{M}w=29.2\cdot10^4$) was used. The density of the sample film 0.2mm thick is 0.919 Mg/m^3 and the degree of crystallinity estimated from the density is 48%. The time-of-flight (TOF) measurements of QENS were made using KENS-LAM. The analytical method used is the same as that described in the preceding paper. In this case, however, the intensity of elastic scattering was corrected for the degree of crystallinity of the sample since we discuss the motion only in the amorphous region. The Q-dependence of the elastic incoherent structure factor (EISF) or intensity ratio of elastic to total scattering is shown in Fig. 1 with the result of polyisobutylene rubber as reported in the preceding

paper. The EISF behavior of polyethylene is similar to that of polyisobutylene, which suggests that the number of jump sites is 2 to 3. Fig. 2 shows the results about the width Γ of QENS part at various Q-values. The same Γ-value is obtained both for the unswollen polyethylene film and for the film swollen in CCl_4; this means that the observed motion is intramolecular. On the other hand, the Γ of polyisobutylene is lower than that of polyethylene, or the average time between successive jumps of polyisobutylene is longer than that of polyethylene. Such results are reasonable because polyisobutylene has two methyl side groups in the monomeric unit $-C(CH_3)_2-CH_2-$, while polyethylene has no side group. The motion of the atomic group of larger mass is slower than that of smaller mass.

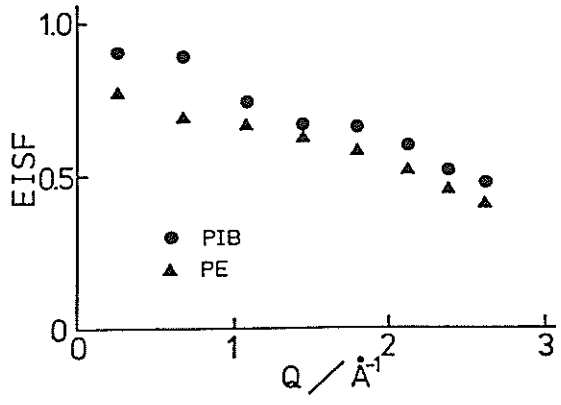

Fig. 1 Elastic to total intensity ratio(EISF) vs. Q for polyethylene and polyisobutylene.

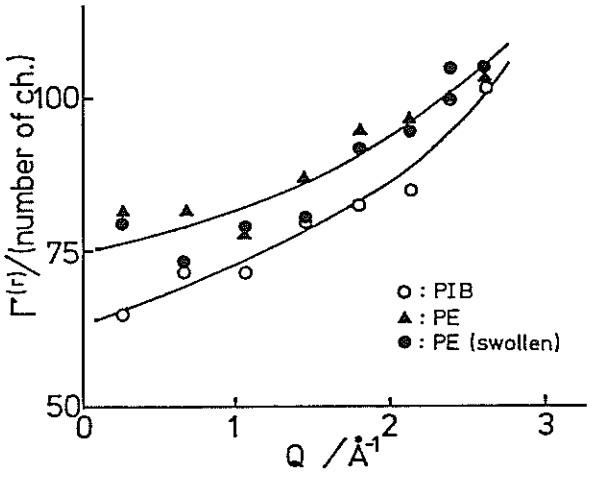

Fig. 2 Half width of quasielastic peak vs. Q for polyisobutylene, polyethylene and swollwn polyethylene.

Quasielastic Neutron Scattering from Polyelectrolyte Solutions

Ichiro Noda*, Yuji Higo* and Kazuhiko Inoue+

* Department of Synthetic Chemistry, Faculity of Engineering, Nagoya University, Nagoya 464

\+ Department of Nuclear Engineering, Hokkaido University Sapporo 060

Preliminary experiments were made on quasielastic neutron scattering (QENS) from polyelectrolyte solutions to study the effect of charge on local motions of a polymer chain. For this purpose we used poly(sodium acrylate)s (NaPA'S) having two different degrees of ionization α=0.1 and

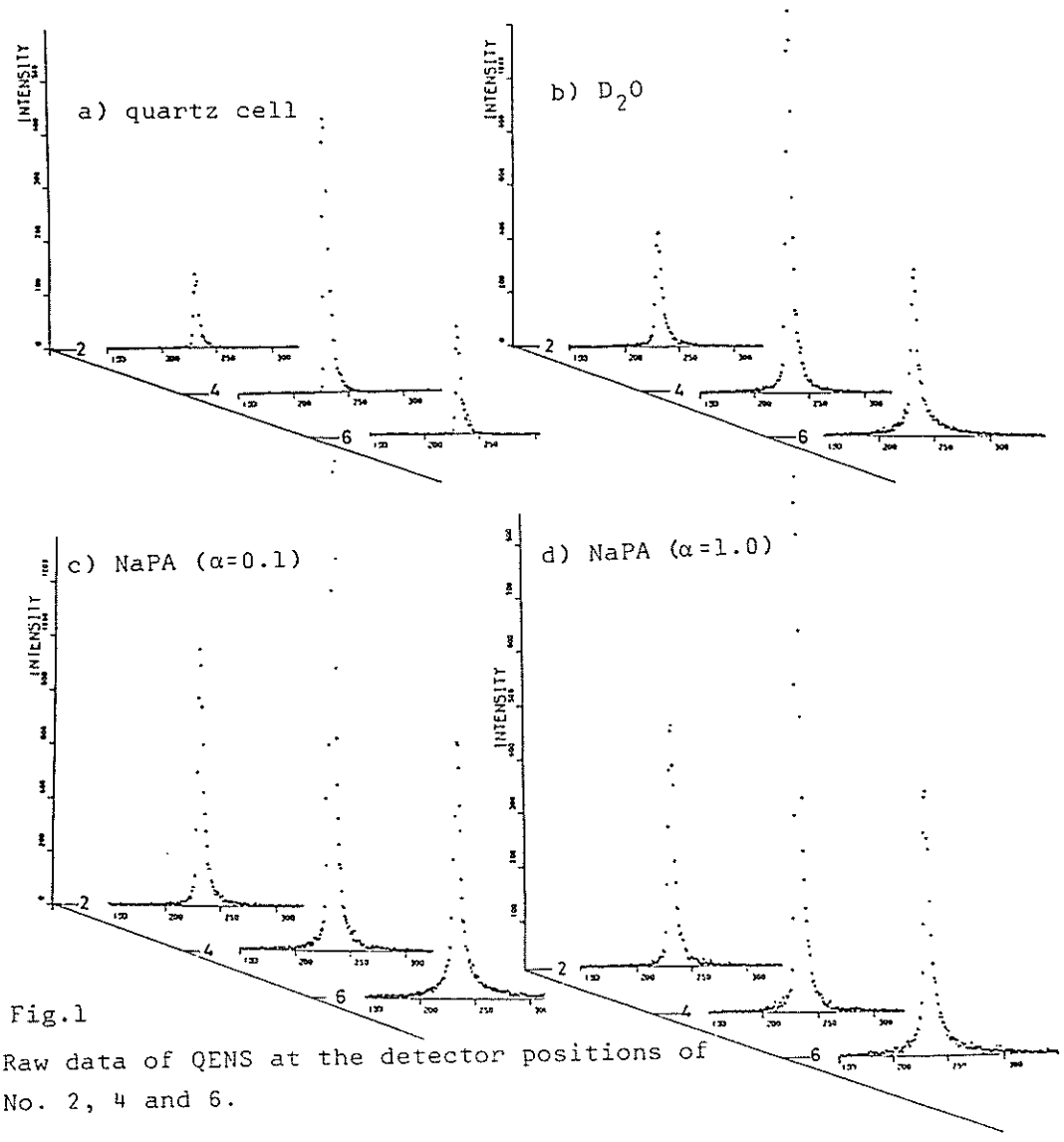

Fig.1
Raw data of QENS at the detector positions of No. 2, 4 and 6.

1.0 as samples and D_2O as a solvent. The concentrations of NaPA'S with α=0.1 and 1.0 were 0.1 and 0.12g/cm^3, respectively. We used a quartz cell of coaxial cylinder in stead of a standard aluminum cell to avoid ionic contaminations from the cell. The measurements of QENS from NaPA'S in D_2O were carried out at room temperatures using the LAM spectrometer at KEK. Fig.1 shows the raw scattering data at the detector positions of No.2, 4 and 6, and Fig.2 shows, as an example, the spectra corrected with the difference of intensity at the detector position of No.2. These data indicate that the background scattering from the quartz cell and D_2O considerably contribute to the spectra of the sample solutions. Fig.3 shows, as an example, the spectra of NaPA'S with α=0.1 and 1.0 at the detector position of No.2 after subtracting the background. This preliminary experimental result suggests that the degree of ionization may influence on the QENS spectra, in orther words, the local motions of chain. Further carefull experiments are necessary to have a definite conclusion.

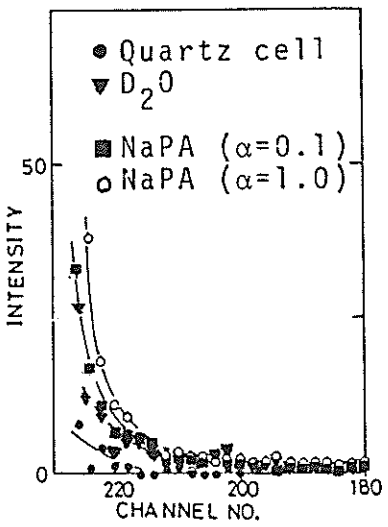

Fig.2 Corrected spectra at the detector position of No.2

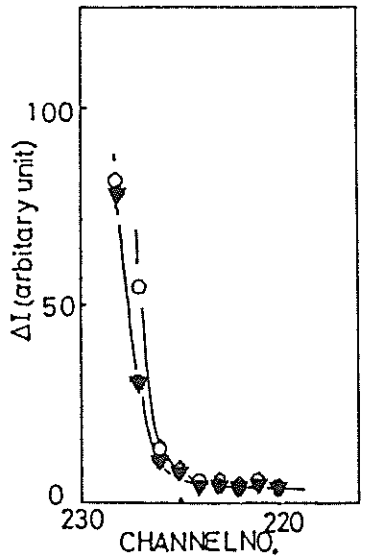

Fig.3 QENS spectra of NaPA's with α=0.1(▼) α=1.0(○)

Quasi-Elastic Neutron Scattering Study of α-Lactalbumin Solution

Yoshinobu Izumi, Yasuhiro Miyake, Shintaro Sugai,
Kunihiro Kuwajima, and Kazuhiko Inoue*

Department of Polymer Science, *Department of Nuclear Engineering,
Hokkaido University, Sapporo 060

The reversible denaturation of α-lactalbumin has been investigated experimentally from various points. The protein undergoes three state denaturations involving the native, the stable intermediate, and the fully unfolded states, on treatment with guanidine hydrochloride (Gu-HCl). The folding mechanism of the proteins has been discussed and a probable model of folding based on these experimental results has been postulated. A systematic diffraction study has been made to confirm the model of folding but it has been limited to the study on the static structures. Among the diffraction methods, neutron scattering provides a powerful technique to study the dynamical properties of protons by which neutrons are quasi-elastically scattered. It is, therefore, interesting to investigate the dynamic structures of α-lactalbumin by quasi-elastic neutron scattering. Neutron scattering measurements were carried out at eight different values of momentum transfer satisfying $0.25<Q<2.5$ ($Q=4\pi\sin\theta/\lambda$). The energy spectra for the 0, 1, 2, and 5M Gu-HCl solutions at pH=7.0 are shown in Fig. 1. The Q dependence of the FWHM for these solutions is shown in Fig. 2. From these Figures, as the concentration of Gu-HCl is decreased, the motion of the proton becomes small, which reflects the different dynamical structures of α-lactalbumin in different states.

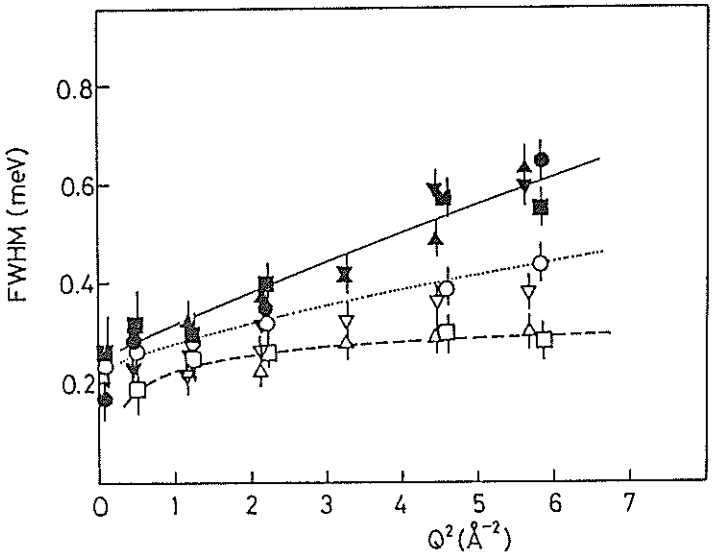

Fig. 2. The Q dependence of the FWHM for 0 (□,■), 1(△,▲), 2(▽,▼) and 5M (○,●) Gu-HCl solutions (open signs) and solvents (filled signs).

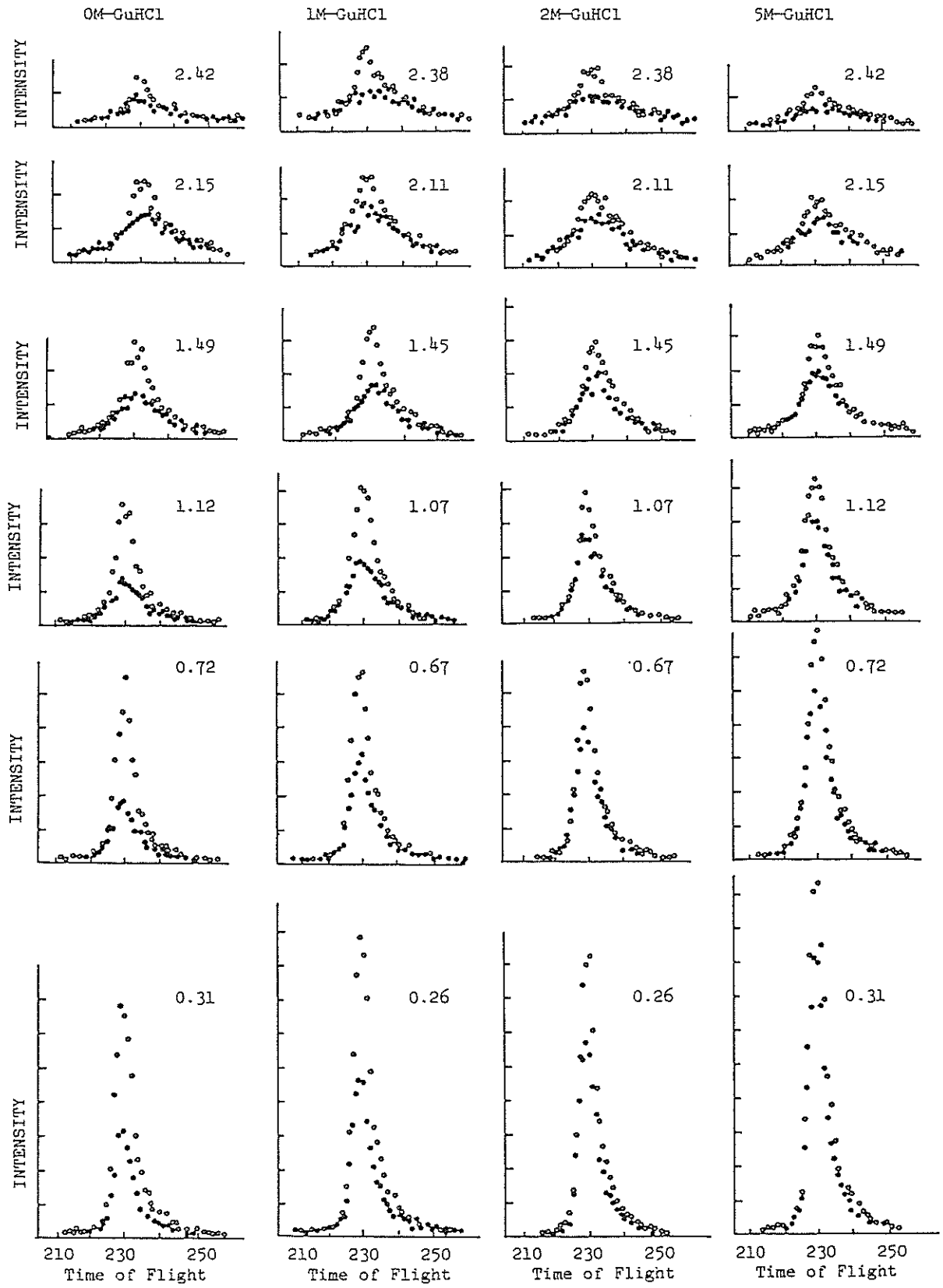

Fig. 1. The energy spectra of QENS for 0, 1, 2, and 5M Gu-HCl solutions (o) and solvents (●) of pH=7.0 at room temperature.

Study of Poly—and Oligo—ether by Neutron Quasi Elastic Scattering

Yasuhiro Miyake, Yoshinobu Izumi, Kazuhiko Inoue*, and Yoshiaki Kiyanagi*

Department of Polymer Science, *Department of Nuclear Engineering,
Hokkaido University, Sapporo 060

Polyethylene glycol (PEG) has a strange property compared with other polymers, because it has a strong intermolecular interaction[1]. Allen et al studied polypropyleneglycol (PPG) and PEG by neutron quasi elastic scattering (NQES)[2]. The results suggest that a small amount of water added to polyether may act as antiplasticizer for the strong interaction. On the other hand, glycerin was studied by NQES[3], which could be illustrated with jump diffusion and oscillatory motion[4]. But studies of liquids with a strong intermolecular force by NQES are not so many. Hence, we attempted to study ether compound over wide range from monomer to polymer by NQES using LAM as preliminary experiment. Commercial samples, which contained water of about 1%, were used and almost all measurements were done at room temperature ($22^{\circ}C$). The obtained results are shown in Figs. and Table. The results obtained from polystyrene in CS_2 are also shown. A central narrow part (mode 1) and a side wings part (mode 2) of NQES intensity are separated by semi—log plot and $S_1(Q,0)$ and $S_2(Q,0)$ are peak intensities of each mode at Q (absolute value of scattering vector) and FWHM—1 is full width at half maximum of mode 1. It is evident from Figs. that experimental errors are found out as yet and NQES of each mode 1 has almost same profile in these compounds and the profiles of NQES in mode 1 of PPG 2000 at $47.5^{\circ}K$ and $175^{\circ}K$ are resemble to the one of vanadium. The dependence of FWHM—1 of PPG on Q is same to Allen et al's value[2]. Debye—waller factors are also small. Therefore, it is necessary to study ether compounds such as PPG, PEG, and oligo—ethers by NQES at high temperature or in solution where intermolecular interaction breaks out. Future investigation will be needed.

1) F.E.Baley, Jr., and R.W.Callard, J. Appl. Polym. Sci., 1, 56(1959).
2) G.Allen, J.S.Higgins, C.J.Wright, J. Chem. Soc. Farad. Trans., 2, 70, 348(1974). G.Allen, J.S.Higgins, Macromolecules, 10, 1006(1977). A. Maconnachie, P.Vasudevan, and G.Allen, Polymer, 19, 33(1978).

3) M.Birr, Z. Physik, 238, 221(1970).
4) T.Springer, Springer Tracts in Modern Phys. 64(1972).

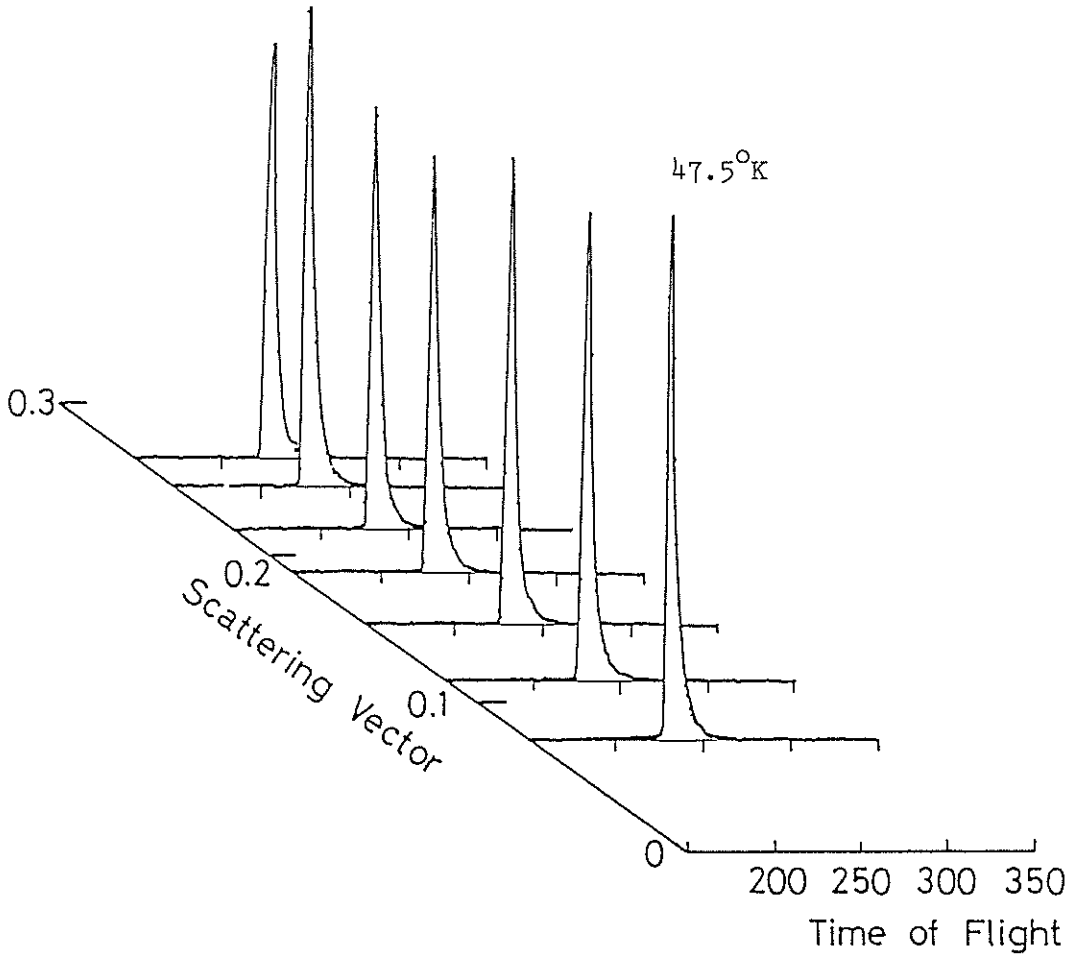

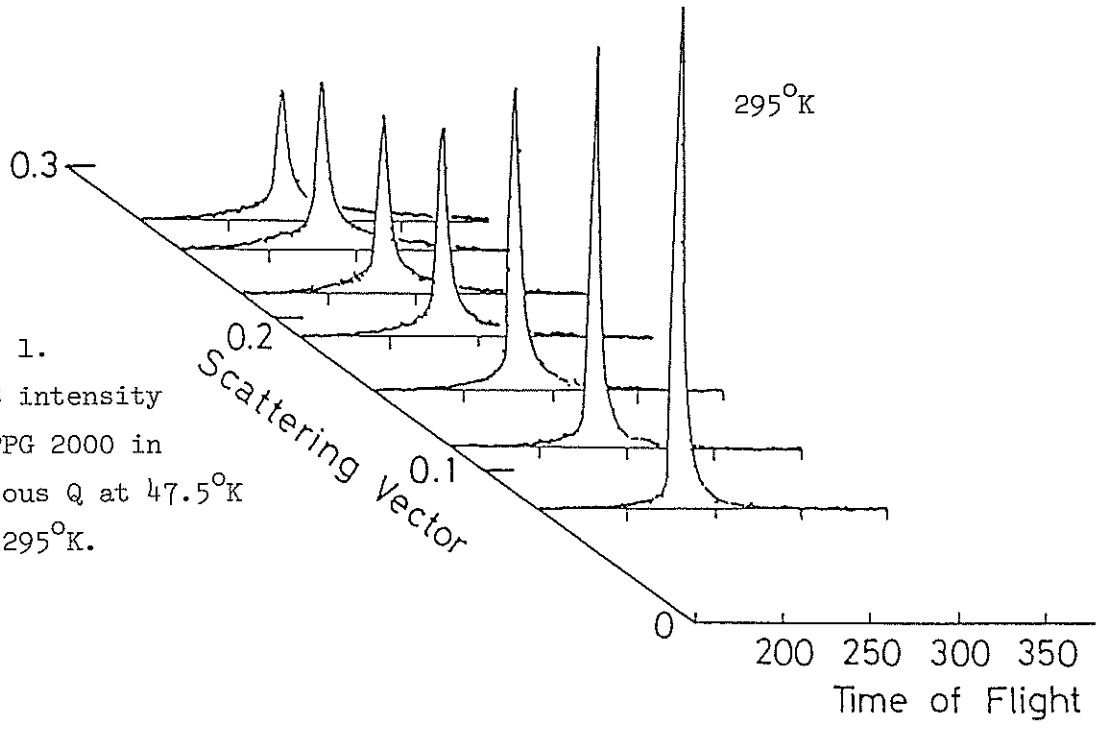

Fig. 1.
NQES intensity of PPG 2000 in various Q at 47.5°K and 295°K.

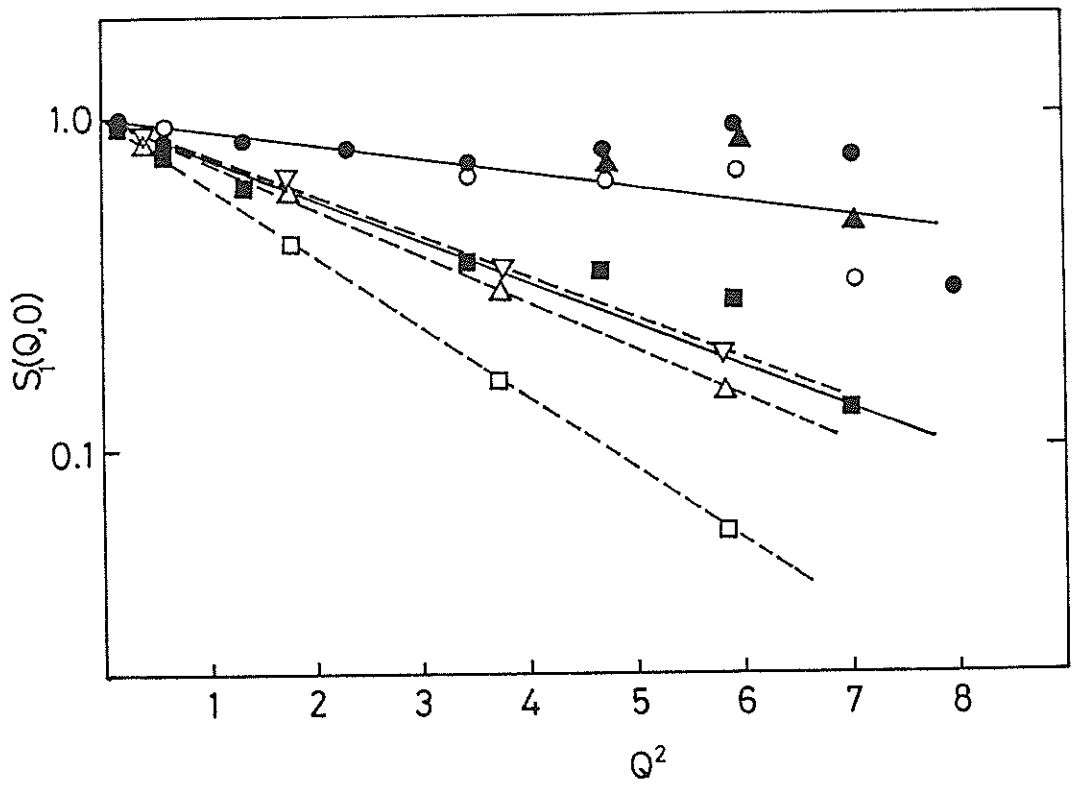

Fig. 2. Debye–Waller factors of various systems: PPG 2000; ■ 295°K, ○ 175°K, ▲ 47.5°K. Polystyrene in CS_2: □ MW=600, △ 17500, ▽ 110000, ● Vanadium.

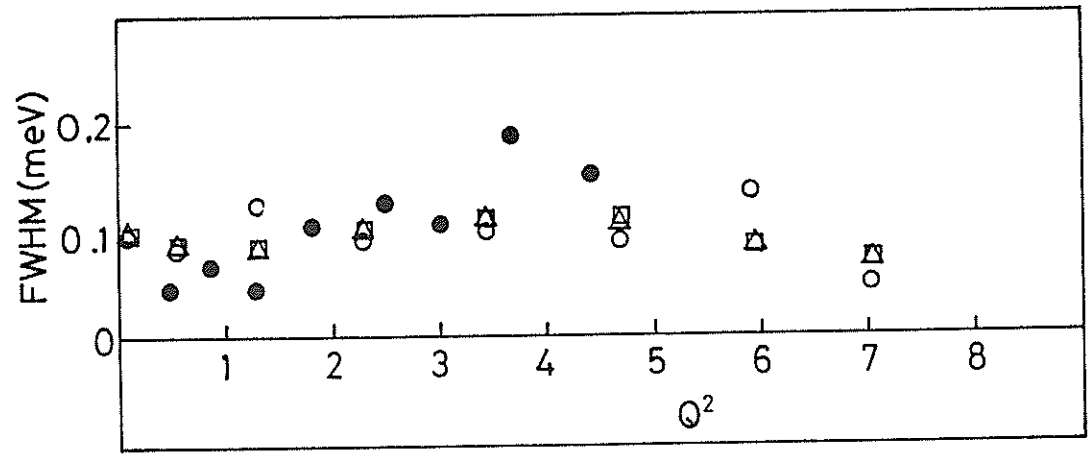

Fig. 3. Dependence of FWHM on Q^2 at 295°K:
○ PPG 2000, △ Propyrene glycol, □ Ethylene glycol,
● Allen et al[2].

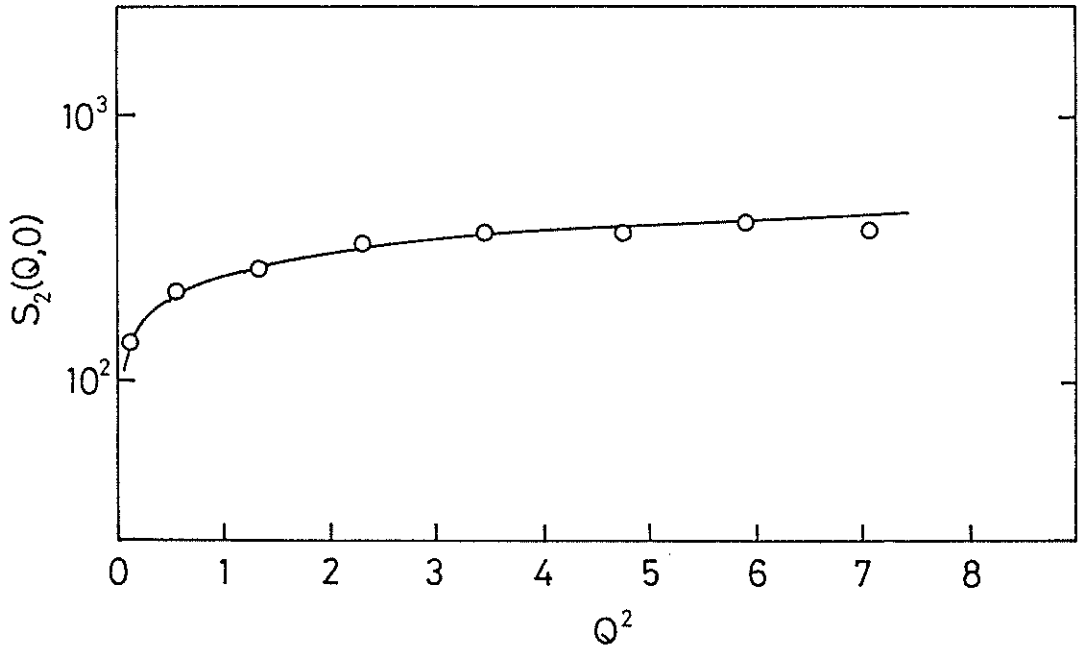

Fig. 4. Dependence of $S_2(Q,0)$ of ethylenglycol on Q^2:
$S_2(Q,0) = 251Q^{0.54}$.

Table

	$\langle u^2 \rangle$, A^2	D_2 (s^{-1})
Ethyleneglycol	0.13	0.66×10^{12}
PEG 400	0.13	0.63
Propyleneglycol	0.13	0.68
Tripropyleneglycol	0.14	0.63
PPG 1000	0.15	0.59
PPG 2000	0.15	0.56

$\langle u^2 \rangle$:mean square amplitude of the oscillating proton.

D_2 :FWHM $\simeq 2\pi D_2$

Study of the Crystal Field in CeBi

Masahumi Kohgi, Takashi Suzuki, Yoshikazu Ishikawa
and Tadao Kasuya

Physics Department, Tohoku University, Sendai 980

Cerium monopnictides exhibit highly unusual magnetic behaviours, namely, anomalously small crystal fields[1], very strong magnetic anistropies[2] and complex magnetic phase diagrams.[3] The last ones are observed for CeBi and CeSb in which the crystal field splitting is especially small. Recently, Takegahara et al.[4] has proposed that the anomalies are well explained by taking account of the mixing between the 4f states and the valence bands. In order to make sure the situation from the experimental side, we are performing the detailed study of the temperature and magnetic field dependence of the crystal field splitting in CeBi and CeSb by means of neutron scattering. In this report some preliminary results for CeBi are shown.

The experiments were carried out with the Large Analyzer Mirror Spectrometer(LAM) at KENS which is the analyzer type (Inverted geometry type) TOF spectrometer using the cold neutrons. The energy of the scattered neutrons was fixed at 4.59 meV by 70 pyrolytic graphite chips which constitute a pseudo-spherical mirror about 9 by 13 cm, per one scattering angle. The polycrystalline CeBi sample was sealed in a cylindrical aluminum container 14mm in diameter and 100 mm long.

In Fig. 1-(a), -(b) and -(c) are shown typical energy spectra of neutrons scattered from CeBi at 300, 40 and 21K, respectively. The qualitative feature of the spectra is essentially the same as the previously reported data by Furrer et al.[5] and Herr et al.[6]. However, our data are distinguished from them by some points as follows. At the paramagnetic state(300 K, 40 K), the spectra other than the incoherent elastic peak are like quasi elastic scattering. However, there can be clearly seen shoulders below 1 meV, and their positions seem to be temperature dependent (0.5 meV at 300 K and 0.7 meV at 40 K). This point is not clear in the data of Furrer et al.[5]. At 21 K, on the other hand, there is a well-resolved inelastic peak at about

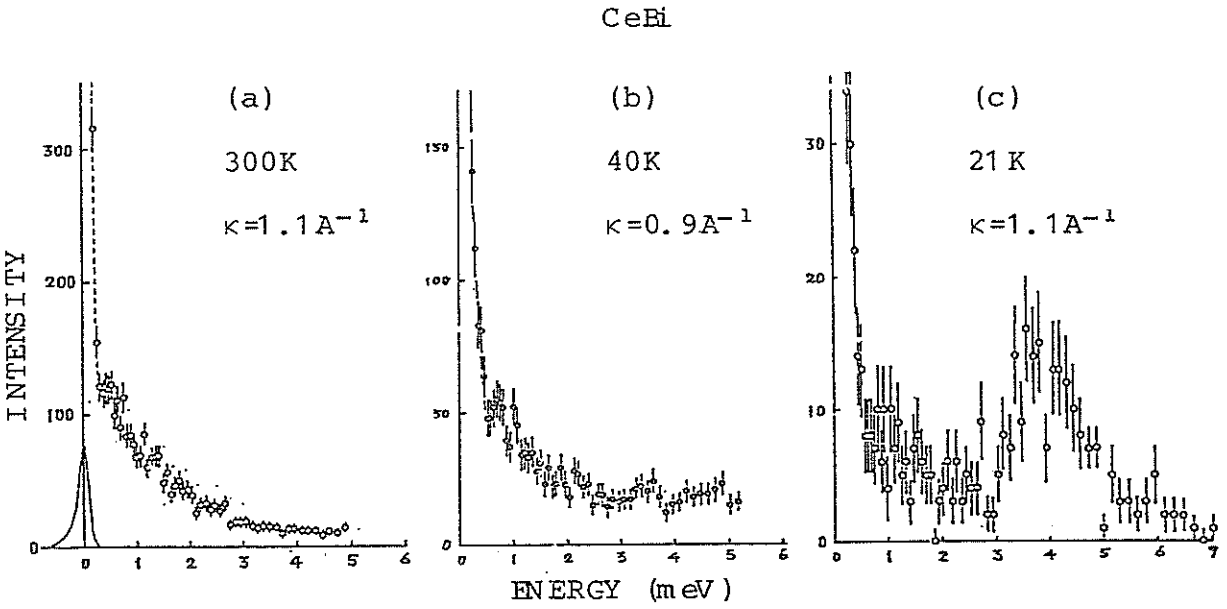

Fig.1 Energy spectra of neutrons scattered from CeBi at (a) 300K, (b) 40K, (c) 21K. Solid curve in (a) shows the resolution of LAM spectrometer.

3.7 meV, though the data of Herr et al.[6] shows only a shoulder at nearly the same energy. It is considered that these new facts are owing to the higher resolution of the LAM spectrometer. The further experiments will be soon done.

references

1) R.J.Birgeneau, E.Bucher, J.P.Maita, L.Passell and K.C.Turberfield: Phys. Rev. B8(1973) 5345.

2) P.Burlet, J.Rossat-Mignod, H.Bartolin and O.Vogt: J.de Phys.40(1979) 47.

3) J.Rossat-Mignod, P.Burlet, J.Villain, H.Bartolin, W.Toheng-Si, D.Florence and O.Vogt: Phys. Rev. B16(1977) 440.

4) K.Takegahara, H.Takahashi, A.Yanase and T.Kasuya: Solid State Commun. 39(1981) 857.

5) A.Furrer, W.Bührer, H.Heer, W.Hälg, J.Benes and O.Vogt: Neutron Inelastic Scattering(Vienna:IAEA) p563.

6) H.Herr, A.Furrer, W.Hälg and O.Vogt: J.Phys.C:Solid State Phys. 12(1979) 5207.

Energy-focusing Downscattering Spectrometer and Low Energy Molecular Spectra

Kazuhiko Inoue, Yoshiaki Kiyanagi, Hirokatsu Iwasa and Kiyoshi Jinguji

Department of Nuclear Engineering, Hokkaido University, Sapporo 060

We are now developing an energy-focusing type, downscattering time-of-flight spectrometer. The KENS neutron source is an efficient pulsed source facility in which intense pulsed neutrons are emanated over a relatively wide moderator surface and a high signal-to-noise ratio is expected. The spectrometer consists of a large area crystal analyser mirror and a beryllium filter. 144 pyrolytic graphite crystals are arranged on an optimally curved array so that energy-focusing is achieved. In order to optimize the efficiency of filtering characteristics, the beryllium block has been given a special shape. Fig. 1 shows the instrumental set-up.

The time-of-flight spectra of vanadium in the cases with and without the beryllium filter are shown in Figs. 2 and 3, which indicate the effectiveness of the filter and a measure of the energy resolution. The spectra are represented in Fig. 4 for NH_4Cl, Fig. 5 for the uracil and Fig. 6 for the thymine respectively. In the case of NH_4Cl, the typical inelastic peak due to the rotation of ammonium ions was observed. Broad inelastic peaks due to the hydrogen bonds in the nucleic acid bases were also observed. In these

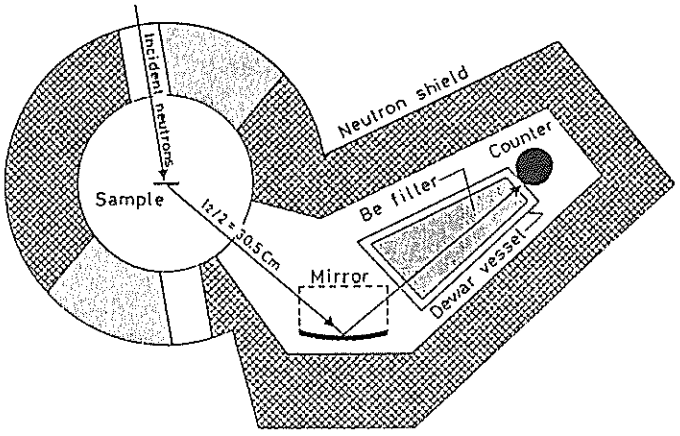

Fig. 1 Energy-focusing downscattering spectrometer. Beryllium filter is cooled by liquid nitrogen.

preliminary measurements the filter was not yet cooled, but the data indicated the intrinsic usefulness of the new spectrometer. A cooling facility for the filter is being tested which is expected to increase the efficiency of the spectrometer threefold.

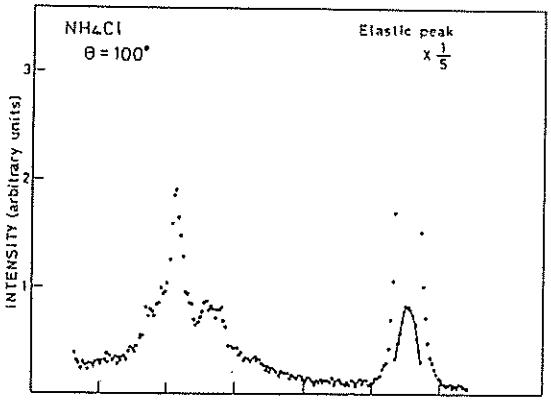

Fig. 4 Time-of-flight downscattering spectrum from NH_4Cl.

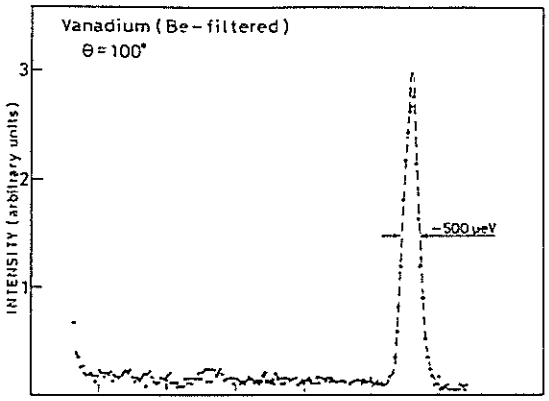

Fig. 2 Typical elastic line from vanadium with the filter.

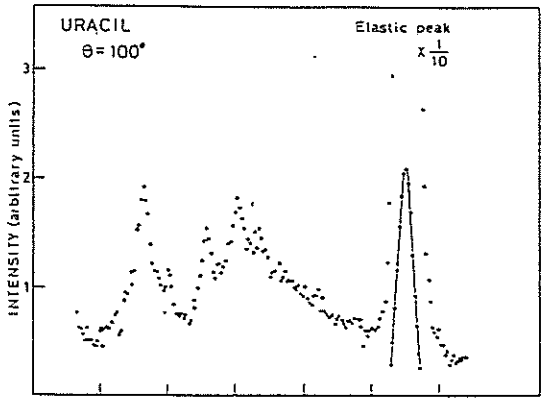

Fig. 5 Time-of-flight downscattering spectrum from the uracil.

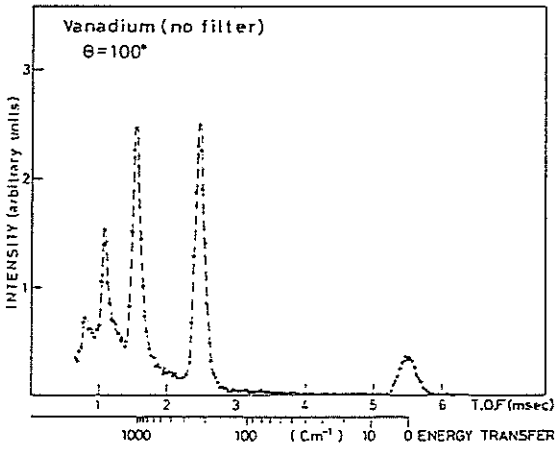

Fig. 3 Higher order lines from vanadium without filter.

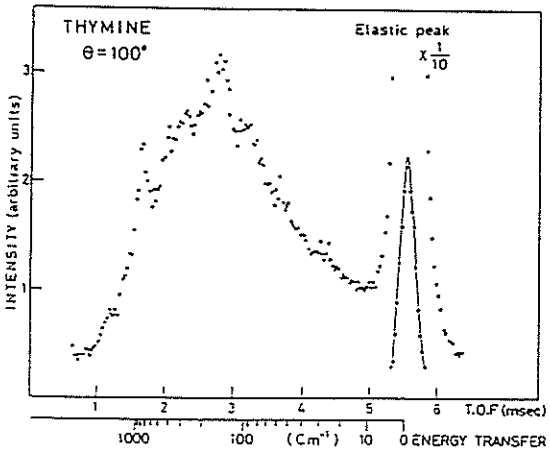

Fig. 6 Time-of-flight downscattering spectrum from the thymine.

Low frequency vibrations in oriented poly(vinyl alcohol) film

Keisuke Kaji, Hiroshi Urakawa, Ryozo Kitamaru,
Kazuhiko Inoue* and Yoshiaki Kiyanagi*

Institute for Chemical Research, Kyoto University, Uji, Kyoto-Fu 611 and *Department of Nuclear Engineering, Faculty of Engineering, Hokkaido University, Sapporo 060

The vibrational modes in poly(vinyl alcohol) have been measured mainly by infrared spectroscopy. The neutron inelastic scattering spectra are not so far reported. In this paper we report the spectra obtained by neutron incoherent inelastic scattering. The sample film was uniaxially drawn four times at 90°C and subsequently heat-treated at 160°C for a few minutes in silicone oil bath. The measurements were carried out for the Q-vectors parallel and perpendicular to the chain using the KENS-LAM-D spectrometer. The spectra obtained are shown in Fig. 1 and 2. The observed new bands are 470 and 560 cm^{-1} for the Q-vector parallel to the chain axis, and a broad band distributing from 10 to 200 cm^{-1} for the Q-vector perpendicular to the chain axis. The latter broad band may be due to the bending mode of the OH side groups, which is very much affected by intermolecular hydrogen bonds. The detailed study will be made using deuterated poly(vinyl alcohol) samples.

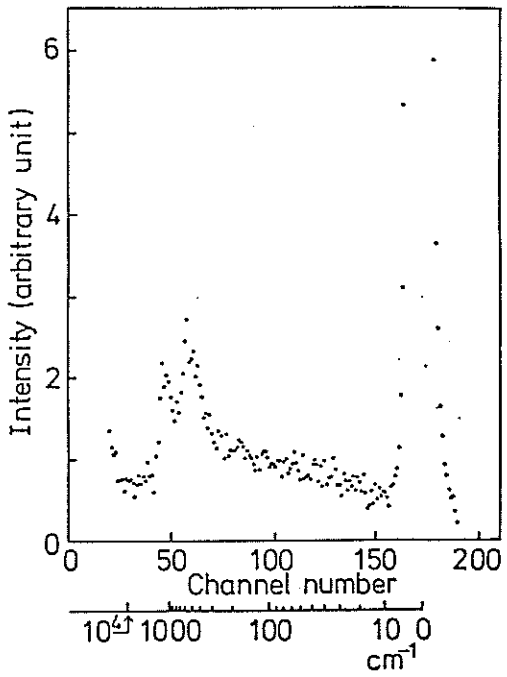

Fig. 1 TOF spectrum of poly(vinyl alcohol) film at scattering angle of 60°. The direction of momentum transfer Q of neutrons is parallel to the chain axis.

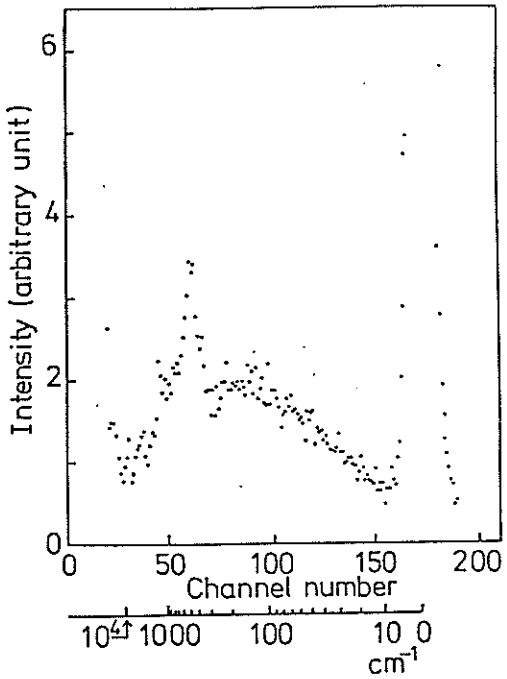

Fig. 2 TOF spectrum of poly(vinyl alcohol) film at scattering angle of 60°. The direction of momentum transfer Q of neutrons is perpendicular to the chain axis.

Low frequency vibrations in oriented poly(isobutylene oxide) film

Keisuke Kaji, Hiroshi Urakawa, Ryozo Kitamaru,
Kazuhiko Inoue* and Yoshiaki Kiyanagi*

Institute for Chemical Research, Kyoto University, Uji, Kyoto-Fu 611 and *Department of Nuclear Engineering, Faculty of Engineering, Hokkaido University, Sapporo 060

In the preceding report the bending mode of the methyl groups in isotactic polypropylene was detected by neutron incoherent inelastic scattering. This mode appeared at about 50 cm^{-1}. If the number of methyl side groups in the monomeric unit increases, it is expected that the band of this mode becomes stronger. For this purpose the similar measurements have been carried out for poly(isobutylene oxide) having two methyl groups in the monomeric unit $-C(CH_3)_2-CH_2-O-$. The sample was uniaxially oriented film and the spectrometer used was KENS-LAM-D. The observed spectra for Q-vectors parallel and perpendicular to the chain axis are shown in Fig. 1 and 2, respectively. When the Q-vector is parallel to the chain axis (Fig. 1), stronger peak is seen at 240 cm^{-1}, which is due to the methyl torsion. A peak at 55 cm^{-1} in Fig. 2 can be assigned to the bending mode of methyl groups. As expected, this peak is stronger than that of polypropylene. The somewhat higher frequency is probably due to the effect of the neighboring methyl group bonded to the same carbon. A shoulder is seen at about 35 cm^{-1}, but this mode is not assigned.

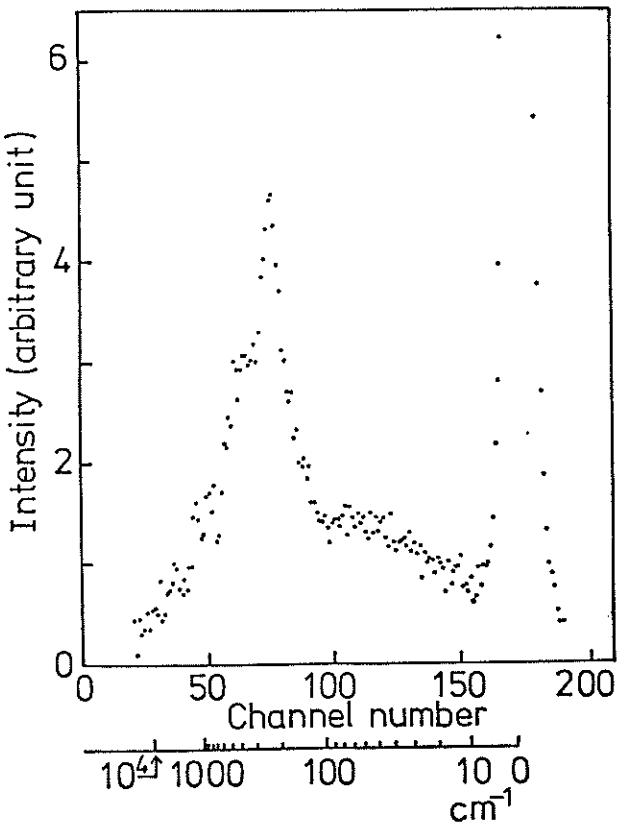

Fig. 1 TOF spectrum of poly(isobutylene oxide) film at scattering angle of 60°. The direction of momentum transfer Q of neutrons is parallel to the chain axis.

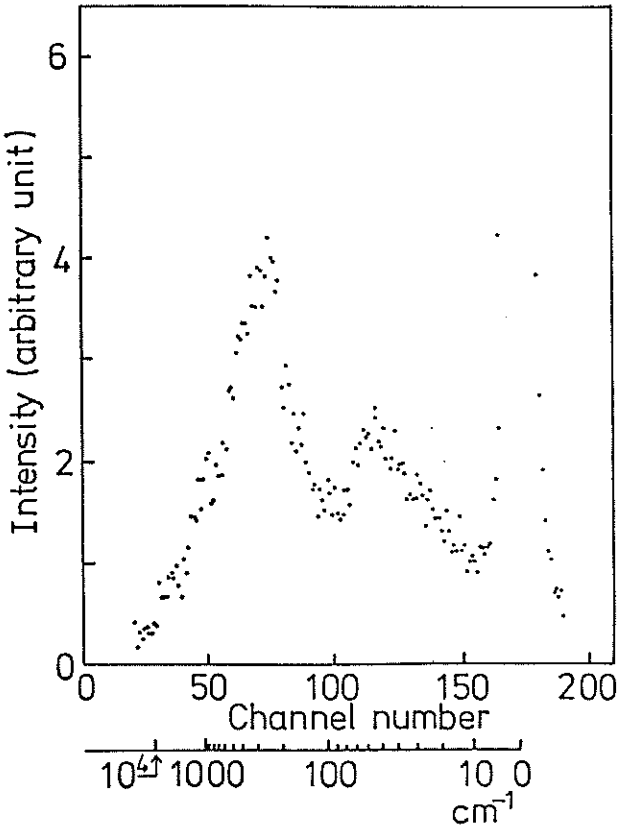

Fig. 2 TOF spectrum of poly(isobutylene oxide) film at scattering angle of 60°. The direction of momentum transfer Q of neutrons is perpendicular to the chain axis.

Low frequency vibrations in oriented isotactic polypropylene film

Keisuke Kaji, Hiroshi Urakawa, Ryozo Kitamaru
Kazuhiko Inoue* and Yoshiaki Kiyanagi*

Institute for Chemical Research, Kyoto University, Uji, Kyoto-Fu 611 and *Department of Nuclear Engineering, Faculty of Engineering, Hokkaido University, Sapporo 060

The vibrational spectra of isotactic polypropylene have been extensively studied by infrared, Raman and neutron inelastic scattering techniques. Most of the previous reports are limited to vibrational modes above 100 cm^{-1}. In several solid polymers with side groups, however, broad Raman bands were observed below 100 cm^{-1} and attributed to the librational motions of the side groups.[1] A simple model was proposed that the pendant side groups, as a whole, oscillating independent of the chain phonons has three normal modes of stretching, torsion and bending. According to this model, the torsional and bending modes are expected to be observed intensely by neutron inelastic scattering. Polypropylene has methyl side groups and the methyl torsion was observed at 240 cm^{-1} by neutron incoherent inelastic scattering.[2] The bending mode of the methyl group of polypropylene, however, is not reported. The purpose of this study is to observe such a bending mode as well as the torsional mode. In order to know the vibrational direction the uniaxially oriented polypropylene film was used and the measurements were carried out using KENS-LAM-D for two sample orientations or Q-vectors parallel and perpendicular to the chain axis. Fig. 1 and 2 show the time-

of-flight spectra of neutron incoherent inelastic scattering for the Q-vectors parallel and perpendicular to the chain axis, respectively. In Fig. 1, a strong peak at 240 cm^{-1} due to the methyl torsion is seen. The peak in Fig. 1 is stronger than that in Fig. 2. The peak at about 50 cm^{-1} in Fig. 2 may be assigned to the bending mode of the methyl side groups. This mode is perpendicular to the chain axis since it disappears in Fig. 1. It means that the methyl side groups oscillate perpendicularly to the chain axis. In the spectrum of Fig. 1, the fine structure is also seen;90, 250, 450, and 1250 cm^{-1} correspond to the frequency modes observed in Raman and infrared spectra.

References

1. J.J.Kim, J.McLeish, A.J.Hyde and R.T.Bailey, Chem. Phys. Let. 22, 503 (1973).
2. C.J.Wright,"Torsion Vibrations in Polymers" in "Structural Studies of Macromolecules by Spectroscopic Methods" edited by K.J.Ivin, Wiley-Interscience Pub. 1976.

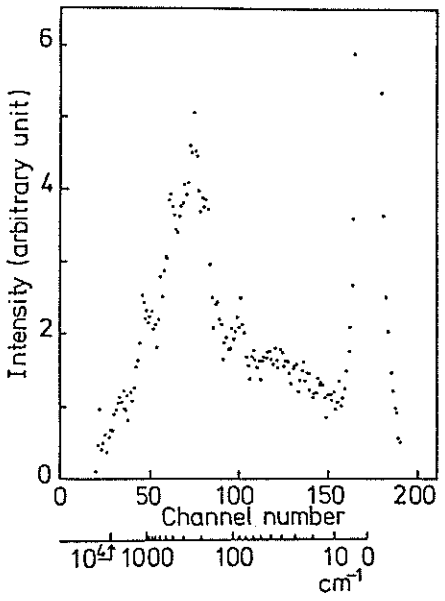

Fig. 1 TOF spectrum of polypropylene film at scattering angle of 60°. The direction of momentum transfer Q of neutrons is parallel to the chain axis.

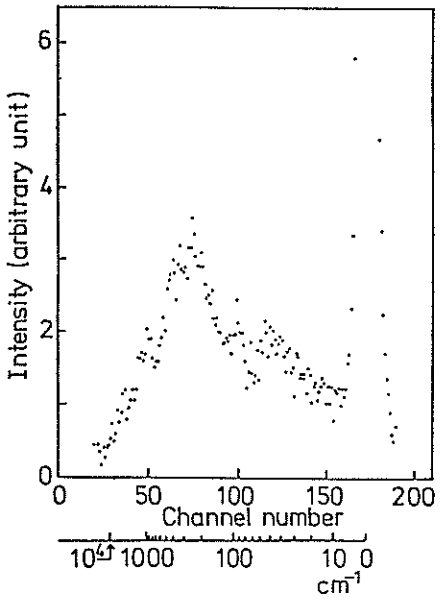

Fig. 2 TOF spectrum of polypropylene film at scattering angle of 60°. The direction of momentum transfer Q of neutrons is perpendicular to the chain axis.

On Neutron Inelastic Scattering of Melanin

Yasuhiro Miyake, Yoshinobu Izumi, Kazuhiko Inoue*, and Yoshiaki Kiyanagi*

Department of Polymer Science, *Department of Nuclear Engineering,
Hokkaido University, Sapporo 060

Melanin is one of biomolecules widely distributed in animal and vegetal kingdoms and has been studied by many workers since about 80 years and then various properties are found out[1]. A property that Melanin is black for sound wave has also been known[2]. Various models for the structure are presented on the basis of the results of physical and chemical measurements. One of them is a plate model which is constituted with 4 or 8 ring molecules such as indole 5, 6 quinone, according to the result of X-ray diffraction using amorphous Melanin[3]. However, the detailed structure of Melanin is not so clear as yet, because Melanin does not crystallize. Furthermore, Melanin is contained in Melanoma (i.e., cancer) and a method of treatment has been investigated by the neutron irradiation on the cancer adhering boron compounds[4]. Then we attempted to study Melanin by neutron scattering to know effects of neutron irradiation. We measured neutron inelastic scattering intensities with DIX using DOPA Melanin and sepia Melanin which was separated from ink sac of cuttlefish, since Melanin has a stacking form of ring molecules and has not a characteristic adsorption band in IR as well as graphite except 1430-1670 cm^{-1}. The obtained results are shown in Figures. It is found out from Figures that inelastic scatterings are seen apparently over 10-650 cm^{-1} and both Melanins have different scattering profiles. Future investigations will be needed using other Melanins like B-16 and Harding-Passey Melanoma Melanins and constituents of Melanin.

1) R.A.Nicolaus, Melanin, 1968, Herman, Paris.
2) R.Kono, H.Yoshizaki, Y.Miyake, Y.Izumi, and J.E.McGinnes, J. Chem. Phys., 75, 4654(1981).
3) C.Shiu-Shin, Thesis, Houston Univ. 1977.
4) Y.Mishima, ed., Kyoto University Research Reactor Ins. Tec. Rep., 195(1980).

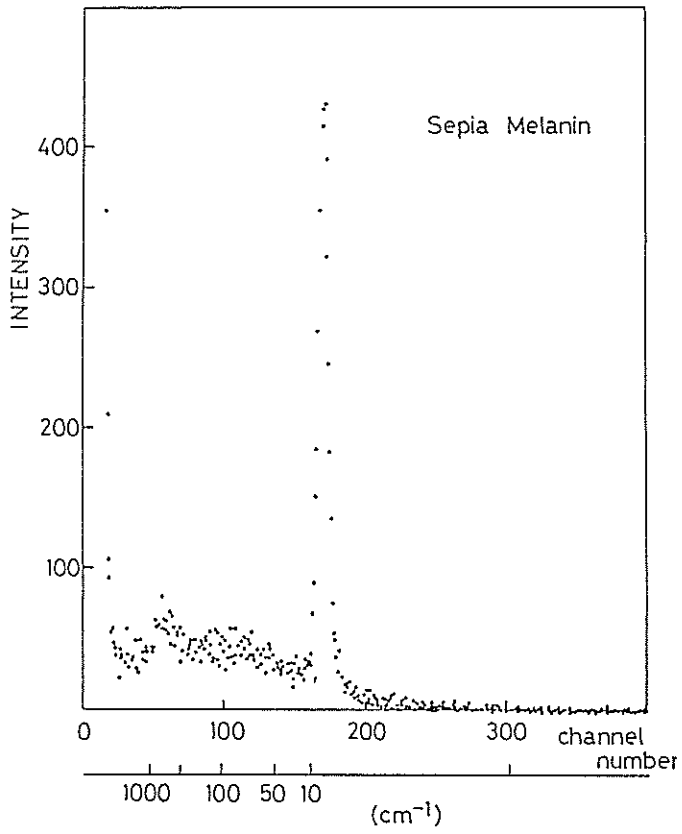
Sepia Melanin
INTENSITY
400
300
200
100
0
100
200
300
channel number
1000
100
50
10
(cm⁻¹)

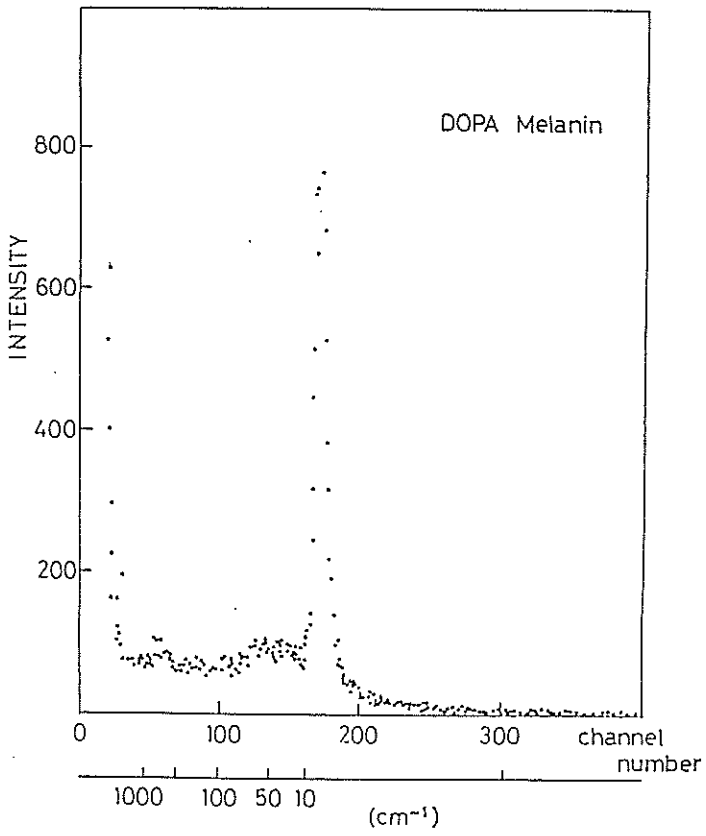
DOPA Melanin
INTENSITY
800
600
400
200
0
100
200
300
channel number
1000
100
50
10
(cm⁻¹)

Small Angle Scattering of Fine Ceramic SiC Powder Measured with White Pulsed Neutron

M. Furusaka and Y. Ishikawa

Physics Department, Tohoku University, Sendai, 980, Japan

The fine ceramic powder of SiC with a definite dimension was measured with the small angle neutron scattering instrument(SAN) installed at KEK in order to examine the quantitative reliability of the spectrometer and to establish the method for corrections. The Q(momentum transfers dependence of the intensity of small angle scattering from spherical particles I(Q) is known to obey approximately the Porod rule in the high Q region. As the converging Soller slit was employed for the correction of the incident beam, the instrument satisfies always the point focussing condition, independent of the sample size. Therefore in the Porod region ($QR >> 1$) the scattering intensity from spherical particles with average radius $\bar{R}$ is approximately given by

$$I(Q) = 8\pi^2\rho^2\bar{R}^2 / Q^4 \qquad (1)$$

, where $Q=4\pi \sin\theta / \lambda$ and ρ is the average scattering length density.

SiC powders used in the measurement was supplied by Prof. Osamura, Kyoto University. The mean radius of the powder $\bar{R}$ was determined by small angle x-ray scattering intensity from the sample I measured with the two dimensional position sensitive detector (2D-PSD) at 5 m is corrected for the incident neutron spectrum, as well as the detector efficiency at each element of 2D-PSD and is plotted against Q on the logalithmic scale in the lower part of Fig. 1. The figure show clearly that the Q^{-4} relation holds only for a high Q region (≥ 0.02 $\mathring{A}^{-1}$) and that the distinct deviation from this relation occurs in the lower Q region.

The deviation was found to be mainly of the instrumental origin ; the effect of the beam stopper. Namely some detector elements 10 x 7 mm^2 in size around the center of 2D-PSD are half covered by the beam stopper 42 x 42 mm^2 in size, resulting in reducing the counting efficiency of these elements. Since, for the lowest angle detector elements, the background level

exceeds the incoherent scattering from water, the accurate determination of the detector efficiency of these elements from the data of water become very difficult, thus introducing a large error for the results from these elements. The situation is clearly seen in Fig. 2 where the scattering intensity measured by a central 1D-PSD (our 2D-PSD consists of the arrays of 43 1D-PSD) is plotted against Q for different neutron wave lengths. The numbers in Fig. 2 correspond to different wave lengths. The intensity at the lowest angle is significantly reduced compared with other points even if the data are corrected for the detector efficiency by water. The detector efficiency of these elements was found to be estimated more accu-

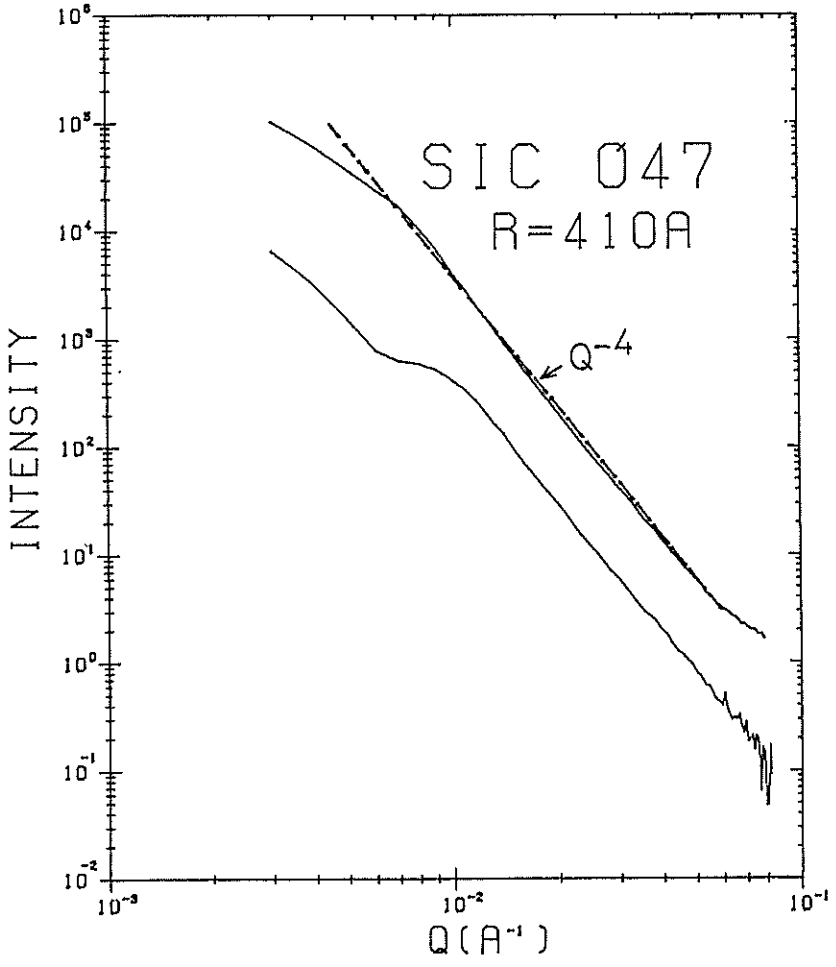

Fig. 1. The lower curve is the scattering function I(Q) obtained without correction for the beam stopper effect. The upper curve is I(Q) corrected for this effect. A broken line represents a $I(Q) = aQ^{-4}$ relation.

rately from Fig. 2 so that the data from these elements coincides with those from other elements. The final I-Q curve thus determined is displayed in the upper part of Fig. 1 which show clearly that the Q^{-4} relation holds now over a large Q region, down to $6.5 \times 10^{-3} A^{-1}$. The deviation of the experimental data from this relation for smaller Q values is at least partly due to the resolution effect. The correction for it can also be done from the wave length dependence of the I-Q curve which is now in progress. The extention of the experimental data to higher Q region than $0.1\ A^{-1}$ using the fixed counter data is also in progress. Therfore our SAN spectrometer can now provide an accurate scattering data over a very wide range of momentum transfers which cannot be performed by a conventional single wave length small angle neutron scattering instrument. Note that our machine needs not make any resolution correction for $Q \geq 1 \times 10^{-1}$ A though we employs a big sample 1.6 x 3.5 cm^2 in size.

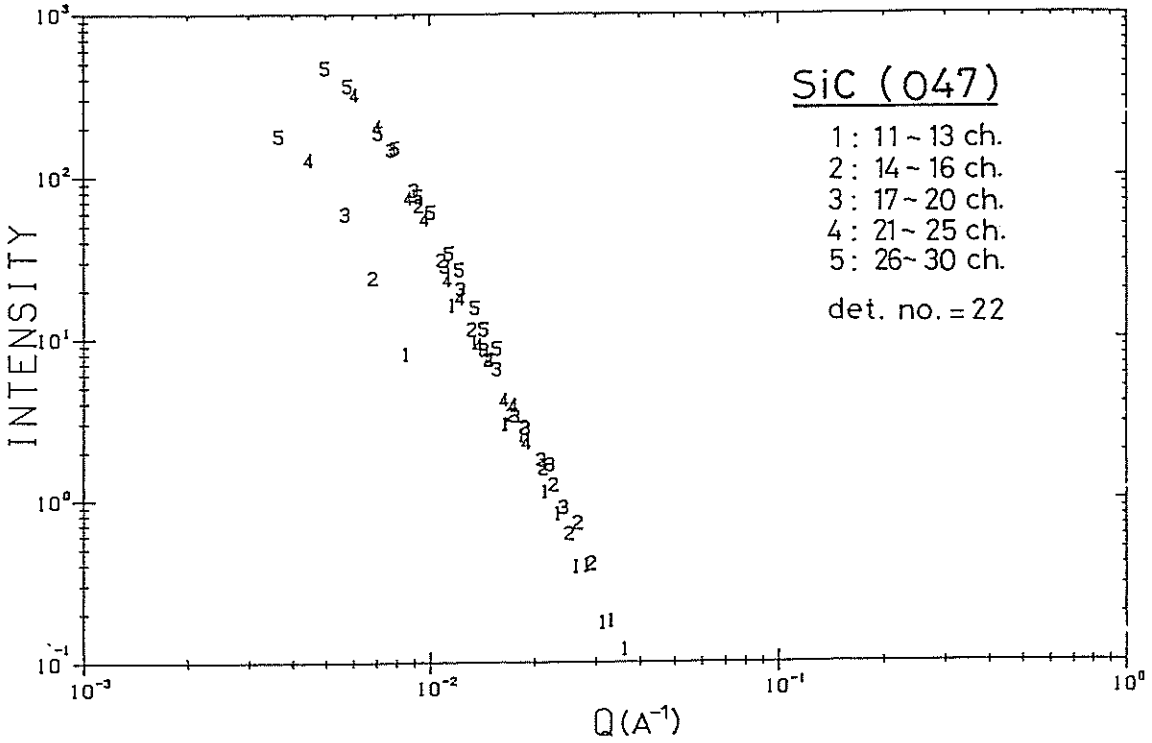

Fig. 2. Raw data from the central 1D-PSD plotted separately for different wave lengths. Numbers corresponds to time channels indicated in the figure.

Studies of Helical Spin Structure of MnSi by KENS Small Angle Neutron Scattering Instrument (SAN)

Yoshikazu Ishikawa, Masatoshi Arai, Michihiro Furusaka and Nobuo Niimura+

Physics Department and +Laboratory of Nuclear Science, Tohoku University Sendai 980

The helical spin structure of MnSi has been studied with KENS - small angle neutron scattering instrument SAN by using a large single crystal. One of the aim of the present study was to examine the accuracy and potential of this machine and another was to sutdy the anomalous critical behaviors at the Néel temperature. The SAN is the unique TOF type small angle neutron scattering instrument which employs the pulsed white incident with wave lengths ranging between 3 $\mathring{A}$ amd 11 $\mathring{A}$. Therefore the satellite Bragg reflections of MnSi, ($\zeta,\zeta,\zeta,$) with the propagation vector q_c= 0.035 $\mathring{A}^{-1}$ were detected at many different detector positions for the different incident neutron wave lengths. Two dimensional displays of the Bragg reflections at four different temperatures are shown in Fig. 1(a)-(d). The propagation vector q_c and the intensity I as well as the line width $\Delta q/q_c$ of the satellites at 13 K were estimated for the different wave lengths λ with a resolution of $\Delta\lambda/\lambda$ = 0.1 and are plotted against either λ or $1/\lambda^2$ in Fig. 2. The uppermost figure shows that the wave vector of the satellites can be determined to be q_c = 0.0345 $\pm$ 0.005 $\mathring{A}^{-1}$ at 13 K in good agreement with the value obtained at ILL[1]. The result provides an evidence that the accuracy of determination of the positions in the two dimensional position sensitive detector (2D - PSD) is satisfactory. The open circles in the middle figure are the scattering intensity obtained for the crystal oriented with the (110) reciprocal lallice plane parallel to the 2D-PSD. This is the configuration where the four satellites ($\zeta,\zeta,\zeta,$) in the (110) plane are detected with equal intnsity. The closed circle is the intensity for the case where the satellite satisfies the Bragg condition. The decrease of the intensity with increasing λ in the latter case is, therefore, due to the extinction

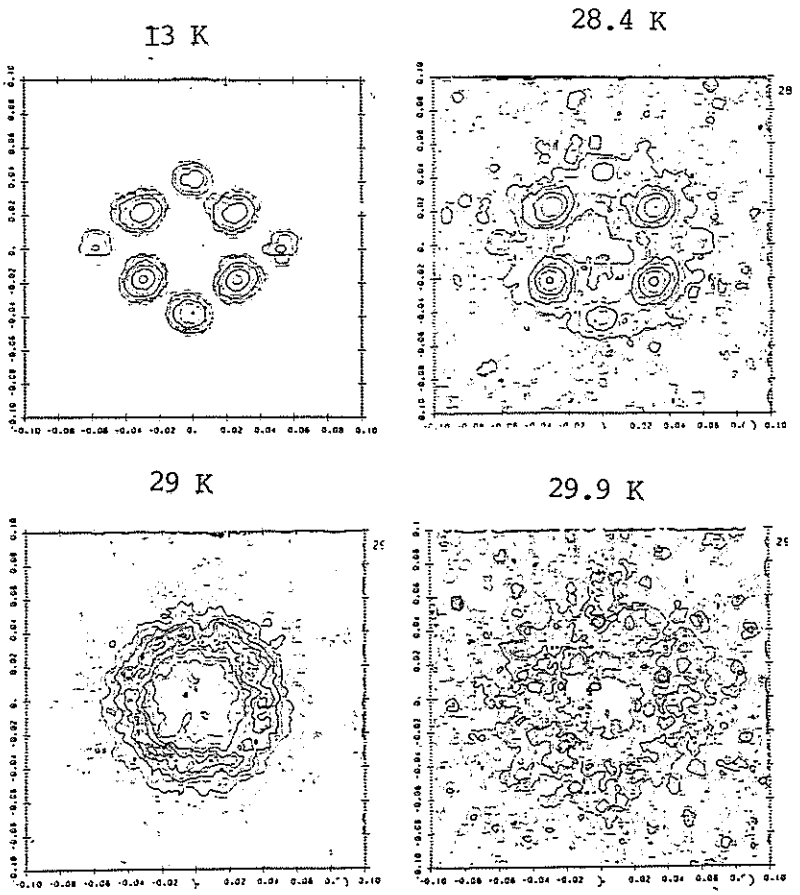

Fig. 1. Two dimensional displays of satellites of MnSi in the 110 reciprocal plane at various temperatures

effect. On the other hand the significant decrease of intensity in the former case is result of deviation from Bragg condition as illustrated in Fig. 3(a). The deviation of the Ewald sphere from the center of the satellite becomes larger for longer wave length and the scattering disappears when the rocking curve of the satellite obtained by rotating the crystal around the Bragg point. The broken line in Fig. 2(b) was calculated by using the rocking curve, which agree satisfactorily with the λ dependence of the intensity. Therefore SAN has an advantage that the rocking curve can be estimated without rotating the crystal. The size of the satellite estimated from the FWHM of the rocking curve is 1.55×10^{-3} $\mathring{A}^{-1}$(FWHM), suggesting the helical spin structure has the domain size of 4060 $\mathring{A}$. The square of the linewidth of the Bragg spot $(\Delta q/q_c)^2$ is plotted against $1/\lambda^2$ in the lower-

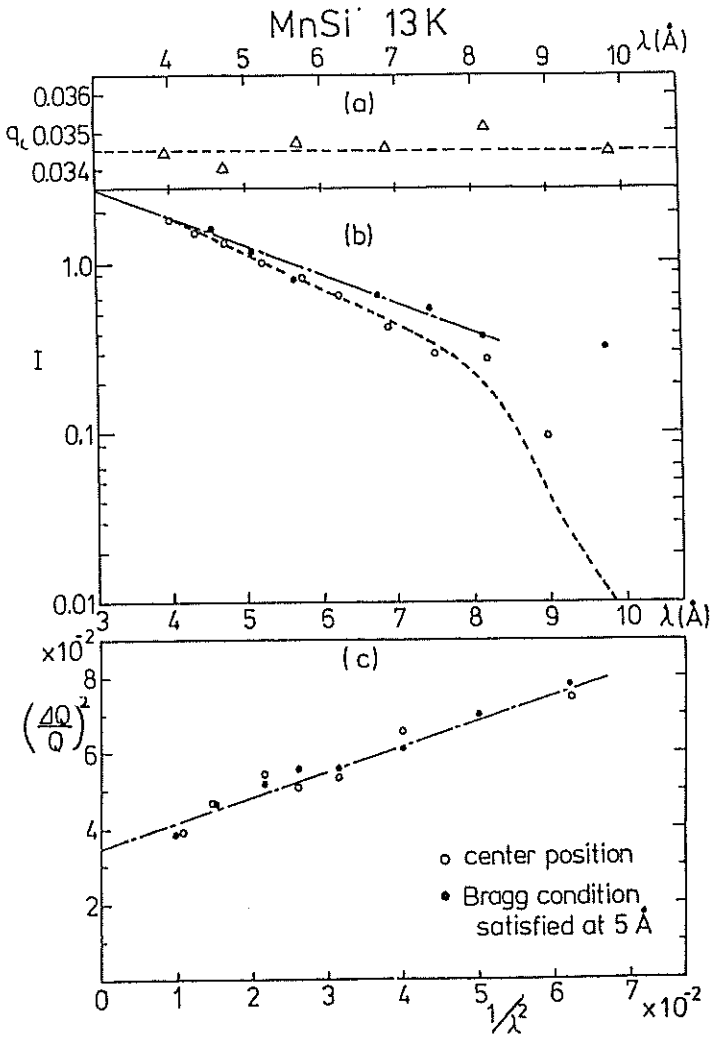

Fig. 2 wave length dependence of q_c, I and $(\Delta Q/Q)^2$ of satellites

most figure. A linear relation between $(\Delta q/q_c)^2$ and $1/\lambda^2$ holds as expected theoretically,but the extrapolation of $(\Delta q/qc)^2$ to $\lambda = \infty$ gives rise to the value $\Delta q/q_c = 0.18$ or $\Delta q = 6.26 \times 10^{-3}$ $\mathring{A}^{-1}$ which is almost four times larger than the value estimated from the rocking curve. This is the problem to be explored further. A preliminary result suggests that this is due to the slight missetting of the1D-PSDs which compose the 2D-PSD. From Fig. 1(b)-(d) we found an interesting temperature evolution of the spin corretation near T_N = 29 K. At T_N the satellites ($\zeta,\zeta,\zeta,$) disappear and the critical scattering develops not around the center. The ring type critical scatter-

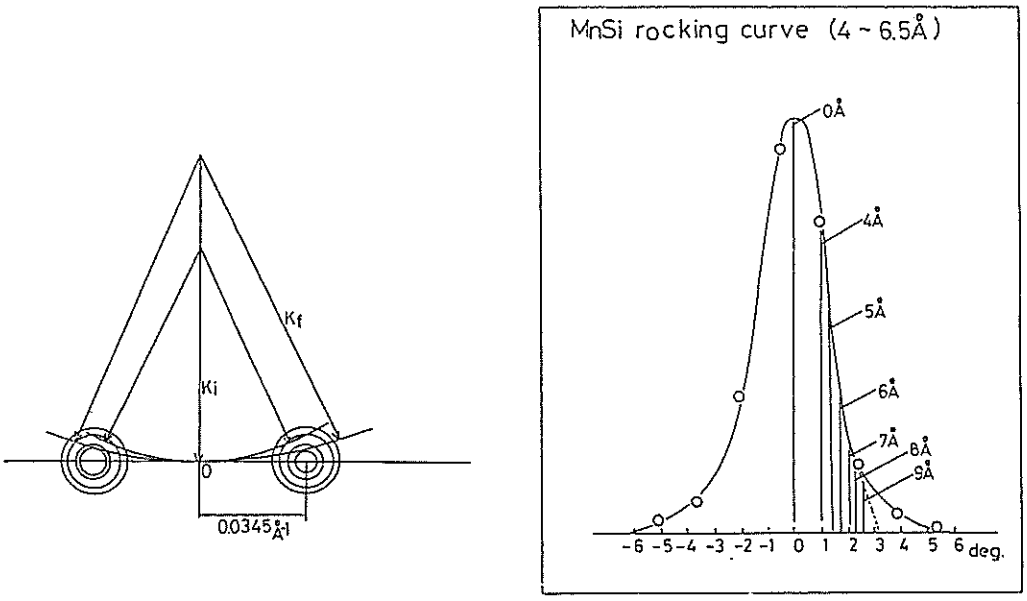

(a) (b)

Fig. 3. reciprocal lattice point of satellites (a) and rocking curve (b)

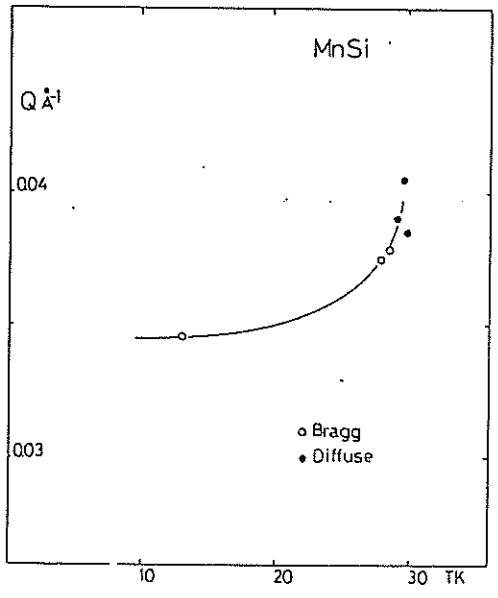

Fig. 4. Temperature dependence of propagation vector q_c

ing almost disappears 1.0 K above T_N. The temperature dependence of the propagation vector q_c is shown in Fig. 4 which indicates that q_c increases with increasing temperature, attaining to the value $q_c = 0.038$ Å^{-1} at T_N, in good agreement with the result obtained at BNL[2].

References

1) Y. Ishikawa, K. Tajima, D. Bloch and M. Roth : Solid State Comm. 19(1976) 525

2) Y. Ishikawa, Y. Noda, C. Fincher and G. Shirane : Phys. Rev. B25(1982) 254

Spinodal decomposition in Fe-Cr Alloys Studied by small Angle Neutron Scattering

M. Furusaka, Y. Ishikawa, S. Yamaguchi* and Y. Fujino*

Physics Department and*Department of Nuclear Engineering
Tohoku University, Sendai, 980, Japan

The kinetics of phase decomposition, especially the difference between spinodal decomposition and nucleation and growth mechanism have been studied by small angle neutron scattering instrument (SAN) installed at KENS. The decomposition as well as magnetic phase diagrams of the alloy system $Fe_{1-x}Cr_x$ have been determined by detecting critical scattering. For $x = 0.4$, the critical scattering was detected at $T_c = 550°C$, which is in agreement with the calculated spinodal temperature. The magnetic critical scattering was also observed at 670°C and 590°C for $x = 0.2$ and $x = 0.3$ respectively, which are consistent with static magnetic measurement. No critical scattering was, however, detected around the spinodal temperture for $x = 0.6$, presumably because of substantial decrease of the diffusion rate for this composition. The results are summarized in Fig. 1, where the experimental points are compared with the calculated phase diagram. The kinetics of the phase decomposition were studied by measuring time evolutions of structure functions S(Q,t,Ta)The samples were quenched into iced water from 1000°C, subsequently annealed at Ta(500°C, 515°C, 540°C) for appropriate time (5min to 50hrs.), quenched and measured at room temperature. S(Q,t,Ta) obtained for $x = 0.4$, the peak of S(Q,t,Ta) shifts towards low Q side as annealing time t goes on, and the time evolution of the peak intensity does not diverge

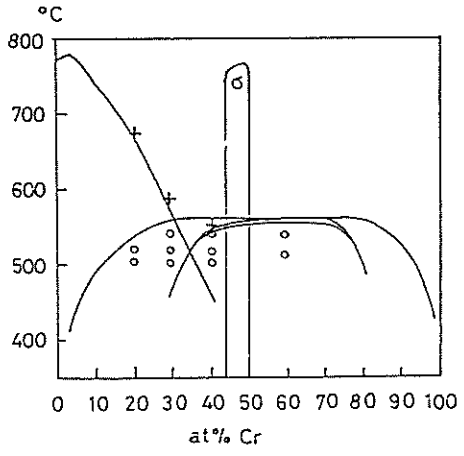

Fig. 1. Decomsposition and magnetic phase diagram of FeCr alloys cross marks:experimental results

exponentially even at the early stage of decomposition, qualitatively in consistents with recent theroy by Y. Saito (J.Phys. Soc. Jpn. 41 (1976) 1129) which takes into account the thermal fluctuations and nonlinear effects. We also found a remarkable result that S(Q,t,Ta) for x=0.3 resembles closely to that of x=0.4 at same annealing temperatures, as seen in Fig. 2, instead of the fact that the annealing temperatures are above the spinodal line for x=0.3. S(Q,t,Ta) of x=0.6 is qualitatively same as that of x=0.4 except the fact that the time evolution is slow corresponding to the low diffusion rate. Small angle scattering was observed even for the as-quenched sample. S(Q,t,Ta) for x=0.2 is distinctly different from other alloys, indicating other kinetics like the nucleation and growth process become important in this alloy.

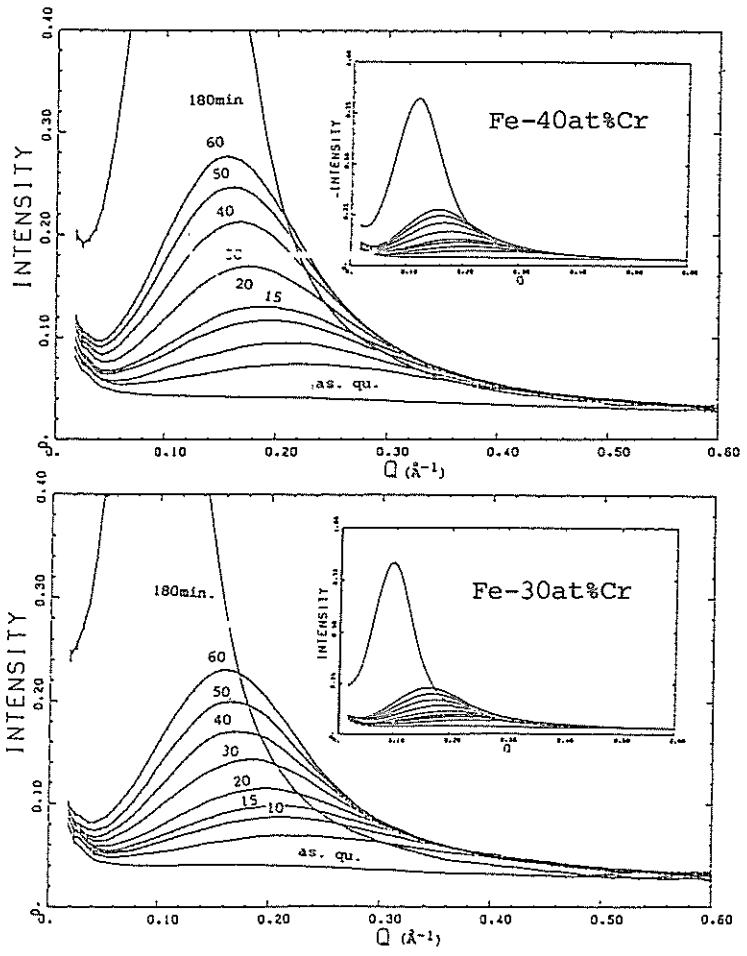

Fig. 2. Time evolution of structure functions phase diagram of FeCr alloys cross marks: experimental results.

Magnetic Correlations in a Competing Interaction System $0.88FeTiO_3$-$0.12Fe_2O_3$ with Spin Glass Behaviors

Yoshikazu Ishikawa, Masatoshi Arai, Norio Saito and [+]Fumihiko Takei

Physics Department, [+]Institute for Iron Steel and Other Metals, Tohoku University, Sendai 980

The paper reports the result of neutron small angle scattering studies on a single crystal of $0.88FeTio_3$-$0.12Fe_2O_3$. The sample has been reported to exhibit the superparamagnetic behaviors above 50 K and the spin glass properties appear at low temperatures. The static susceptibility along the c axis ($\chi_{11}(0)$) in a weak magnetic field of 10 Oe shows a sharp maximum at 38 K, while that in the perpendicular direction $\chi_\perp(0)$ has only a broad maximum around 50 K. The sharp peak is depressed when the applied field is increased as is commonly obseved for the typical spin glasses. The temperature evolution of the magnetic correlations around the 0.0.0. reciprocal lattice point was studied by the SAN spectrometer installed at KENS. The crystal was aligned so as that the c* axis is parallel to the two dimensional counter. Typical examples of two dimensional disply of the scattering profiles measured at three different temperatures, 13 K, 40 K and 45 K are shown in Fig. 1(a),(b), and (c), where the scattering intensity at room temperature had been subtracted as the background. The horizontal direction nearly coincides with the c* axis. The figure shows clearly that the magnetic correlation is quite anisotropic and varies significantly with temperature. A drastic change occurs between 40 K and 45 K. The parallel $\chi_{11}(q)$ and perpendicular $\chi_\perp(q)$ susceptibilities can be separately obtained from the small angle scattering intensity along the c* axis and that perpendicular to it, because the former is proportional to $2\chi_\perp(qc)$, while the latter to $\chi_{11}(q) + \chi_\perp(q)$. In the analysis, we assumed for the simplicity that $\chi_\perp(q)$ is isotropic, which has been proved not to hold exactly by the scattering at high angles, but the errors due to

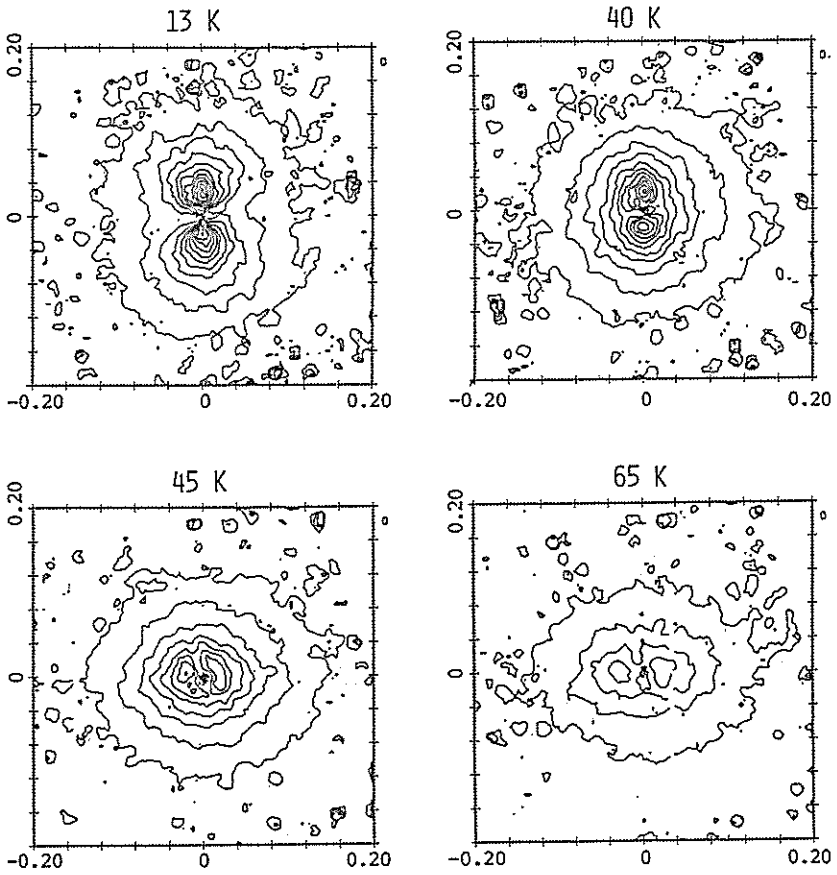

Fig. 1. Two dimensional disply of magnetic correlation in $88FeTiO_3$ at various temperatures

this assumption is rather small. Fig. 2.displays the wave vector dependence of the parallel and perpendicular suceptibilites at 13 K. χ_{11} has a peak at $q_c = 0.028\ A^{-1}$ and the profile for $q>q_c$ can be fitted by the Lorentzian $\chi_{11}(q) = c/\kappa_{11} + q^2$ with $\kappa_{11} = 0.048\ \mathring{A}^{-1}$. The temperature dependences of χ_{11} and $\chi_\perp$ are shown in Fig. 3(a) and (b). The perpendicular susceptibility $\chi_\perp(q)$ has a broad maximum independent of q, while $\chi_{11}(q)$ exhibits an interesting T dependence; $\chi_{11}(q)$ starts to develop below 50 K having the maximum for small q. We have found from the neutron scattering at high angles that 50 K corresponds to the Nêel temperature where the ilmenite type a tiferromagnetic order starts to appear. The maximum of $\chi_\perp$ occurs therefore at T_N. The most eminent results are that the spin glass properties appear only for χ_{11}, the spin component parallel to the c axis and the spin glass transition occurs 12 degrees below T_N. The overall features of the magnetic corre-

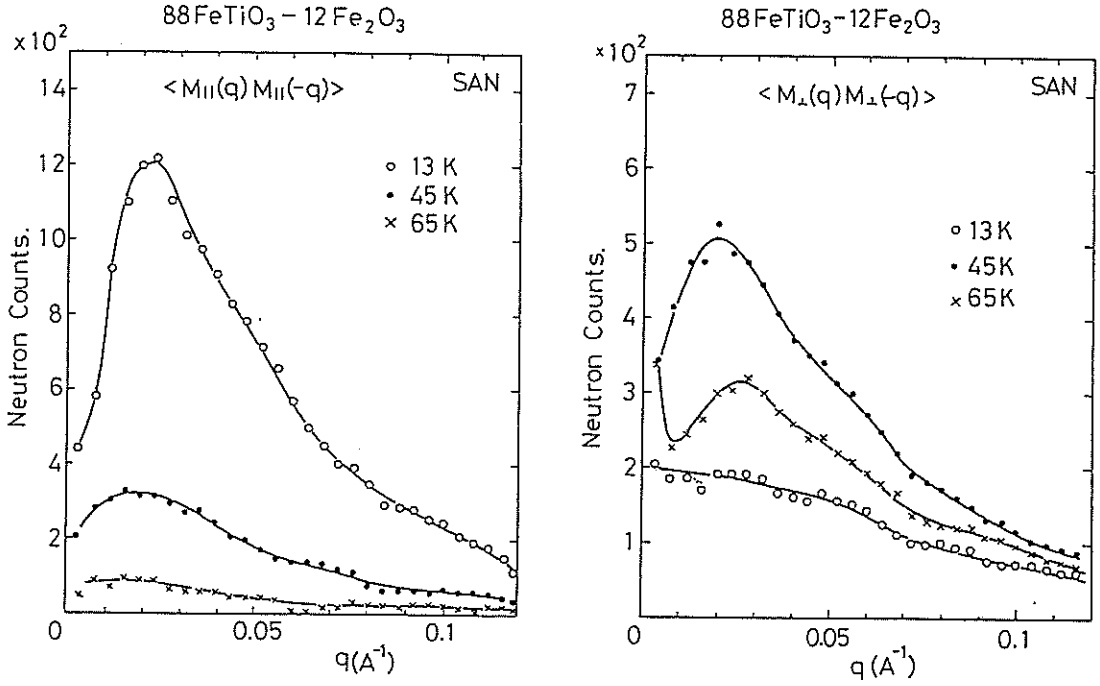

Fig. 2. Wave vector dependences of magnetic correlations $\chi_{11}(q)$ (a) and $\chi_{\perp}(q)$ (b) at different temperature

lations in this ilmenite-hematite system can be understood as follow. Below the Néel temperature of T_N, the c axis component of spins starts to order in parallel, but with a helical modulation of the amplitude with a period of $2\pi/q_c$ = 224 Å, so that the resultant ferromagnetic moment disappears in zero field. The effect of the external field on the spin correlations is reported in a succeeding paper.

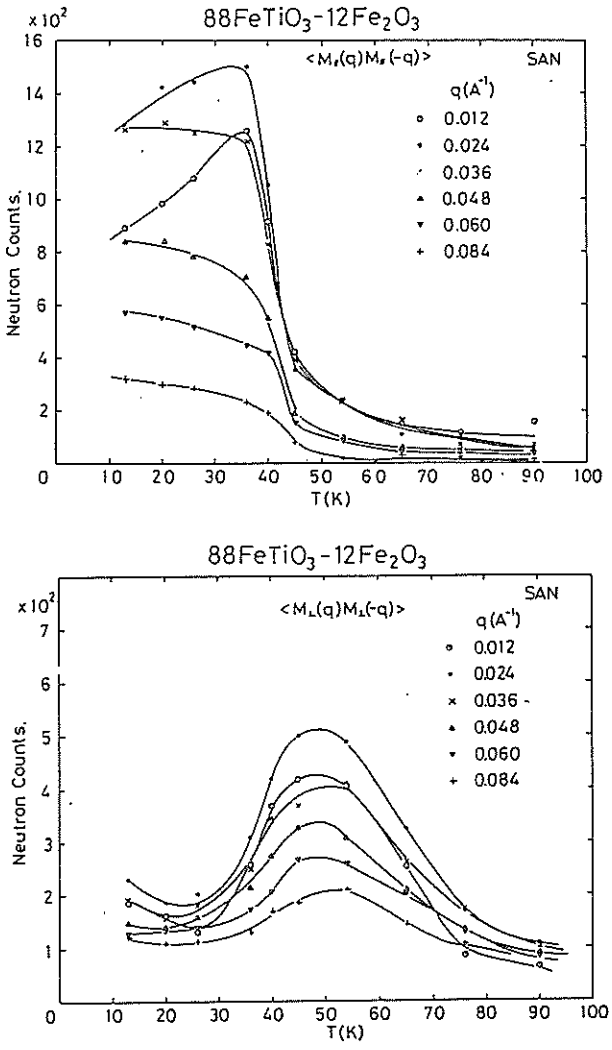

Fig. 3. Temperature dependences of magnetic correlations $\chi_{\parallel}(q)$ (b) and $\chi_{\perp}(q)$ (b) for different wave vectors

Effect of Magnetic Fields on the Spin Glass state of $0.88FeTiO_3$-$0.12Fe_2O_3$

Masatoshi Arai, Norio Saito, Yoshikazu Ishikawa
and Fumihiko Takei

Physics Department, Institute for Iron Steel and Other Metals,
Tohoku University, Sendai 980

Recently we have studied extensively a typical cluster type spin glass system, $0.88FeTiO_3$-$0.12Fe_2O_3$ by means of neutron scattering and static magnetic measurements. The magnetic susceptibility along the c axis $\chi_{11}(0)$ has the sharp peak at T = 38 K in a magnetic field of 10 Oe, but the peak is broaden and is shifted to lower temperature with increasing the external field. The magnetic hysteresis is shifted upward by the field cooling from above 50 K and the thermo-remanence magnetization (TRM) produced shows the relaxation phenomenon. These field effects have commonly been observed in various spin glass systems.

In order to find the relation between the field effect and the magnetic correlations in the spin glass state, we have carried out the small angle neutron scattering experiments in magnetic fields. Typical examples of the observed two dimensional patterns are displayed in Figs. 1(a)-(d). The magnetic field was applied in the horizontal direction which nearly corresponds to the c* axis. Figs.1(a),(b)and(c) are scattering patterns at 12K in zero field, 2.25 KOe and 5 KOe respectively, while Fig.1(d)is the pattern in zero field after the sample was field cooled from 90 K in a field of 5 KOe. The figures show clearly that the peak of scattering along the direction perpendicular to c* is significantly suppressed by the external field. Note that the TRM state (Fig. 1(d)) resembles to the parttern in 2.25 KOe (Fig. 1(b)). The field dependence of the scattering intensity along c* ($2\chi_{\perp}(q)$) and that perpendicular to it ($\chi_{\perp}(q) + \chi_{11}(q)$) are plotted in Fig. 2. for two different wave vectors, which shows that it is only spin correlation of the c axis components $\chi_{11}(q)$ which is strongly affected by the external field. A significant change occurs at 2.2 K Oe which

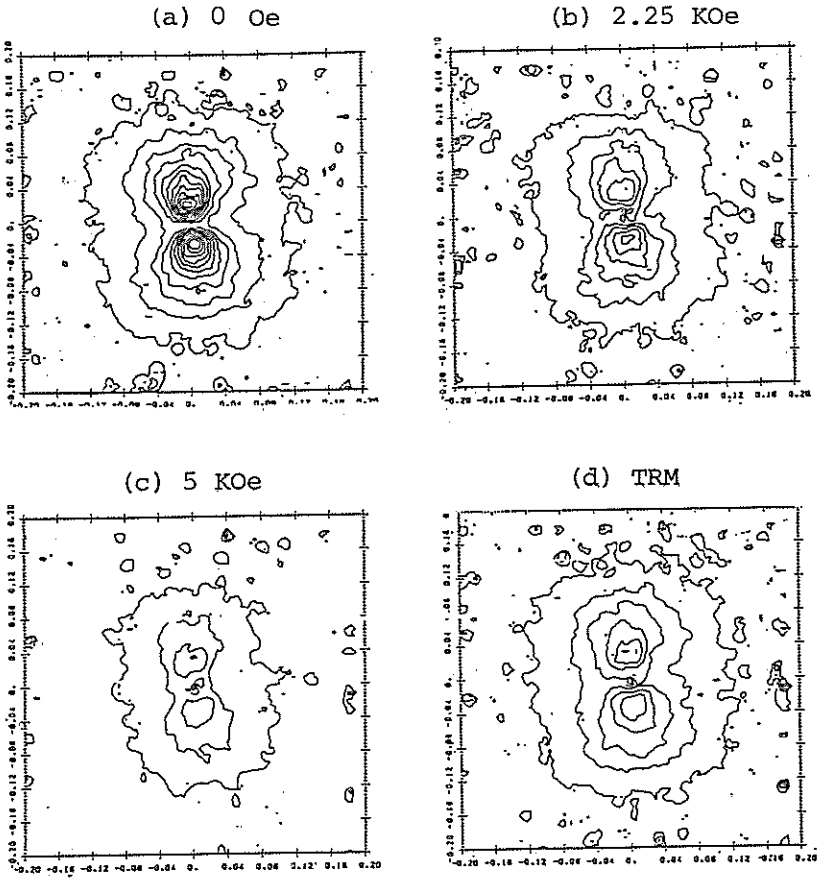

Fig. 1. Two dimensional display of magnetic correlations in 0.88 $FeTiO_3$-0.12Fe_2O_3 in various external fields(a-c) and in the thermo-remanent state(d).

corresponds to the coercive force of the material. The cross mark in the figure is the inverse correlation length κ derived from the Lorentzian fit of the profile ($I \propto 1/\kappa^2+q^2$) which increases with increasing the field. We have measured at the same time the scattering around the (1,0,-0.5) and (1,0,1) reciprocal lattice points by employing the fixed single counters. The former corresponds to the antiferromagnetic Bragg point, while the latter to the ferrmagnetic one. The intensity of the scattering around (1,0,-0.5) is not affected by the field, but that around (1,0,1) decreased with increasing the field as is demonstrated in Fig. 3. In 0.88 $FeTiO_3$-0.12Fe_2O_3, the ferromagnetic clusters of order of 120 Å exists

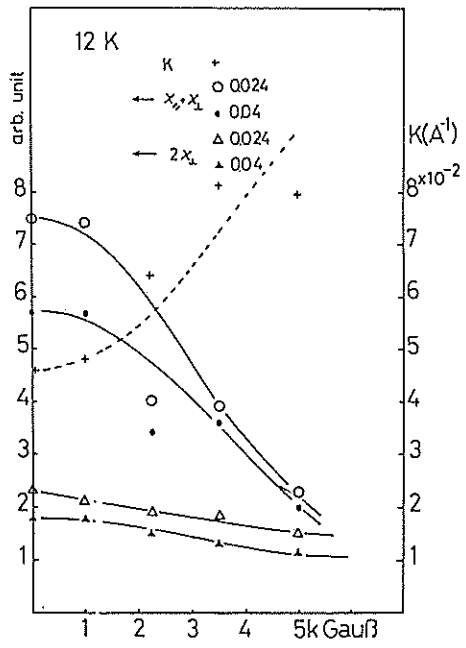

Fig. 2. Field dependence of the scattering intensity along $c^*(2\chi_\perp(q))$ and that perpendicular to it $(\chi_\perp(q) + \chi_{//}(q))$ plotted for q = 0.024 and 0.04 A^{-1}. Cross marks exhibit the inverse correlation length K.

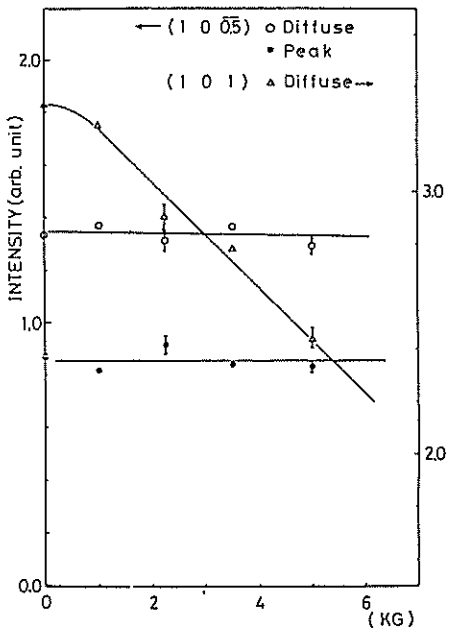

Fig. 3. Integrated intensities of (1,0,1) and (1,0,-0.5) measured with the fixed single counters plotted against the external field.

below 100 K, the ferromagnetic alignment inside the cluster is antiferromagnetically modulated below 50 K, resulting in the diffuse scattering around (1,0,-0.5). The spin glass state below T_g = 38 K is the result of antiferromagnetic alignment of the resultant ferromagnetic moments of the clusters. Our experiment has depicted that the field effect is due to the reorientation of the reusltant moment of the cluster. The spin configuration inside the cluster is not affected by the field of 5 KOe. We believe that our experiment results give a strong support of the cluster model of this substance.

Small Angle Scattering from Polystyrene Latex with KENS Pulsed Neutron Source

Kimio Kurita, Osamu Hasegawa, Shinya Nakajima
Michihiro Furusaka* and Yoshikazu Ishikawa*

College of Science and Technology, Nihon University, Tokyo 101
*Faculty of Science, Tohoku University, Sendai 980

For the purpose of testing KENS-SAN apparatus, the neutron scattering from polystyrene latex with known particle diameters was carried out.

Apparatus: Wave length λ of the cold neutron used in the experiment was $3\text{Å} \leq \lambda \leq 12\text{Å}$. The intensity maximum was observed at $\lambda=5\text{Å}$. Distance between the sample and the two dimensional position sensitive detector(2D-PSD) composed of 43 1D-PSD was 5m. The direct beam was focussed on the center of the detector by use of converging Soller slit. Intensity of the incident beam was 7×10^4 n/cm^2.s and area of the beam at the sample was 3.5 x 1.4 cm^2. Sample cell was made by fused quartz and the thickness of the sample was 2 mm.

Sample: Concentration of the particles of polystyrene latex (Dow chem., mean diameter: 693 Å, Standard deviation: 60 Å) was 1 % in aq. solution of D_2O(90%). Distribution of the diameter of the particles measured by electron microscopy is shown in Fig.1.

Measurements: By use of KENS-SAN facility excess scattering intensity of the latex against D_2O(90%) was determined after the transmission correction was made for both of the solution and solvent. The incident neutron spectrum as well as the detector efficiency of each element of 2D-PSD was corrected for by using the data of incoherent scattering from water.

Results: Observed scattering intensity with the resolution of dq=0.003 is plotted by full circles against the momentum transfer q in Fig.2. The solid curve was calculated by taking account of resolution of spectrometer and distribution of particle sizes. The agreement between the observation and this curve is fairly satisfactory except the data for the low q region, where other kinds of corrections were found to be required paper.

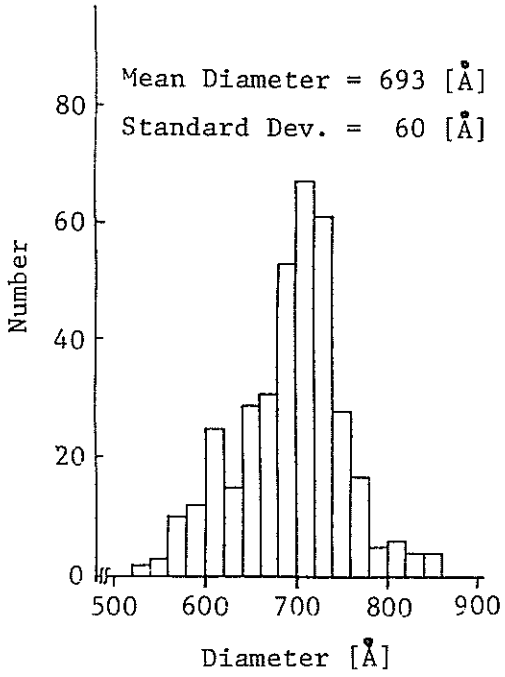

Fig.1 Particle diameter distribution of polystyrene latex determined by electron micrograph.

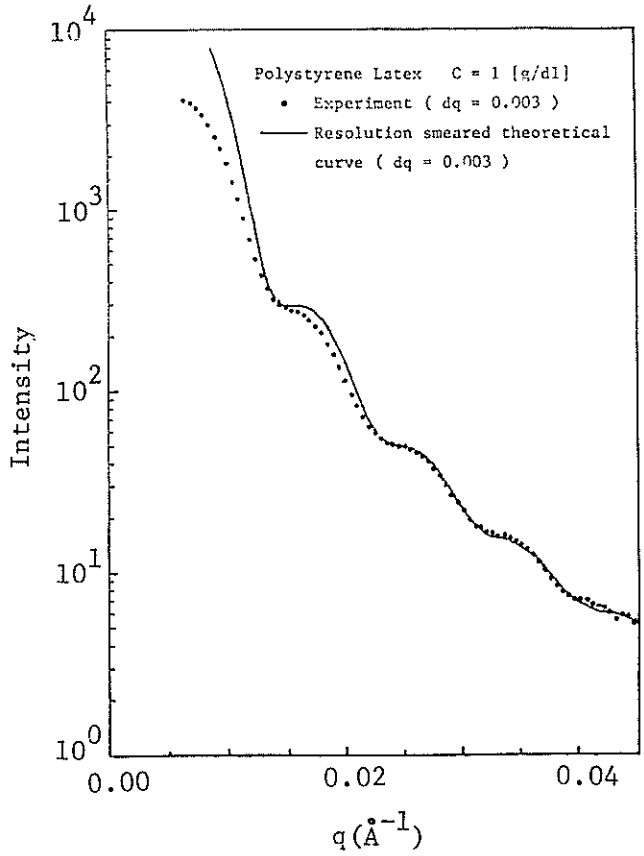

Fig.2 Observed scattering intensity and the theoritical curve for polystyrene latex.

Small-Angle Neutron Scattering from Semi-dilute Polymer Solutions
—— Compensation Temperature in Semi-dilute Solutions

Kimio Kurita, Osamu Hasegawa, Shinya Nakajima, Eiichi Wada
Koji Okano*, Michihiro Furusaka** and Yoshikazu Ishikawa**

College of Science and Technology, Nihon University, Tokyo 101
*Faculty of Engineering, University of Tokyo, Tokyo 113
**Faculty of Science, Tohoku University, Sendai 980

KENS-SAN facility was used for the measurements of compensation points of semi-dilute polymer solutions which have not been determined experimentally. It is well known[1),2)] that in the case of dilute polymer solutions, due to the contribution of the three-body interaction (the ternary cluster integral β_2) of polymer segments the compensation temperature $\tilde{\Theta}$ is shifted from the Flory Θ temperature at which the binary cluster integral β_1 of the segments becomes zero.

In this report we discuss the $\tilde{\Theta}$ point in semi-dilute solutions of polystyrene in deuterated cyclohexane.

When the excluded volume effect is so small that the parameters $z_1 \equiv \beta_1 b^{-3} N^{1/2}$ and $z_2 \equiv \beta_2 b^{-6}$ are both sufficiently smaller than unity the density-density correlation function of polymer segments in semi-dilute solutions can be theoretically calculated by using the ring approximation,[3),4)] here b^2 being the mean square length of a segment, N the number of segments in a polymer chain. And we obtain the scattered intensity of SANS as

$$I(q)^{-1} = I(0)^{-1}(1 + \xi^2 q^2), \tag{1}$$

$$\xi^{-2} = 6(MA^2)^{-1} + 12N_A A^{-2} B_1 C + 36N_A{}^2 A^{-2} B_2 C^2, \tag{2}$$

where C is the weight concentration(g/cm^3), N_A is Avogadro's number, M is the molecular weight of polymer, and A^2, B_1 and B_2 are defined respectively as $MA^2 = Nb^2$, $M^2 B_1 = N^2 \beta_1$ and $M^3 B_2 = N^3 \beta_2$.

Sample

The sample used was living polystyrene (Press. Chem., $M = 2.9 \times 10^5$, $M_w/M_n \leq 1.06$) dissolved in deuterated cyclohexane.

Apparatus

The excess scatterings were measured by the same apparatus described in the preceeding report[5] except the new camera length of 3m.

Results

The measured excess scattering intensity was in good agreement with Eq.(1) and the concentration dependence of the correlation length ξ was found to obey Eq.(2) for each temperature near Θ as shown in Fig.1. Fig.2 shows the temperature dependences of B_1 and B_2 thus obtained. We recognize from these results that we actually have the concentration dependent compensation temperature in semi-dilute solution below the point where the binary cluster integral vanishes.

References

1) P.G.de Gennes: Scaling Concepts in Polymer Physics, Cornell University Press,1979.

2) I.Webman, J.L.Lebowitz and M.H.Kalos: Macromolecules,14,1495(1981).

3) H.Miyakawa, N.Saito and K.Moro: RPPPJ.,24,37(1981)

4) M.A.Moore: J.Phys.(Paris),38,265(1977).

5) K.Kurita, et al.: KENS REPORT II (1982).

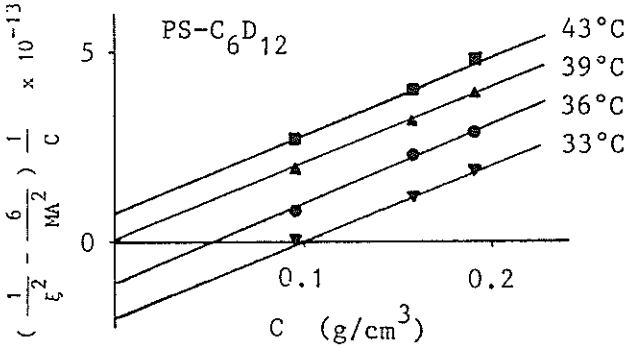

Fig.1. Concentration dependence of ξ at various temperatures.

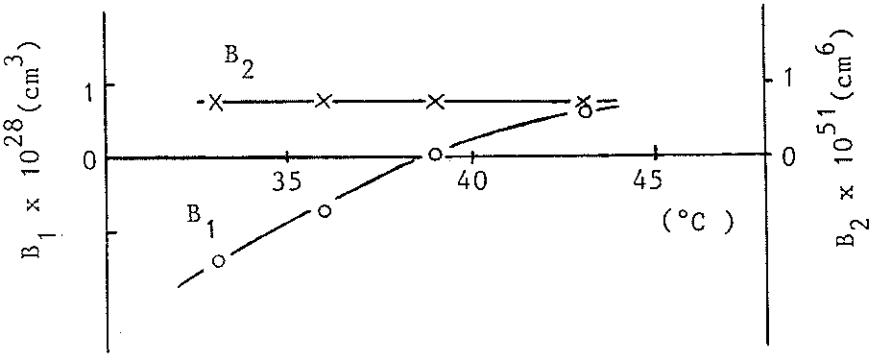

Fig.2 Temperature dependences of B_1 and B_2.

Small Angle Neutron Scattering by the Purple Membrane and Collagen

Toshio Mitsui, Toshiaki Hamanaka, Yoshinobu Izumi*,
Nobuo Niimura**, Michihiro Furusaka*** and Yoshikazu Ishikawa***

Faculty of Engineering Science, Osaka University, Toyonaka, Osaka.
*Faculty of Science, Hokkaido University, Sapporo,
**Laboratory of Nuclear Science, ***Faculty of Science,
Tohoku University, Sendai.

It is expected that the small angle scattering instrument (SAN) is used to study the structure analysis of the biological materials. The small angle neutron scattering experiments of purple membrane and collagen were carried out in order to check the feasibility of the SAN, since the structures of these substances are well known.

The purple menbrane is a fraction of the cell membrane of Halobacterium halobium, and contains only one species of protein, bacteriorhodopsin which forms a 2-dimension hexagonal lattice in liquid bilayer. About 50mg of membrane fragment were used for scattering experiments and a set of data was collected for 7 hours. Fig. 1 shows the spectra originating from the periodic stacking of the lamellae. The inserted figure is an enlargement of the part of the higher order reflections.

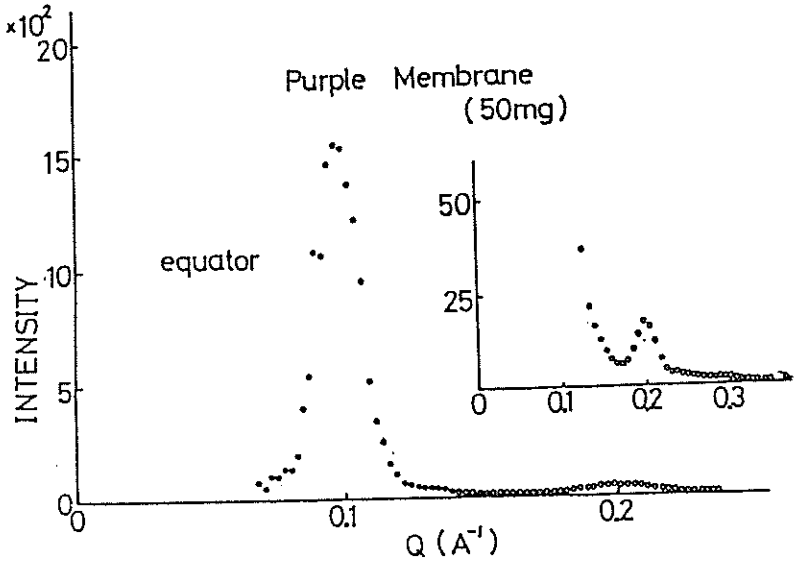

Fig. 1. Diffraction pattern originating from the periodic stacking of the lamellae.

Fig. 2 shows the Bragg reflections originating from the 2-dimensional crystalline lattice in the membrane.

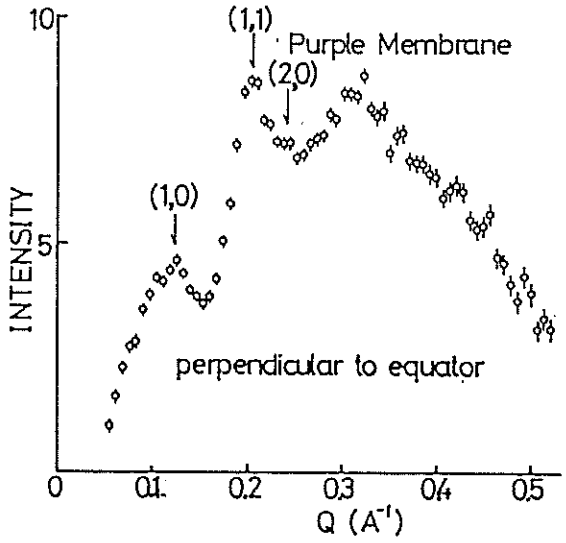

Fig. 2 The Bragg reflections originating from the 2-dimensional crystalline lattice in the purple membrane.

Collagen is a typical biological fibre with the advantages of being easy to handle. It consists of a single type of rod-shaped molecule which constructs a regular periodic structure, of which the period is about 670Å along the fibre axis. The small angle neutron scattering from the collagen of the deer tendon was carried out by the use of the SAN. The size of specimen was 2mm in thickness, 18mm in width and 33mm in length. The data were collected for 4.5 hours. Fig. 3 shows the result. Bragg reflections from the 1st order to the 5th order were observed. The integrated intensities of the 1st and the 3rd Bragg reflections are explained well by the generally accepted model. The period observed was 677Å.

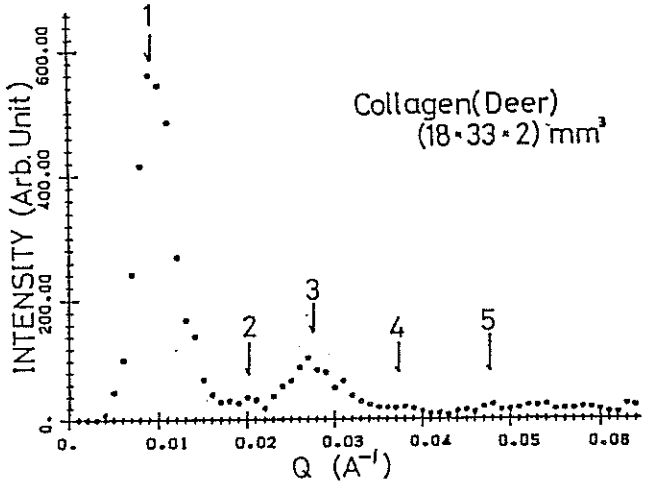

Fig. 3 Diffraction pattern by the deer collagen. Collagen is offered from Department of Veterinary Science, Hokkaido University.

It is concluded that the study on the structure analysis of the biological materials by using the SAN is feasible.

Small Angle Neutron Scattering Studies of the Structure of Nucleosome Cores at Low Ionic Strength

Kazuei Mita, Mitsuo Zama, Sachiko Ichimura, Nobuo Niimura*, Mitsuhiro Hirai** and Yoshikazu Ishikawa**

Division of Chemistry, National Institute of Radiological Sciences, Chiba 260; * Laboratory of Nuclear Science, Tohoku University, Sendai 982; ** Physics Department, Tohoku University, Sendai 980

The nucleosome core particle, consisting of 146 base pairs of DNA wrapped around an octamer of two each of the inner histones H2A, H2B, H3 and H4, constitutes the first level of DNA packaging in chromatin. Recent reports that conformational transitions are induced in the nucleosome core in low salt concentration are of interest because the low-salt conformation may relate to possible conformational states of nucleosomes in the transcriptionally active chromatin. However, little is known about the detailed mechanisms of the conformational transition. Neutron scattering is one of the most powerful techniques to reveal the mechanisms of the conformational changes of nucleosome cores, because the structural behaviors of the DNA and the histones can be detected separately by the contrast variation method. This paper describes the results of small angle neutron scattering studies made by KENS-SAN of nucleosome core solutions from chicken erythrocytes over the range from 10 to 0.04 mM Na^+. Fig.1 shows the effect of ionic strength on the radii of gyration, R_G, calculated from the slopes of the Guinier plots from nucleosome cores in 65 and 100% D_2O. In 65% D_2O where DNA is matched out, a single transition, in which R_G increases from 34 to 43A, occurs at about 1 mM ionic strength with decreasing the ionic strength from 10 mM. No loss of the secondary structure of the histones was observed by circular dichroism over the range of the ionic strength examined. Therefore the fact indicates a substantial change in the tertiary or the quaternary structure of the histone octamer in the nucleosome core at low ionic strength ($\lesssim$ 1 mM). Interestingly, a single transition, in which R_G decreases from 40 to 36A, occurs also near 1 mM ionic strength with decreasing ionic strength from 10 mM of nucleosome cores in 100%

D_2O. For an inhomogeneous but centrosymmetric body, the radius of gyration, R_G, will vary as: $R_G^2 = R_I^2 + \alpha/\bar{\rho}$, where R_I is the radius of gyration at infinite contrast and $\bar{\rho}$ the difference between the mean scattering density of the nucleosome core and that of the solvent. α has the significance of a mean square distance of fluctuations from the center of shape. Fig.2 dipicts the relationship between R_G^2 and $1/\bar{\rho}$ of nucleosome cores obtained from the present data. The positive slope for the nucleosome core in 10 mM ionic strength demonstrates that the radius of gyration for the material with higher scattering density (the DNA) is greater than that for the material of lower scattering density (the histones), that is, the mass of DNA is concentrated toward the outside of the particle, in agreement with the results by other authors [1,2]. On the other hand, the negative sign of α for the nucleosome cores in 0.02 mM EDTA implies that the mass of histones is concentrated toward the outside of the particle. One of the possible ways to describe the conformation of the nucleosome core induced by low salt may be that, the histones locate outside of the particle accompanied by an alternation of the tertiary and/or the quaternary structure of the histone octamer.

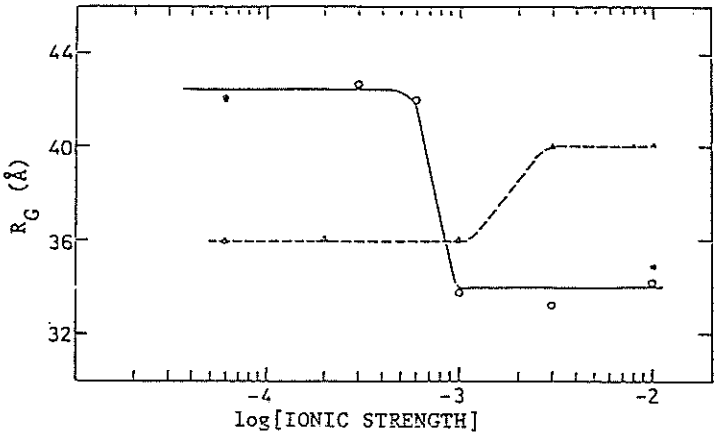

Fig.1. Plots of R_G vs the logarithm of the ionic strength. ——,65% D_2O; ----,100% D_2O.

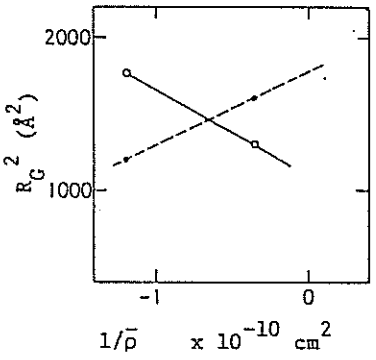

Fig.2. Variation of R_G^2 as a function of $1/\bar{\rho}$.

———, 0.02 mM EDTA;
-------, 10 mM NaCl/0.02 mM EDTA.

References

1. Pardon,J.F. et al.(1975)Nucleic Acids Res. 2,2163-2176
2. Suau,P. et al.(1977)Nucleic Acids Res.4, 3769-3786

TOP Performance

Yasuo Endoh, *Susumu Ikeda, Hitoshi Ono, Yukio Sasaki,
Setsuo Mitsuda and Mitugu Onodera

Department of Physics, Tohoku University, Sendai 980
and
*National Laboratory for High Energy Physics, Tsukuba Ibaraki 305

TOP has been operated as the polarised neutron diffractometer with a polarisation analyser since the last April . Although the detailed report describing of this spectrometer, performance etc. is in preparation[1], results of the beam polarisation measurments are described here. An experimental set up to measure the polarisation is shown in Fig. 1 schematically. A spin flipper of the Drabkin coils which has an excellent flipping efficiency indpendent of the wave length is placed at approximately centre of the guide magnet channel between the polariser and the sample table. These coils sit inside the double layered permalloy cylinder which shields the stray field and even the earth magnetic field. The current direction of the first coil can be automatically altered which produces the sudden change of the magnetic field at the middle point of the coils. Then neutron spins follow nonadiabatically these fields, which functions the spin flipping to the magnetic field produced by the second coil. The switching time coincides with the proton Booster pulses so that the magnetic field really changed the direction at the time when the neutron bunch pass away from the second coil in the flipper. The gate circuit of neutron counting is also coincident with the neutron pulses. Furthermore the distributer of the neutron counting was attached to the data acquisition system. Therefore the neutrons labelled as the neutron spin directions or signs are accumulated to the different memories in the system. Measurements were carried out in the manner described by Kendrick et al[2] and the flipping ratio were determined using a shim plate. Since the absorption effect by the shim plate is not negligible, these values were obtained after the correction from the raw data. Fig. 2. are plotted

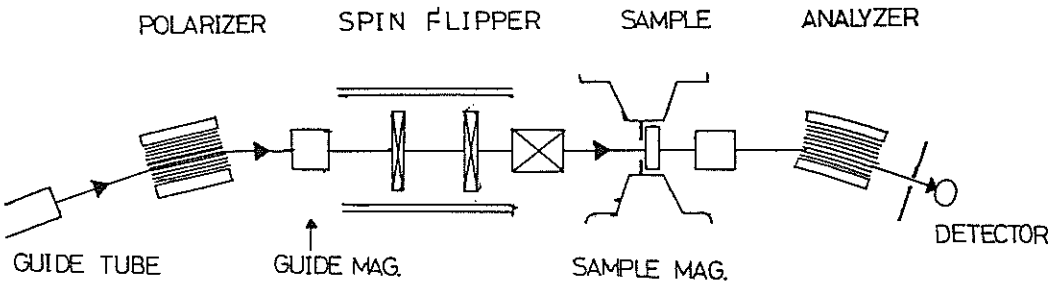

Fig. 1. Experimental set up of TOP spectrometer for the purpose of the determination of beam polarisation. Note that TOP is regularly used as the TOF diffractomter and as the diffractometer with the polarisation analyser

the polarisation, flipping efficiency against the wave length in the range of 3.5 A - 9 Å. Note that these values are defined for the beam cross-section of 10 mm x 10 mm. Our maximum beam is 20 mm wide x 50 mm long. For this wide beam polarisation reduces by 3 % at the maximum which is still acceptable for most of the practical experiments. The mean reflectivity of the polariser is evaluated to be 90 % ; which implies that about 40 % of the incident neutrons from the guide tube are effectively used in the experiment. At present we study the diffuse scattering from various magnetic substances like ultra fine particles, the small angle scattering and the polarisation analysis for, both transmitted and scattered beams. Neutron spectrum moduration is also demonstrated by applying the simple concept that neutron polarisation density (P) rotates around the magnetic field just as the rigid spin rotation. In the present demonstration a rectangular coil in which the uniform vertical magnetic field is supplied was put on the sample table keeping the same arrangement of Fig. 1. When the bunch of polarized neutrons along the beam path enter into the rectangular coil, polarization rotates and therefore the phase angle of the polarisation axis changes when neutron beams go out of the coil, because we are dealing with the polychromatic neutrons. When we look at the neutron spectrum after the

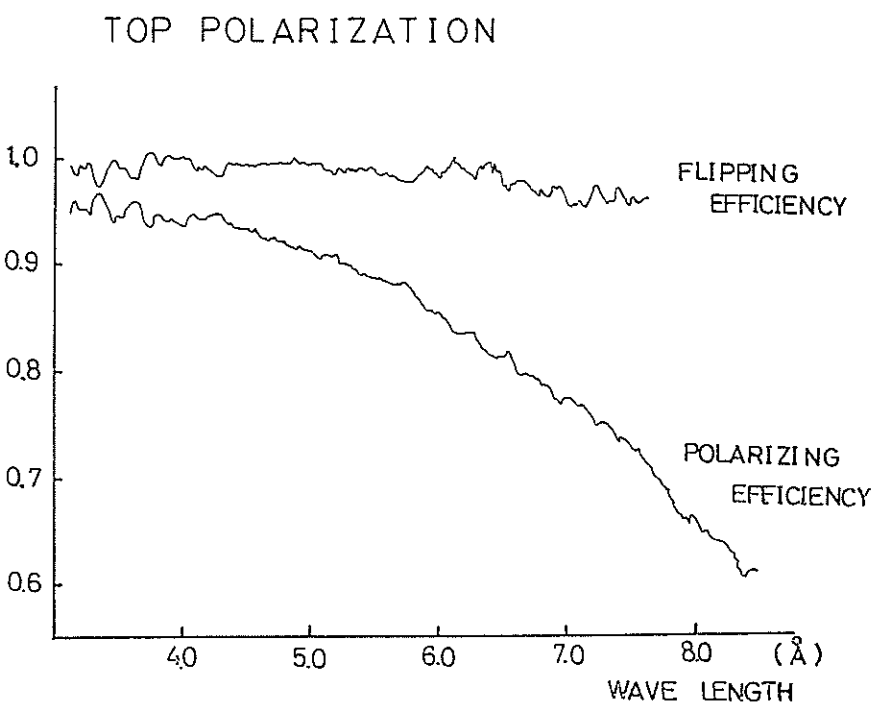

Fig. 2. Wave length dependence of the polarisability and flipping efficiency of the TOP neutron beam. Beam cross-section is 10 mm x 10 mm.

polarisation analyser the spectrum is considerably modurated as shown in Fig. 3. This demonstration also gives an important concept for the neutron spin echo technique for the pulsed spallation sources.[3] We will test very near future the feasibility of NSE by using a proto type set up which is now under construction. Our polariser and analyser of the curved Soller type magnetic mirror are not perfectly satisfactory due to the lower polarizability and the continuous effort to develope the techniques is ultimately necessary until we will be able to supply a high quality polariser.

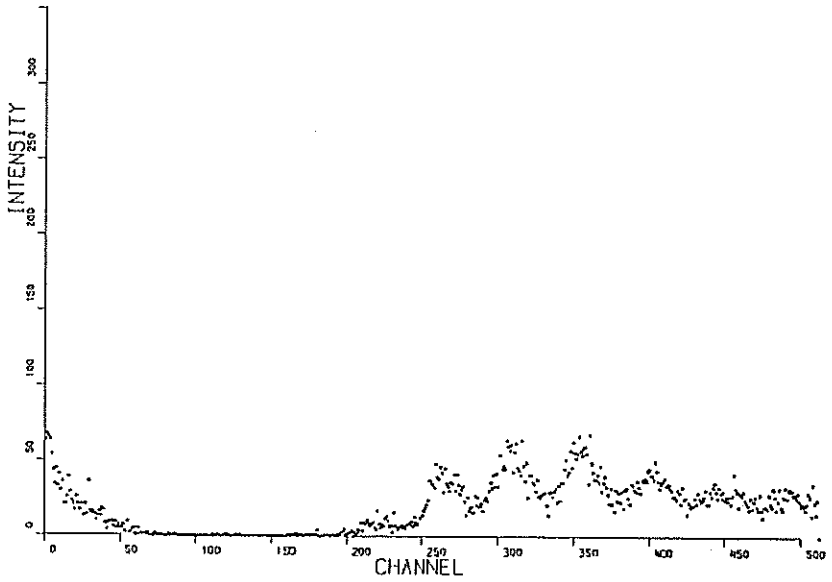

Fig. 3. Neutron spectrum moduration
This exmple is obtained by applying 20 Oe
for the path length of 50 mm.

References

1) Y. Endoh, S. Ikeda, H. Ono, Y. Sasaki, S. Mitsuda & M. Onodera in preparation

2) H. Kendrick, S. A. Werner & A. Arott Nucl. Inst Meth. 68(1969)50

3) F. Mezei : " Neutron Spin Echo " Springer Verlag

Polarised neutron diffraction from the artificial superlattice films - investigation of the effect of the surfaces on the ferromagnetism -

Hitoshi Ono, Yasuo Endoh, *Nobuyoshi Hosoito, Teruya Shinjo and **Susumu Ikeda

Department of Physics, Tohoku University, Sendai 980

* Institute for Chemical Research, Kyoto University, Uji, Kyoto 611

and

** National Laboratory for High Energy Physics, Tsukuba, Ibaraki 305

Polarised neutron diffraction was carried out on the TOP spectrometer using artificial superlattice films (ASFS). The primary concern in the present studies is to elucidate the surface or/and interface effects on the ferromagnetic order. Since neutrons can penetrate deeply into most of substrances, the surface contributions in the scattering is very small. Therefore the AFS samples were obtained which consist of multiple bilayers of ferromagnetic and non magnetic metals. ASFS were perpared by the sequential evaporation onto the glass substrates by means of the electron gun technique. The evaporation was controlled by the dedicated micro computer detecting the rate of the film thickness during the operation. These films obtained by this method form a periodically stratified lamella structure. We have observed several sharp diffraction peaks, whose diffraction position exactly fits to the inverse thickness of the bilayer monitering by the thickness detector.

The magnetic properties in such ferromagnetic ASFS are studied by using long wave polarised neutrons which facilitate the precise determination of the anomalies due to the surface effects.[1,2] If the values of the flipping ratio with respect to the diffraction orders are varied, the magnetic density distribution along the direction normal to the film layers must be varied within these magnetic layers. In other words the spatial structure in the magnetic scattering potential along the normal direction to the plane different from that of the nuclear potential creats the moduration in the magnetic scattering amplitude with respect to the scattering momentum

transfer.

In the present experiments from FePd and FeSb AFS, the values of the flipping ratios in the first and the second ordered magnetic superlattice reflections are different, which immediately implies the spatial moduration in the magnetic sturcture possibly due to the surface effects. Since the flipping ratio of the strong reflection is independent of the wave length, the extinction effect may not be serious. The effect of temperature as well as the magnetic field were studied. These experimental results are summarized in the figure.

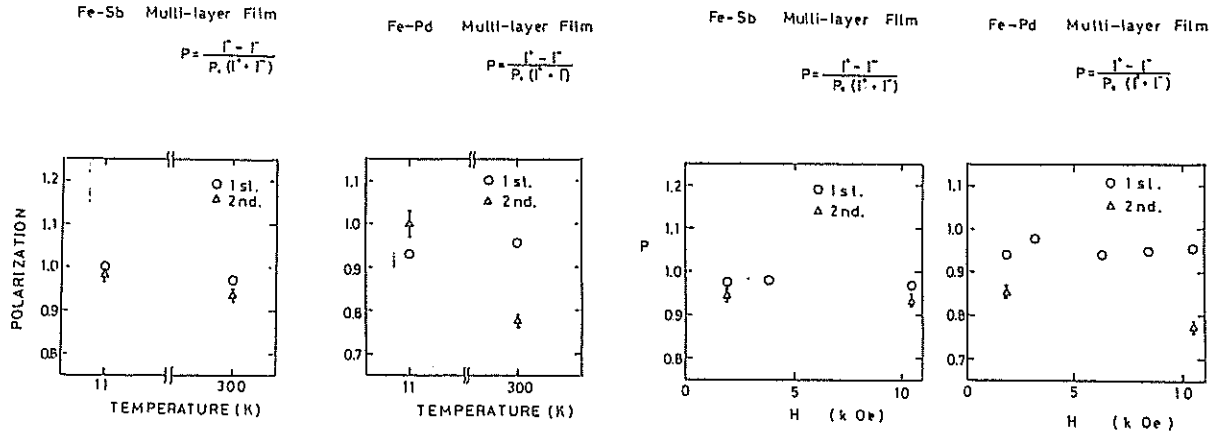

Fig. 1. Temperature and Field dependence of the flipping ratio in FePd and FeSb ASFS. Note that the quantities are in the unit of polarisation.

It is clear that the magnetic behaviors in FePd and FeSb ASFS are different with each other. These results suggest that an Fe magnetic moment at the interfaces may be reduced due to the surface effects. The anomalies are stronger in FePd ASFS. It is necessary, however, to examine with more intense and higher polarised beams in order to determine difinitive surface effects. Nevertheless present demonstration just shows the feasibility of polarised neutron diffraction to the interesting surface problems.

References

1) M. Sato, K. Abe and Y. Endoh; J.de phys. C2 40 72 (1979)

2) M. Sato, K. Abe and Y. Endoh and J. Hayter; J.phys. C13, 3563 (1980)

Depolarisation of pulsed polarised neutrons by the magnetic alloys

Y. Endoh, S. Mitsuda and *S. Ikeda

Department of Physics, Tohoku University, Sendai 980

and

*National Laboratory for High Energy Physics, Tsukuba Ibaraki 305

Neutron polarisation can be regarded as the "classical spin", which means that the operater S for the neutron spin is determined by the "classical equation of motion. Therefore the change of polarisation state in passing through a region of the magnetic field Hi is also comprehended as the change of the "spin" state rotating in the effective field in the region.

(1) The parallel component of the polarisation to Hi is unchanged. While,

(2) the perpendicular component precesses about Hi with the frequency ω_i.

$$\omega_i = \gamma \, Hi \tag{1}$$

When we think about depolarisation of polarised neutrons by the magnetic substance of the finite length, we should follow the motion of the neutron "spin" by using the equation of motion. The solution of this equation, P(t), provides the explicit time dependence of the polarisation. Following the famous paper by Halpern and Holstein, P(t) must be written as

$$P(t) = D\,(\underline{n},t) \cdot \underline{P}(0), \tag{2}$$

where $D(\underline{n},t)$ represnts a pure rotation matrix with respect to the orientation of the field $\underline{n}$, and the time inteval, t. If the neutrons pass through numbers of domains where the magnetic field inside a domain is kept constant and it varies in neightouring domains, the final value of the polarisation is given as,

$$P_N = D(\underline{n}_N,\ t_N) \cdot D(\underline{n}_{N-1},\ t_{N-1}) \cdot \cdots \cdot D(\underline{n}_1\ t_1) \cdot \underline{P}(0). \tag{3}$$

Since we handle the polychromatic neutrons, we can easily study the time dependent, or dynamical behaviors of the depolarisation. We just demonstrate it as follows. In order to understand the physical concept, we try to consider a simple case, where polarised neutrons pass a ferromagnetic plate, of d in thick, consisting of many magnetic domains, of δ in size. Let's send polarised neutrons along x axis. Polarisation axis is fixed at z axis. Magnetic field was applied along z axis which forces the polarisation outside a plate fixed along z axis. Inside a plate, the magnetic induction Bi is presumably random in direction, but in each domains both the magnitude and the direction of the induction are assumed to be a constant. Then the average of (B) should be zero.

$$(B_x^2) = (B_y^2) = (B_z^2) = 1/3\, B^2, \quad (B_U^i B_V^j) = 0 .$$

If the domain size is large compared with the Larmor period, neutrons pass through every domain with several rotations along Bi. It means that neutron polarisation before entering this particular domain cannot be kept when neutrons go out . Therefore the final polarisation state outside the plate is given as simple form of

$$\underline{P}_f = 3^{-d/\delta}\, \underline{P}_o , \qquad (4)$$

which is independent of neutron velocity.

However as for the opposite case of small domains comparable to the Larmor period, faster neutrons pass through them with less than a period, but slower do with more than one rotation. Consequently the final polarization is dependent on the neutron velocity v.

$$\underline{P}_f \sim \underline{P}_o \exp \{ -1/3\, g^2 (Bi^2)\, \delta d/v^2 \} \qquad (5)$$

We performed the depolarisation measurements by the ferromagnetic alloys of thin elliptic plate. An $Fe_{65}Ni_{35}$ plate was served as the former example of the large domains, while an $Fe_{85}Cr_{15}$ has the small domains if this alloy is quenched from the molten state. Note that in these crystals the multidomain states are realized even in the medium field up to $\tilde{\sim}$ 1 tesla. Polarised neutrons were sent to the sample and the polarisation change after the transmission was detected by the polarisation analyser. In Fig. 1 polarisation is plotted with respect to the square of the wave length. It clearly shows the feature of the velocity dependence in case of $Fe_{85}Cr_{15}$ quenched sample. When the depolarisation was measured in the case

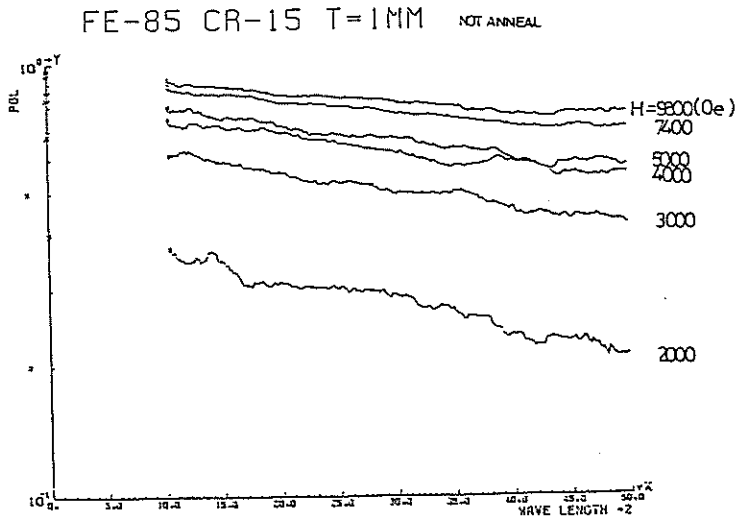

Fig. 1. Polarisation of the neutron beams after the transmission through 1 mm thick $Fe_{85}Cr_{15}$ crystal. It was quenched from the molten state.

of the transmission by an annealed $Fe_{85}Cr_{15}$, the polarisation loss was not seen as shown in Fig. 2. Finally in the transmission results from the $Fe_{65}Ni_{35}$ alloy the depolarisation seems to be independent of the neutron wave length as was expected. We are now going to study the dynamic depolarization studies on the interesting problem of "the critical slowing down" of the spin diffusion and "the reentrant transition from the ferromagnetic to the spin glass state".

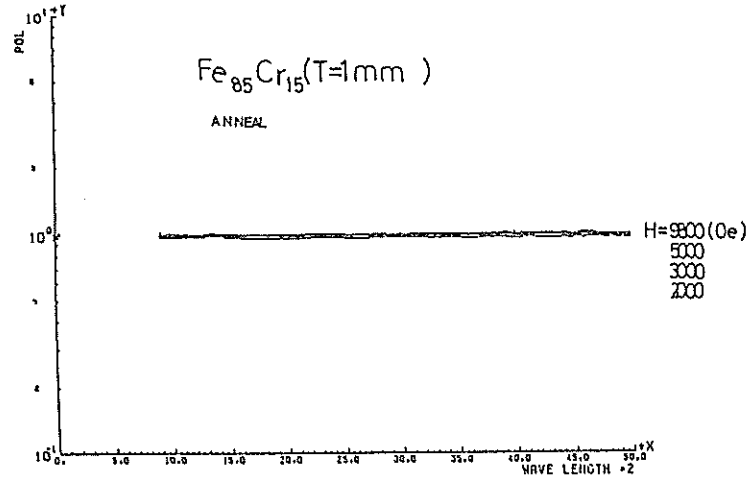

Fig. 2. Polarisation after the transmission of the annealed $Fe_{85}Cr_{15}$

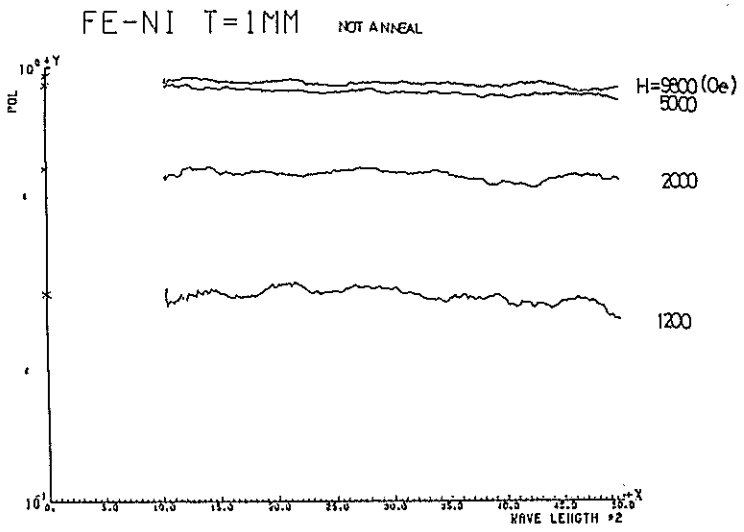

Fig. 3. Polarisation after the transmission of the quenched $Fe_{65}Ni_{35}$

Reference

O. Halpern and T. Holstein, Phys. Rev. 59 (41) 960

MAGNETIC STRUCUTRE OF Ni FINE PARTICLES

Susumu IKEDA

National Laboratory for High Energy Physics, Tsukuba, Ibaraki 305

Yasuo ENDOH

Department of Physics, Tohoku University, Sendai 980

Polarised neutron diffraction measurements provide us unambiguous informations about the surface magnetization in the ferromagnets. The flipping ratio changes with the momentum transfer Q, in other words the surface effect on the ferromagnetism produces an anomalous magnetic form facter. Furthermore the flipping ratis never changes with Q due to the atomic structural moduration. In order to elueidate the effect of the surface and/or interface on the magnetism by using neutron diffraction techniques we must choose such materials as thin films or fine particles since the relative fraction of surface volume of these materials is quite larger than that of usual samples. Besides studies on the artificial superlattice filsm we carried out experiments on the ferromagnetic ultra fine particles. In the latter case we must collect the flipping ratios of the diffuse magnetic scattering with relatively wide range of Q. By this reason we think that TOF method should be feasible.

Ni fine particles are commercially available. We purchased these particles with the specification of the mean size of about 100A, which are obtained by the evaporation in the argon atmosphere. Particles are presumably covered with NiO layers. We carefully compressed them into the pelet by the hydranlytic press. The pelet was situated between the magnetic pole pieces of the electramagnet by which we applied the vertical field up to 1.1 Tesla.

We used 5 detecters which cover from 0.05 A^{-1} to 0.3 A^{-1} in Q range. Spin flipping was functioned evey 2500 msec when the pulses are at rest. Typical TOF patters are shown in Fig.1. The flipping ratio was determined from the data after the currection taking account of the beam polarisation and the flipping efficiency. We plotted the Q dependence of the flipping ratio which are shown in Fig.2. It is quite obvious that the flipping ratio has maximam around 0.10 A^{-1} in Q at room temperature, while this maximum porition seems to shift smaller in Q at 20 K. Note that the maximum value of 1.6 in the flipping ratio and the peak position are in quite good agreement with these obtained by Sato and Hirakawa.

Although our demonstration is not quite new we are sure that the present method measuring the flipping ratio with wide range of Q is very powerful tool to define the magnetic form factor which is largely modified by the effect of surface.

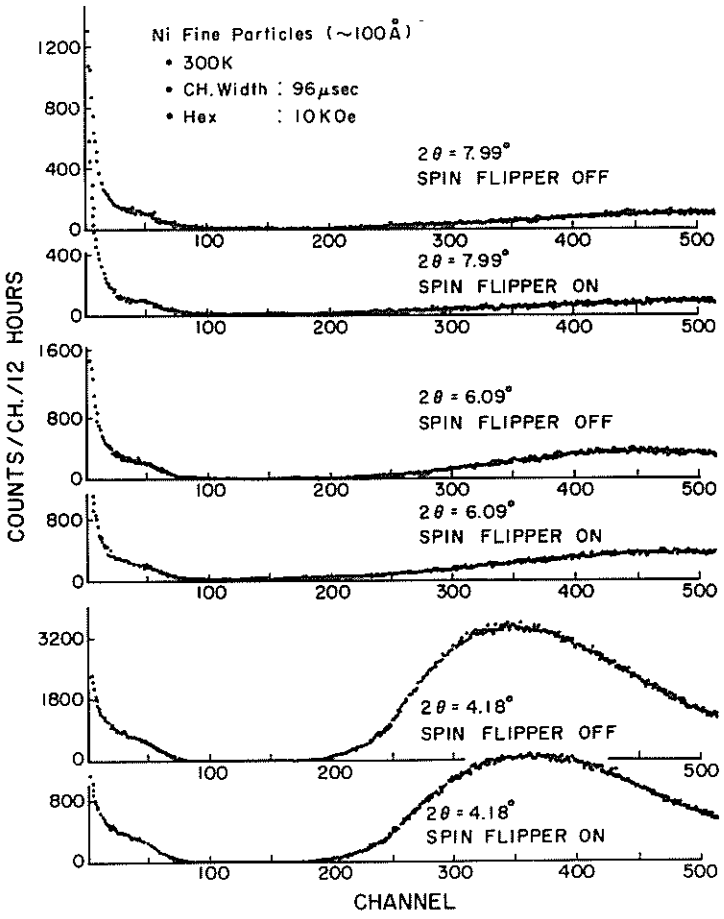

Fig. 1 Raw Data of Polarized Neutron Scattering

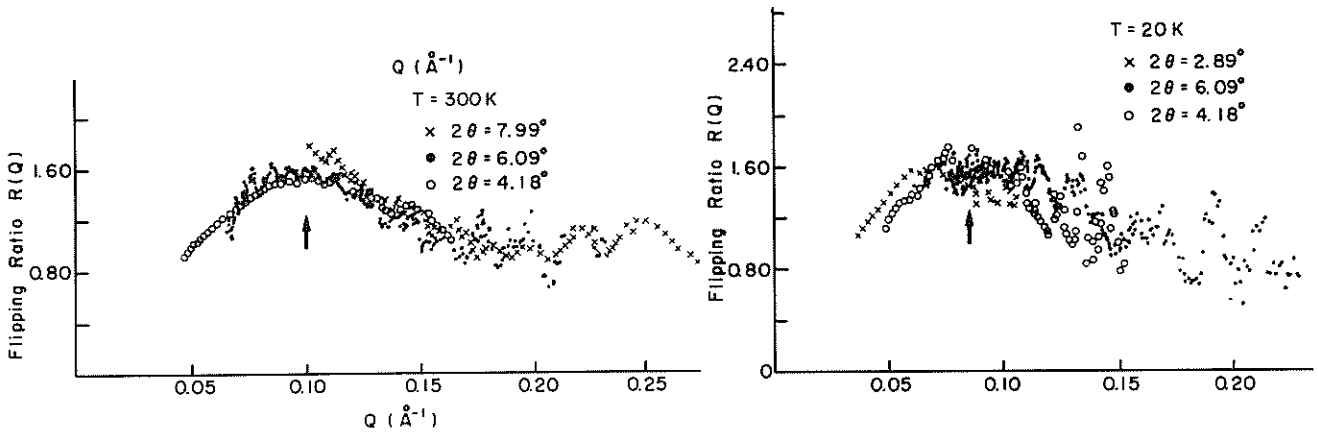

Fig. 2 Flipping Ratio of Ni Fine particles

References

1) M. Sato and K. Hirakawa : J.Phys.Soc.Japan, Vol.39, No.6 (1975)1467
2) Y. Endoh, S. Ikeda, H. Ono, Y. Sasaki, S. Mitsuda and M. Onodera : KEK Report-III(1982)

Some Experiments by using TOP

Takayoshi Takeda, Shigehiro Komura, *Yasuo Endoh and **Susumu Ikeda

Faculty of Integrated Arts and Sciences, Hiroshima University, Hiroshima 730
* Faculty of Science, Tohoku University, Sendai 980
** National Laboratory for High Energy Physics, Tsukuba 305

A performance test of a polariser, and preliminary studies of separation of nuclear and magnetic peaks and of paramagnetic scattering were performed by using a time of flight spectrometer with an optical polariser (TOP) which consists of a neutron polarising system, a magnetic channel with a Drabkin-type spin flipper and a diffractometer with a movable detector arm on which a polarization analysing system can be set [1].

Performance Test of Polariser

A Soller-type polariser with curved magnetic mirrors [2] was constructed for a neutron small angle scattering spectrometer at KUR [3]. Its dimensions and design characteristics were as follows: length L = 300 mm; radius of curvature R = 19.66 m; channel width a = 0.4 mm; number of channel, 80; total beam cross section, 50 mm(height) x 36 mm(width); the polarising material is $Co_{60}Fe_{40}$ alloy evaporated on a Mylar foil. The polarising efficiency and transmission measurements were made by measuring the flipping ratio when the polariser was set on the detector arm as an analyser. The characteristic cut-off wavelength was near 3.7 A. The polarising efficiency and transmission were 0.9 and 0.4,respectively, near λ = 4 A.

Isothermal Separation of Nuclear and Magnetic Peaks

When the neutron polarization is parallel to the scattering vector $\vec{K}$ ($\hat{P}\cdot\hat{K} = 1$), the partial cross sections for Bragg scattering are

$$\frac{d\sigma^{++}}{d\Omega} = \frac{d\sigma^{--}}{d\Omega} = \sum_{ij} \exp(i\vec{K}\cdot(\vec{r}_i - \vec{r}_j)) b_i b_j^{*} \quad , \qquad (1)$$

and

$$\frac{d\sigma^{+-}}{d\Omega} = \frac{d\sigma^{-+}}{d\Omega} = \sum_{ij} \exp(i\vec{K}\cdot(\vec{r}_i - \vec{r}_j)) p_i p_j^{*} (\vec{S}_i\cdot\vec{S}_j^{*} + i\hat{z}(\vec{S}_i \times \vec{S}_j^{*})) \quad , \qquad (2)$$

where $\vec{S} = \vec{S} - (\vec{S}\cdot\hat{K})\hat{K}$ and $\hat{z}//\hat{P}$. The magnetic scattering is spin-flip

and the nuclear scattering is non-spin-flip [4]. For many antiferromagnets, some of magnetic peaks will come at same scattering angle as a nuclear peak. The magnetic intensities are usually obtained by subtraction of nuclear intensities measured at a temterature above the Néel point. Sometimes, this procedure involves large Debye-Waller corrections, or more seriously, the crystal structure may change at or below the Néel point. The isothermal separation of nuclear and magnetic peaks is very useful to such cases. A preliminary study of this technique was performed for α-Fe_2O_3 . The results are shown in Fig. 1. Magnetic peaks (1 1 1) and (1 0 0) were not observed in the spin-flipper-off(non-spin-flip) but in the spin-flipper-on(spin-flip) TOF spectra.

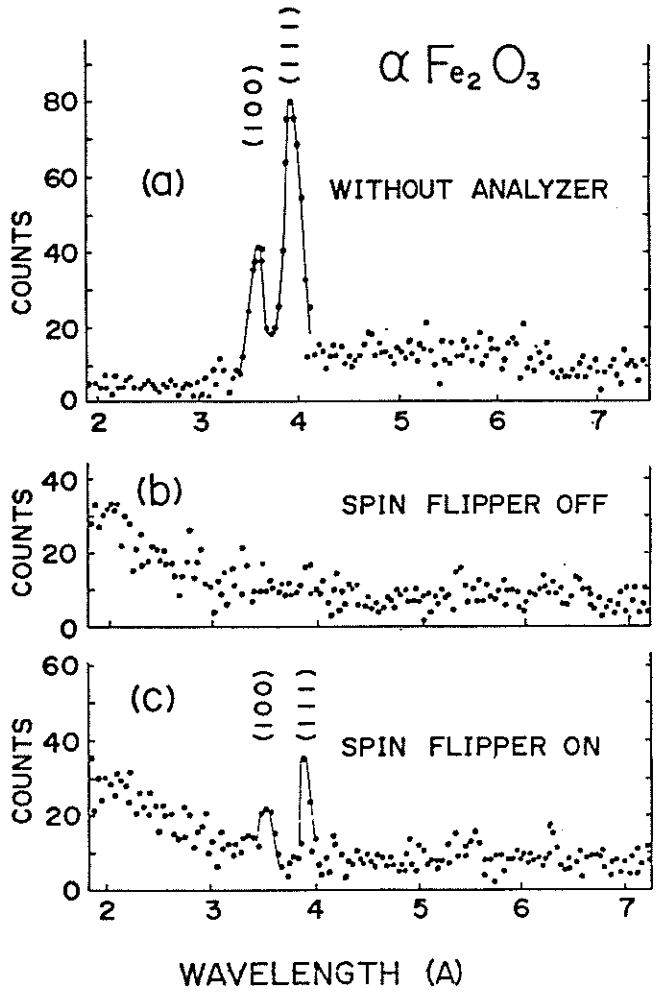

Fig. 1. TOF spectra of α-Fe_2O_3 when $2\theta = 50°$ and $\hat{P}\cdot\hat{K} = 1$. Isothermal separation of nuclear and magnetic peaks by using the neutron polarization analysis technique.

Paramagnetic Scattering

The partial cross sections for paramagnetic scattering are

$$\frac{d\sigma^{++}}{d\Omega} = \frac{d\sigma^{--}}{d\Omega} = \frac{1}{3}\left(\frac{\gamma e^2}{2mc^2}\right)^2 f(\vec{K})^2 g^2 S(S+1)\left(1 - (\hat{P}\cdot\hat{K})^2\right) , \qquad (3)$$

and

$$\frac{d\sigma^{+-}}{d\Omega} = \frac{d\sigma^{-+}}{d\Omega} = \frac{1}{3}\left(\frac{\gamma e^2}{2mc^2}\right)^2 f(\vec{K})^2 g^2 S(S+1)\left(1 + (\hat{P}\cdot\hat{K})^2\right) . \qquad (4)$$

If $\hat{P}\cdot\hat{K} = 1$, the scattering will be entirely spin-flip. If $\hat{P}\cdot\hat{K} = 0$, the scattering will consist of equal parts of spin-flip and non-spin-flip[4]. With polarization analysis, many of the most difficult problems in analysis of paramagnetic scattering data are completely avoided , whereas isotope disorder, multiple Bragg, thermal diffuse(phonon), Bragg, nuclear spin incoherent and paramagnetic scattering may be present in the usual diffuse scattering experiment.

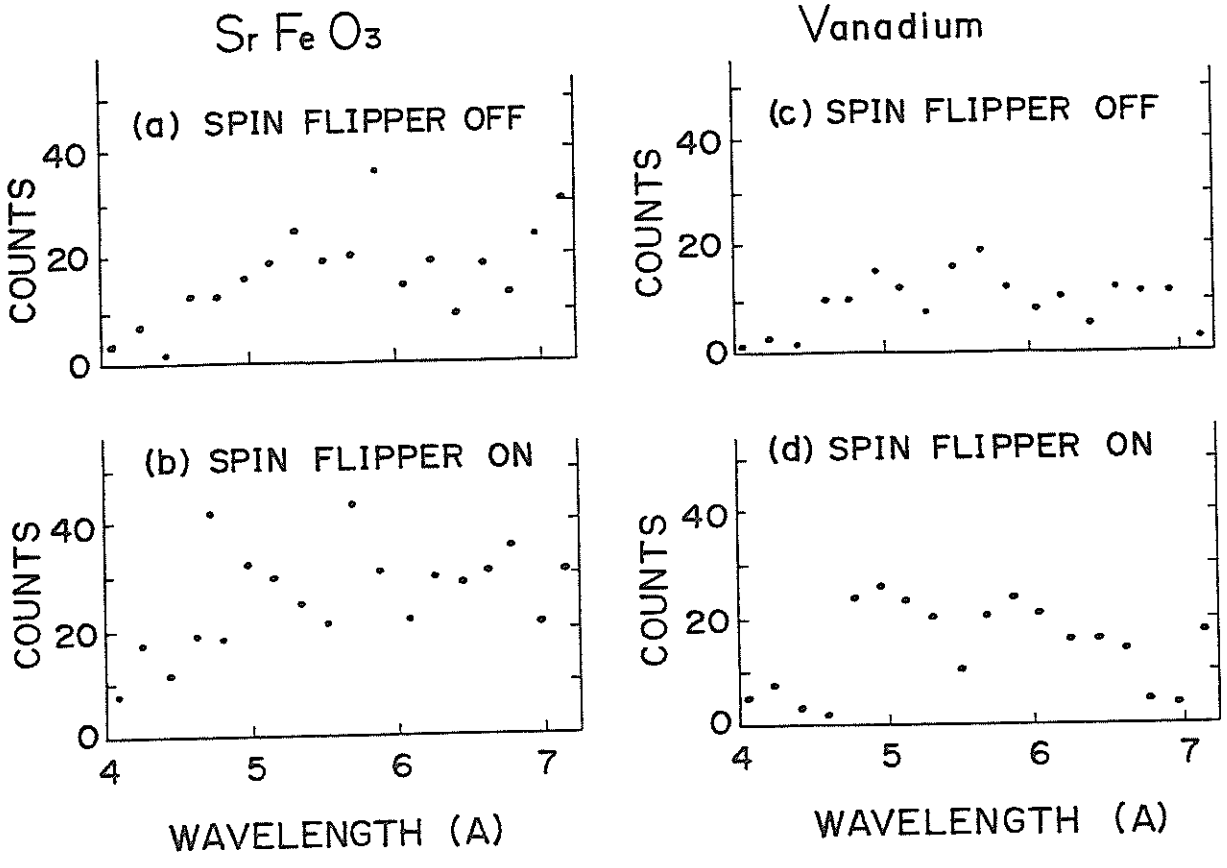

Fig. 2. TOF spectra of $SrFeO_3$ and vanadium when $2\theta = 15°$ and $\hat{P}\cdot\hat{K} = 1$. Paramagnetic scattering by using the neutron polarization analysis technique.

In $SrFeO_3$ with a helical spin structure, the intensity of the (0 0 0) satellite peak in neutron diffraction is lower than that expected from other satellite peaks [5]. The magnetic form factor $f(\vec{K})$ at small scattering vectors $\vec{K}$ will reflect the effects of conduction electron polarization and covalency. Therefore, the paramagnetic scattering experiment of $SrFeO_3$ was performed by using the neutron polarization analysis technique in order to know $f(\vec{K})$ at low $\vec{K}$. Vanadium was used as a standard sample. The scattering from vanadium is nuclear-spin-incoherent scattering whose partial cross sections are

$$\frac{d\sigma^{++}}{d\Omega} = \frac{d\sigma^{--}}{d\Omega} = \frac{1}{3} B^2 I(I+1) \quad , \qquad (5)$$

and

$$\frac{d\sigma^{+-}}{d\Omega} = \frac{d\sigma^{-+}}{d\Omega} = \frac{2}{3} B^2 I(I+1) \quad . \qquad (6)$$

The results are shown in Fig. 2 , where background counts were subtracted. Though the statistical error was too large to know $f(\vec{K})$, the spin of Fe S was estimated to be 2.1 if we assumed that $f(\vec{K}) = 1$ and summed up the intensities over $K = 0.23 \sim 0.41\ A^{-1}$.

References

1) Y. Endoh, J, Mizuki, Y. Sasaki and H. Ono: KENS Report II (1981) 609.

2) J. B. Hayter, J. Penfold and W. G. Williams: J. Phys. E 11(1978) 454.

3) S. Komura, T. Takeda, H. Fujii, K.Osamura, K. Mochiki and K. Hasegawa: to be published in Proc. Yamada Conference VI (1982).

4) R. M. Moon, T. Riste and W. C. Koehler: Phys. Rev. 181 (1969) 920.

5) T. Takeda, S. Komura and N. Watanabe: Ferrites, ed. H. Watanabe, S. Iida and M. Sugimoto (Center for Academic Publications Japan, 1981) 385.

Temperature Dependence of the Magnetic Excitation in Antiferromagnetic γFeMn Alloy

Keisuke Tajima, Kenji Kanai,† Yoshikazu Ishikawa†
and Shoichi Tomiyoshi††

Physics Department, Faculty of Science and Technology,
Keio University, Hiyoshi, Yokohama 223

†Physics Department, ††Institute for Iron, Steel and Other Metals,
Tohoku University, Sendai 980

The f.c.c. γFeMn alloy exhibits an itinerant antiferromagnetic character.[1] The magnetic excitations in this material were measured by means of 3-axis spectrometer as reported in Ref.2) and it was found that the spin wave dispersion curves are steep and diffuse in the $\hbar\omega$-q space, which seems to be the typical feature in an itinerant antiferromagnet.[3] The measurements have been extended both in the $\hbar\omega$-q space and in the temperature range by using the MAX spectrometer. The experiments were performed along the [100] direction around the (100) and (110) reciprocal lattice points at various temperatures up to 1.5 T_N. The time of flight spectra observed at several temperatures are shown in Fig.1. Two

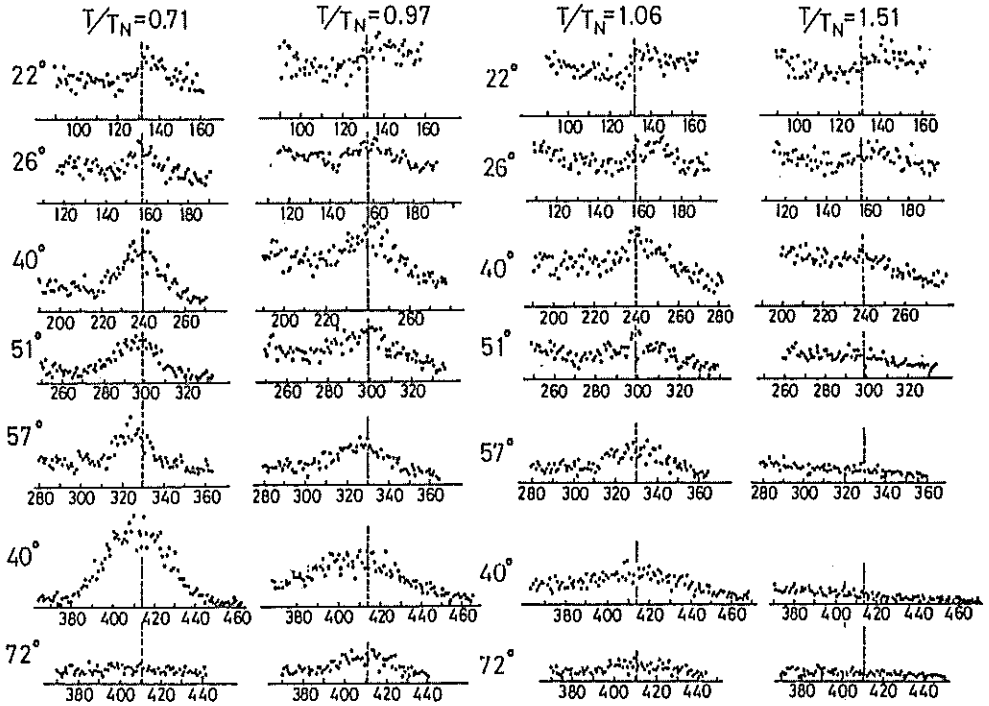

Fig. 1. The time of flight spectra observed at several temperatures. Vertical dotted lines indicate the position corresponding to the (110) or (100) reciprocal lattice point. The scattering angle is shown in each spectrum.

peaks, one on each side of a reciprocal lattice point, should be observed. However, they could not be separated from each other, mainly because of their short life times of the magnetic excitation. The contour maps of the scattering intensity may be constructed from the observed spectra after various instrumental corrections such as the volume of the resolution functions and the reflectivity of each analyser crystal as well as the intensity of the incident neutron beam flux. Preliminary results are shown in Fig.2. These contour maps clearly show that the low energy

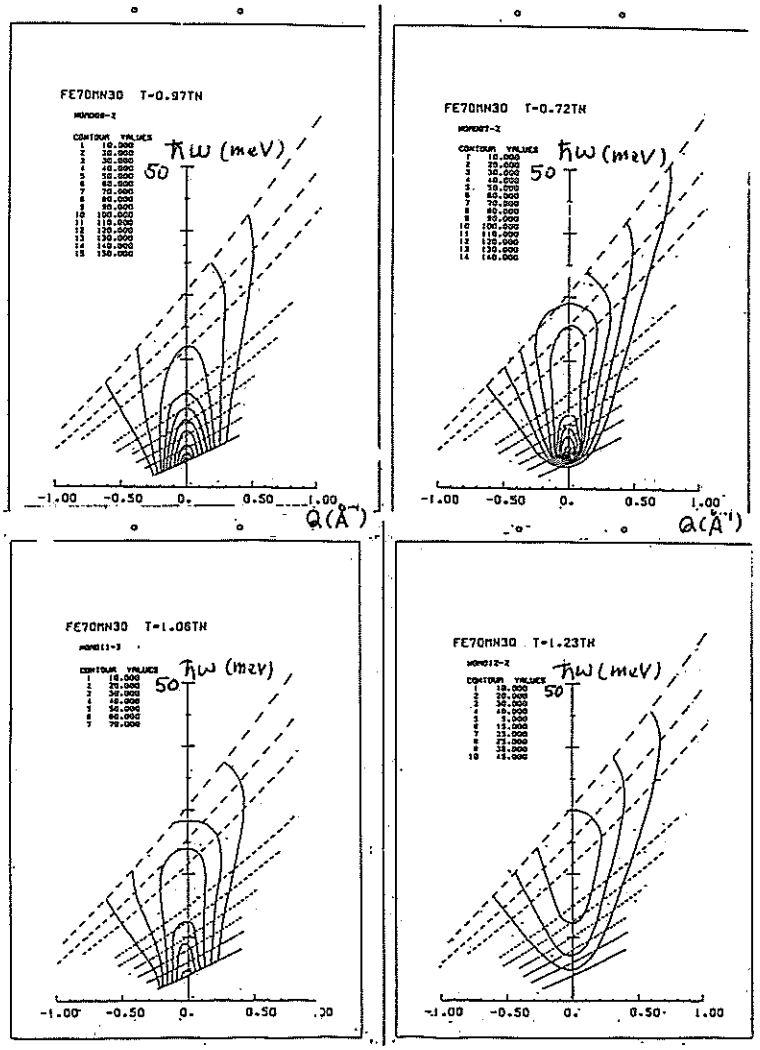

Fig. 2. The contour maps of the scattering intensity after instrumental corrections. (Preliminary)

excitations are renormalized and smeared out just above T_N while the intensities and life times of the higher energy excitations remain almost unchanged even at $T=1.5\ T_N$. Further measurements are now in progress.

References

1) e.g., Y. Endoh and Y. Ishikawa; J. Phys. Soc. Jpn. 30 (1971), 1614.
2) K. Tajima et al.; J. Phys. Soc. Jpn. 41 (1976), 1195.
3) e.g., M.J. Gillan; J. Phys. F 3 (1973), 1874.

A HIGH RESOLUTION CRYSTAL SPECTROMETER FOR HIGH ENERGY INCOHERENT NEUTRON SCATTERING

Susumu IKEDA and Noboru WATANABE
National Laboratory for High Energy Physics
Oho-machi, Tsukuba-gun, Ibaraki-ken, 305, Japan

Kenzo KAI
The Research Institute for Iron, Steel and Other Metals
Tohoku University, Sendai, 980, Japan

Sadae YAMAGUCHI
Department of Neuclear Engineering, Faculty of Engineering
Tohoku University, Sendai, 980, Japan

A high resolution crystal spectrometer has been built and operated at KENS. The instrument will make possible large energy transfer incoherent neutron scattering in the range $\varepsilon = 0.05 \sim 1$ eV, with resolution of about $\Delta\varepsilon/\varepsilon = 0.02$ in the entire range of energy transfer. The instrument is an inverted geometry type; the scattered neutrons are detected at a fixed energy by a large analyzer crystal, while the incident neutron energy is determined from the measured total time of flight, t, using the following relation,

$$t = \frac{L_i}{V_i} + \frac{L_f}{V_f} , \qquad (1)$$

where L_i, L_f, V_i, and V_f are incident (i) and scattered (f) flight paths lengths and neutron velocities, respectively.

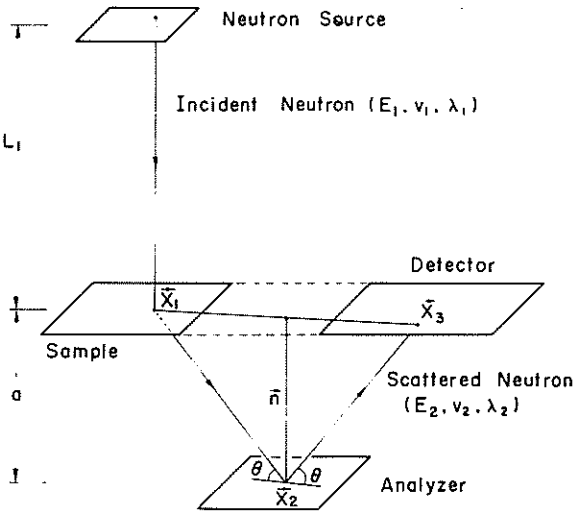

Fig. 1 Principle of Spectrometer

In this type of spectrometer, generally speaking, uncertainty in the second term becomes large due to the finite extent of sample, analyzer, and detector. This reflects on the first term through the equation and results in the poor definition of the incident energy. If we put the sample and the detector on a plane, and set the analyzer parallel to this plane as shown in Fig. 1, then two dimensional focussing is realized in time of flight between sample and detector. This focussing geometry make it possible to improve the energy resolution without sacrificing the geometric counting efficiency. A prototype spectrometer of this type was developed and operated at Tohoku linac[1-3]. In the new machine at KENS, signal to background ratio has been largely increased with an improved energy resolution. Momentum transfer, Q, is rapidly increased with energy transfer, ε, due to the low final energy, but the spectrometer will be useful for the measurements of the local mode of hydrogens in metalic hydrides, for the molecular spectroscopy, etc., where the value of Q is not crucial and the Q-dependence is not so important. Similar instruments were operated also at the pulsed neutron facilities of Harwell linac[4], ZING-P' at Argonne[5], and WNR, at Los Alamos[6]. Figure 2 shows the spectrometer configuration.

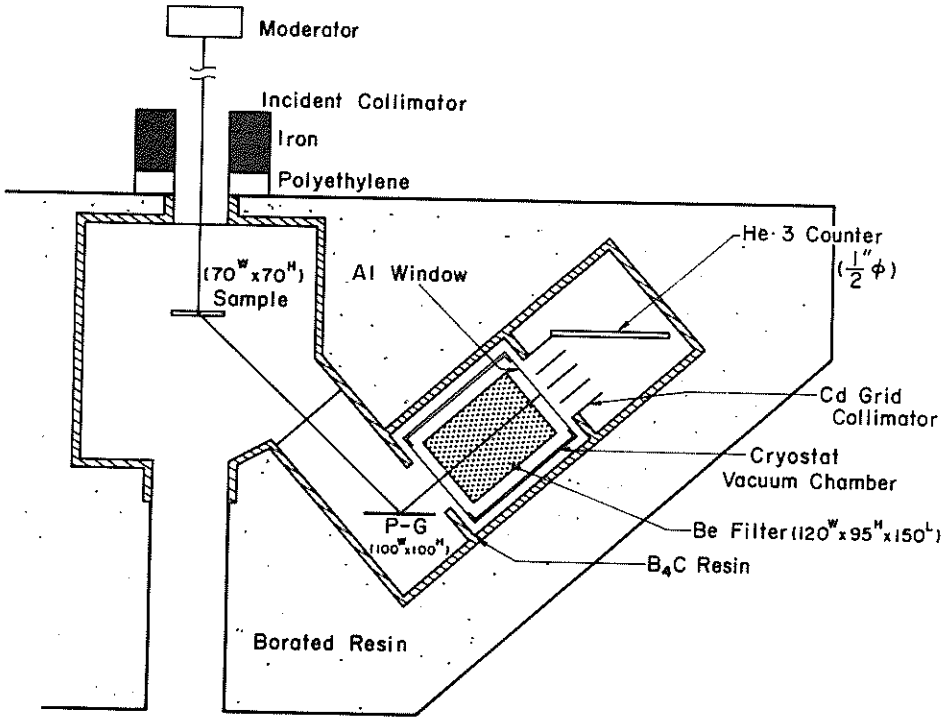

Fig. 2 Spectrometer configuration

The instrument has been installed at H-7 beam hole which views the surface of a moderator (polyethylene slab at room temp.) perpendicularly. Maximum beam size at sample position is 7 cm^W x 7 cm^H. In order to minimize the ambiguity of the incident flight path length, a plane sample is set perpendicularly to the beam at L_1 = 5.299 m. The analyzer crystal is a 10 cm x 10 cm pyrographite (mosaic spread 1.2°). Bragg angle of $\theta_B \sim 43°$ is used, and 002 reflection corresponds to E_f = 4 meV. Eight He-3 proportional counters, 1/2 inches in diam. and 12 inches in active length filled to 20 atoms pressure, are set in horizontal direction to form a detector plane. In the present configuration, center line distance between sample and analyzer, and that between analyzer and detector are 36 cm respecively which correspond to inter plane distance a = 24.228 cm. A beryllium filter (9.5 cm^H x 12 cm^W x 15 cm^L) cooled to liquid nitrogen temperature is used between analyzer and detector with a post cross collimator made of cadmium, in order to eliminate neutrons due to higher order reflections. Sample-analyzer-detector system is buried in a shield box of 2 cm thick B_4C and 25 cm thick borated resin wall.

Extensive studies of the energy resolution were performed by a Monte Carlo computer simulation for sample-analyzer-filter detector system. Figure 3 shows the effect of the mosaic spread, β, in the analyzer crystal on the time distribution of the scattered neutrons, which indicates that mismatch in time focussing due to the finite value in β is not significant in this spectrometer. The most probable value of t_f is determined to be t_f = 821 μsec from this result.

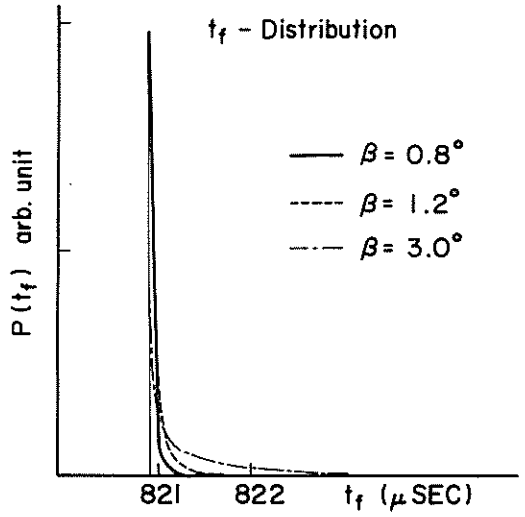

Fig. 3 Time distribution of scattered neutrons due to finite mosaic spread

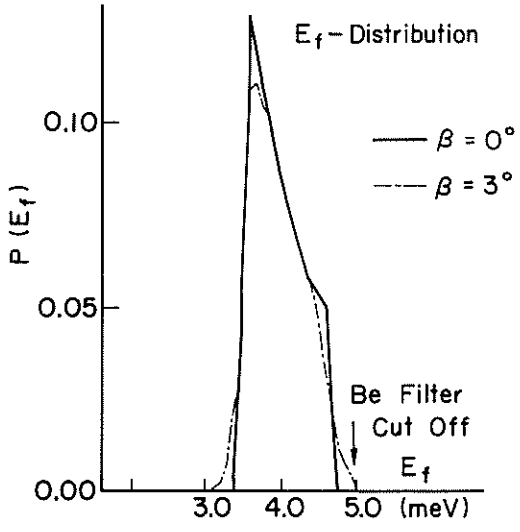

Fig. 4 Energy distribution of scattered neutrons

Figure 4 shows the calculated energy spectrum of the scattered neutrons. The width is fairly wide which is consistent with measurement, and from this distribution, mean value of E_f is determined to be $\overline{E}_f$ = 3.9 meV.

The effect of the finite size and circular cross section of the detector was also studied. Even with 1/2" diam. counter, the effect seems significant, and if necessary we can improve the resolution by placing a proper cadmium mask, with a sacrifice in counting efficiency by about 30 %. Calculated values of the total and partial resolution are shown in Fig. 5 as a function of energy transfer.

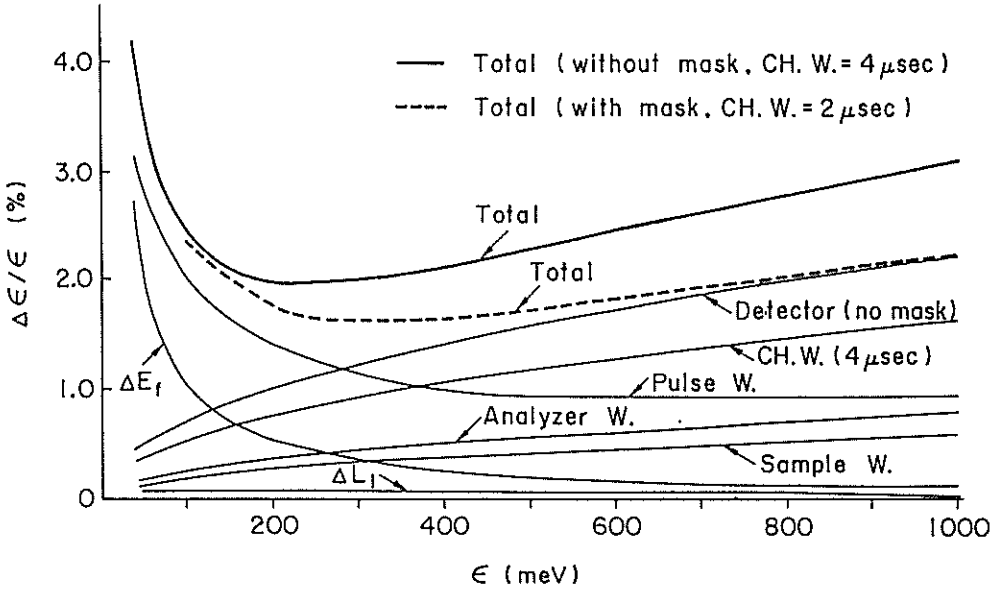

Fig. 5 Total and partial energy resolution

In order to test the performance of the spectrometer, local vibration mode of hydrogens in various metalic hydride samples has been measured[7-8]. In Fig. 6 is shown a typical raw data of TOF spectrum obtained from TiH_2 at room temperature which demonstrates the extremely low background level compared to the results obtained at other laboratories. Even at the time corresponding to $\varepsilon = \infty$, background is low enough to observe a small step increase in the spectrum at this time. Higher performance in the energy resolution is demonstrated in Fig. 7 in the form of double differential cross section which is obtained from the raw data in Fig. 6. Higher harmonics are clearly observed up to 5th order with their fine structures.

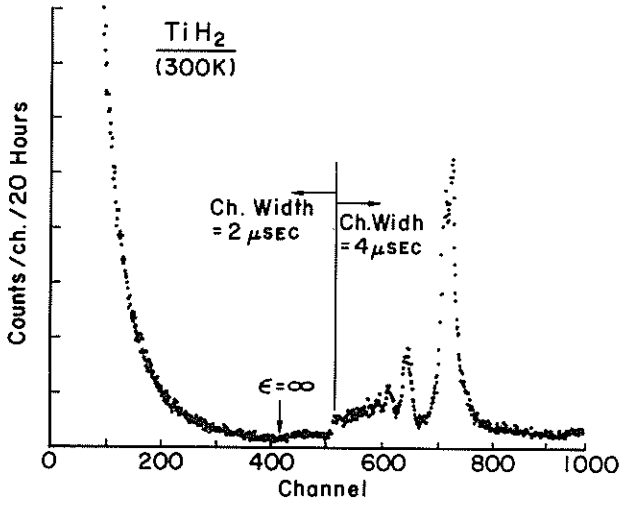

Fig. 6 TOF spectrum (raw-data) of TiH_2

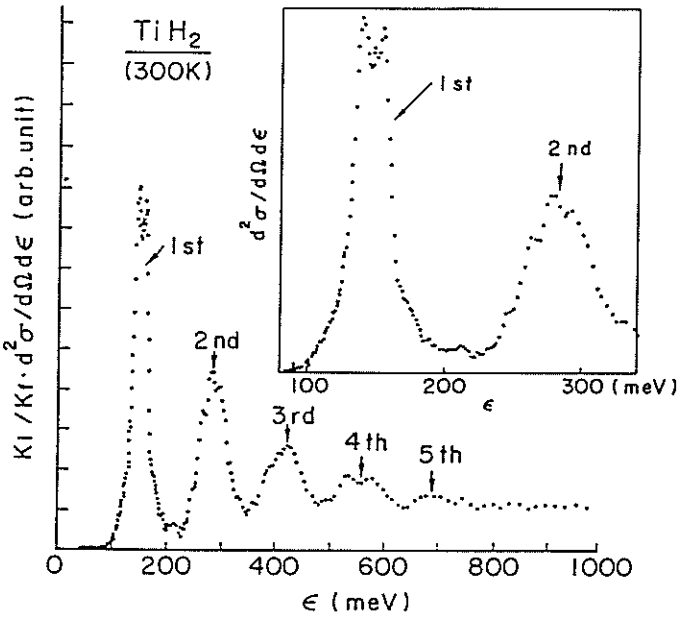

Fig. 7 Double differential cross section of TiH_2

References

1) N. Watanabe, M. Furusaka and M. Misawa, Research Rep't. Lab. Nucl. Sci., Tohoku Univ. 12 (1979) 72 (in Japanese).

2) M. Furusaka, N. Watanabe and H. Asano, ibid. 12 (1979) 83 (in Japanese).

3) N. Watanabe and M. Furusaka, KENS Report I, KEK Internal 80-1 (1980) 181.

4) D. H. Day and R. N. Sinclair, J. Chem. Phys. 55 (1971) 2870.

5) K. Sköld, K. Crawford and H. Chen, Nucl. Instrum. Methods 145 (1977) 117.

6) J. Eckert, R. N. Silver, A. Soper, P. J. Vergamini, J. Goldstone, A. Larson, P. A. Seeger and J. Yarnell, Proc. ICANS-IV (1981) 434.

7) S. Ikeda, N. Watanabe and K. Kai, KENS Report III, KEK Internal (1982).

8) K. Kai, S. Ikeda and N. Watanabe, ibid.

Fine Structure of Localized Models in Metal Hydrides

S. Ikeda and N. Watanabe

National Laboratory for High Energy Physics
Oho-machi, Tsukuba-gun, Ibaraki-ken, 305, Japan

K. Kai

The Research Institute for Iron, Steel and Other Metals
Tohoku University, Sendai, 980, Japan

The localized mode frequency spectra of hydrogens in metal hydrides provide important information about these system. Especially detailed shape or the structure, and location of the optical peaks up to higher harmonics is important to discuss anharmonic potential of hydrogen. However, none of these data was reported in the literature. We have measured the localized mode of ZrH_x (x = 1.41 and 1.93) and $TaH_{0.5}$ by a high resolution down scattering neutron spectrometer, CAT[1], at KENS.

Figures 1 and 2 show the preliminary results of measured spectra of $ZrH_{1.41}$, $ZrH_{1.93}$ and $TaH_{0.5}$. Higher harmonics were clearly observed up to 5th harmonics. Furthermore, their fine structures were observed, for the first time, in higher harmonics as well as in fundamentals.

The locations of the peaks are listed in Table 1. It is obvious that the frequencies for higher harmonics are shifted by appreciable amounts from the respective harmonic positions, and from these frequency shifts we can determine the anharmonicity parameters of the hydrogen potential. The striking feature of the fine structures in the higher harmonics is that the separation or the split of the subpeaks in the respective orders becomes more pronounced at higher harmonics.

	1st (meV)	2nd (meV)	3rd (meV)	4th (meV)	5th (meV)
$ZrH_{1.93}$ (300 K)	138 145 154	257 274 293	389 415	500 531	644 677
$ZrH_{1.41}$ (300 K)	137 141 146	260 274 297	394 433	493 531 565	644 666
TiH_2 (300 K)	139 148 154 171	263 280 304	394 405 433	523 565	678 740
$TaH_{0.5}$ (300 K)	122 130 162 167	223 236 277 318			
$TaH_{0.5}$ (30 K)	124 130 161	225 239 277			

Table 1. Location of Localized Mode

In the fundamental peak for $ZrH_{1.93}$, there are two sub-peaks at about 138 meV and 145 meV with a shoulder at about 154 meV. The results is consistent with the reported values by Couch, et al.[2] There exists a distinct difference between the fine structures of $ZrH_{1.41}$ (cubic) and those of $ZrH_{1.93}$ (tetragonal), especially in the 2nd harmonics. (See Fig. 1(a) and (b).)

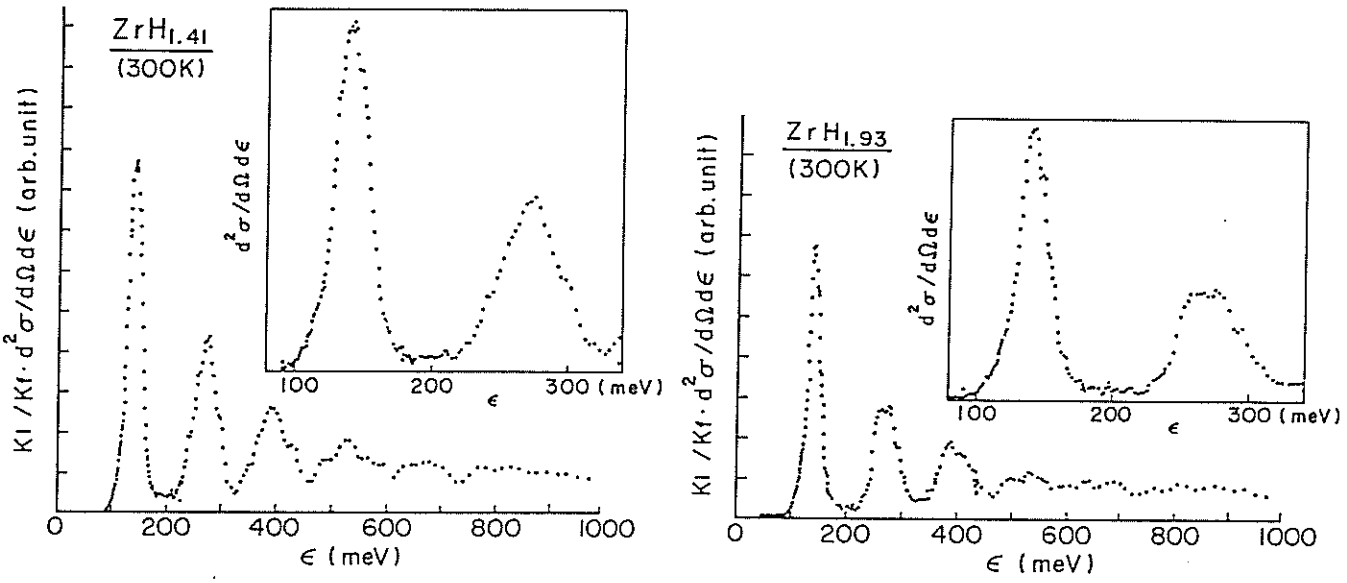

(a) (b)

Fig. 1 Double Differential Cross Section of $ZrH_{1.41}$ (a) and $ZrH_{1.93}$ (b)

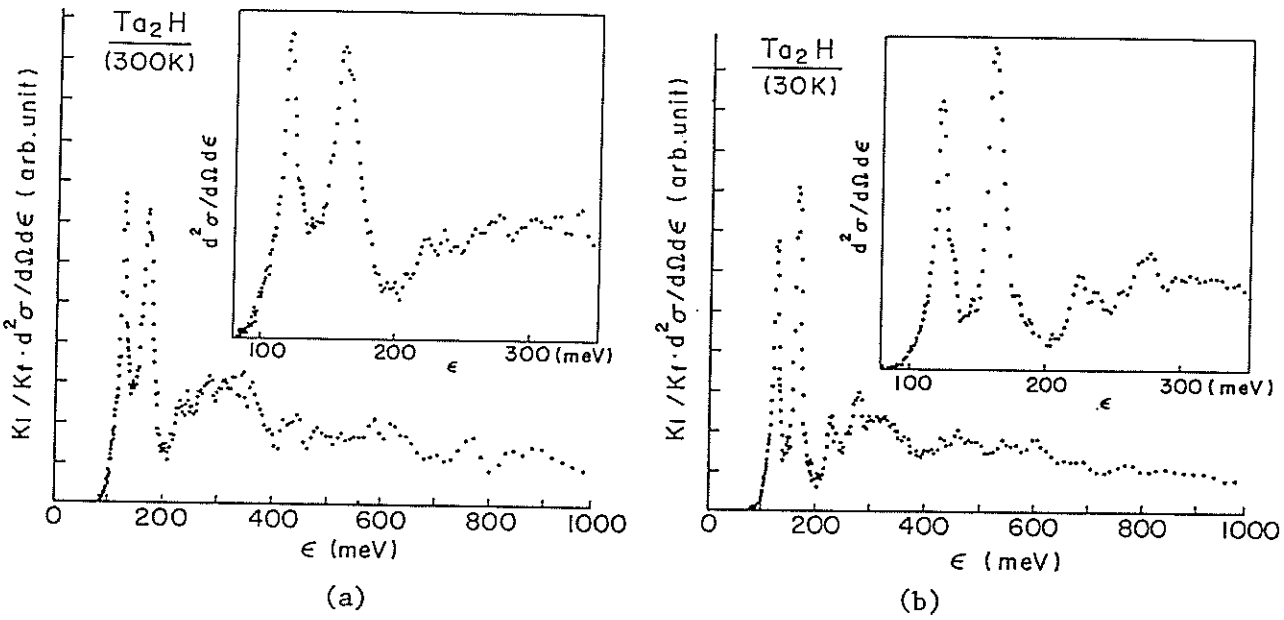

Fig. 2 Double Differential Cross Section of TaH_2 (300 K) and TaH_2 (30 K)

In $TaH_{0.5}$ at room temperature, the lower fundamental peak ($\sim$ 120 meV) has a shoulder at about 130 meV, and the higher fundamental ($\sim$ 160 meV) splits into two peaks. Hempelmann, et al. have measured $TaH_{0.08}$ and fitted the higher fundamental peak by two Gaussians[8]. The present results are qualitatively consistent with theirs. They have found the second harmonics of the lower fundamental at about 227 meV which may correspond to our peak at 223 meV. In the present spectrum, many extra peaks are observed above this energy (See Fig. 2(a)). Some of them may be attributed to the multi-phonon contribution of the fundamentals. Assignement of the peaks are now in progress. Similar measurements at low temperature were performed to observe well defined second harmonics, and the results are shown in Fig. 2(b).

References

1) S. Ikeda, N. Watanabe, K. Kai and S. Yamaguchi: "A High Resolution Crystal Spectrometer for High Energy Incoherent Neutron Scattering" KENS report-III (1982).

2) J. G. Couch, O. K. Harling and Lavern. C. Clune: Phys. Rev. B 4 (1971) 2675.

3) R. Hempelmann and D. Richter: Z. Phys. B - Condensed Matter, 44 (1981) 159.

LOCAL ENVIRONMENT AROUND HYDROGEN ATOMS IN HYDROGENATED $NiTi_2$ ALLOY GLASS BY HIGH RESOLUTION NEUTRON SPECTROMETER

K. Kai, S. Ikeda*, N. Watanabe* and K. Suzuki

The Research Institute for Iron, Steel and Other Metals
Tohoku University, Sendai 980, Japan
*National Laboratory for High Energy Physics, Oho-machi,
Tsukuba-gun Ibaraki-ken 305, Japan

Recently hydrogenated metallic glasses are interesting from fundamental points of view and from practical ones.

In order to investigate a local environment experienced by hydrogen atoms residing in the central hole of polyhedral unit structures of metallic atoms, we have measured the optic vibration of hydrogen atoms in crystalline TiH_2, $NiTi_2H_{0.9}$, $NiTi_2H_{0.5}$ and a glassy $NiTi_2H_{0.5}$ using a high resolution crystal analyser T-O-F spectrometer(CAT) [1] installed at a spallation neutron source of KEK.

$NiTi_2$ alloy glass ribbons were prepared by rapidly-quenching the melts in Ar gas atmosphere. Hydrogen atoms were charged into $NiTi_2$ alloy glass at 130°C under about 30 atoms pressure, and also charged into $NiTi_2$ crystals at 300°C.

Figure 1 shows the measured spectra of optic mode. The spectrum was measured up to several hundreds meV with extremely high signal to background ratio and very high energy resolution ($\Delta E/E \sim 2\%$ in the entire energy transfer range). The striking new result of this work is the observation of well defined higher harmonics of the local mode in glassy metallic hydride. Higher harmonics in the glassy sample are clearly observed up to 4th or 5th order at low temperature as in crystalline sample, while a rapidly damping oscilation occurs beyond 3rd higher harmonics at room temperature.

The location and width of the optic peaks in Fig. 1 are summarised in Table 1: (1) The location of 2nd or 3rd harmonics is found to be shifted by about 10 meV or 35 meV respectively from the

harmonics positions $n\hbar\omega_1$ (n=2,3...) in glassy sample as well as in crystalline ones, which implies anharmonicity for hydrogen potential is significant in this system. (2) The low-energy shoulder appearing at $\hbar\omega \leq 100$ meV in the crystalline $NiTi_2H_{0.5}$ is also found in the glassy state. According to X-ray and neutron diffraction of crystalline $NiTi_2H(D)_{0.5}$ [2], H or D atom occupies the 8b or 16d (octahedral) site as well as the 8a (tetrahedral) site. The low-energy shoulder seems to be contributed from hydrogen atoms in the octahedral site. Hydrogen atoms in the glassy state are trapped in the nearly same environment as appears in the crystalline state. (3) Considerable peak broadnings are present in the glassy state even at low temperature, which are accompanied by shift of the peak by ~5% to lower energy respective to the crystalline state. This result suggests some contributions from the chemical and topological disorders in the local environment around hydrogen atoms as well as the hydrogen-hydrogen interaction as shown in the $\beta \rightarrow \alpha$ order-disorder phase transition of $NbD_{0.85}$ [3].

References

1. S. Ikeda, N. Watanabe and K. Kai, this report.
2. H. Buchner, M. A. Gutijar, K-D. Beccu and H. Säufferer, Z. Metalkd. 63 (1972) 497.
3. D. Richter and S. M. Shapiro, Phys. Rev. B 22 (1980) 599.

Table 1. Central positions and line widths of the 1st, 2nd and 3rd optic vibrational modes in glassy and crystalline $(NiTi_2)H_x$ alloys, and TiH_2 crystal.

(meV)

	1st peak		2nd peak		3rd peak	
	$\hbar\omega$	FWHM	$\hbar\omega$	FWHM	$\hbar\omega$	FWHM
a-$(NiTi_2)H_{0.5}$ R. T.	139 ± 2	74 ± 5	271 ± 3	106 ± 10		
L. T.	138 ± 2	66 ± 5	281 ± 3	93 ± 10	405 ± 10	140 ± 20
c-$(NiTi_2)H_{0.5}$	146 ± 2	36 ± 5	282 ± 3	67 ± 10	406 ± 8	90 ± 20
c-$(NiTi_2)H_{0.9}$	140 151 ± 2	47 ± 5	282 ± 3	90 ± 10	408 ± 8	130 ± 20
TiH_2	138 149 ± 2	31 ± 2	260 281 ± 3	55 ± 5	390 424 ± 8	96 ± 10

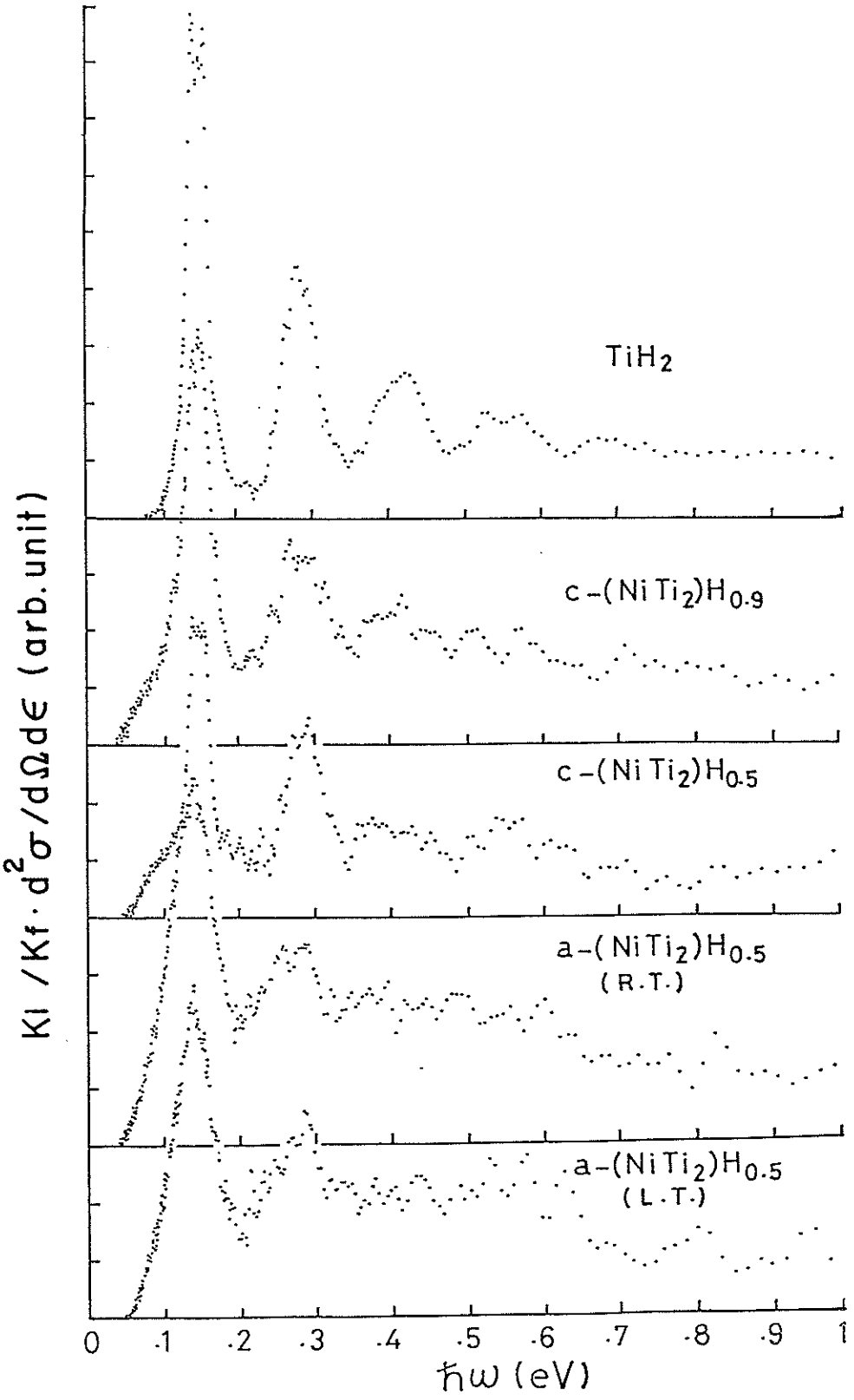

Fig. 1. Energy spectra of the optic modes from glassy and crystalline $(NiTi_2)H_x$ alloys, and TiH_2 crystal. Coordinate shows (double differential cross section)X$[k_i/k_f]$. k_i and k_f are the incident and scattered neutron wave vectors.

Four-circle Single Crystal Diffractometer (FOX)

Isao Kawada, Mitsumasa Isobe, Fujio Okamura,
Nobuo Niimura* and Jimpei Harada**

National Institute for Research in Inorganic Materials,
Sakura-mura, Ibaraki 305.
* Laboratory of Nuclear Science, Tohoku University, Sendai 982.
** Department of Applied Physics, Faculty of Engineering, Nagoya University, Nagoya 464.

In March 1981 this diffractometer was installed at the H1 beam hole of KENS. The possible applications of this diffractometer are:

(i) Structure analysis with elastic Bragg reflections.
(ii) Diffraction measurements under high or low temperatures etc.
(iii) Detailed investigations of 2- or 3-dimensional reciprocal space (including diffuse scattering) in case of equipping 1- or 2-dimensional position sensitive detectors.

This instrument has a large χ-circle (inner diameter = 500 mm). χ-circle plane is located 100 mm outside the θ-circle axis and ϕ-circle axis. The four axes are controlled by pulse-motors with an accuracy of 0.01°. Each axis has three modes of rotating speed as shown in Table 1. as well as inching movement. The possible measurement range of 2θ is from -50° to 163°. Until March 1982 the angle setting was performed by manual, because the controlling microcomputer system has not yet been accomplished.

Two incident collimators of B_4C are provided with the opening of 30 mm in diameter and 300 mm in length or 10 mm in diameter and 300 mm in length. One of them is used by an experiment. Two sets of half slits (top and bottom, left and right) with small $^{10}B_4C$ edges are equipped before the receiving slit. The receiving slit is a sintered B_4C block with an opening of 10 mm in diameter and 20 mm in length.

The detector is Helium-3 proportional counter of 1" in diameter and 6" in active length filled to 9.5 atm. of enriched ^3He (Reuter-Stokes RS-P4-0806-246).

Three steps of attenuators can be set before the incident collimator but have not yet been equipped. The flight path length from the target to the detector has been determined to be 627.3 cm. The schematic drawing of FOX is given in Fig. 1. and the measurable energy range (wave length) at each 2θ angle setting is shown in Fig. 2. Diffraction patterns of single crystals of silicon (r.t.) and $BaTiO_3$ (at 125° C) are shown in Fig. 3. In Fig. 4. indices until 0026 of pyrolytic graphite can be recognizable ($Q \simeq 24$). Fig. 5. shows distinct Bragg reflections of vanadium single crystal.

Table 1. Rotating speeds of four axes (degree/minute)

	Fast	Middle	Slow
2θ	120	50	2
ω	120	50	2
χ	270	50	2
ϕ	540	50	2

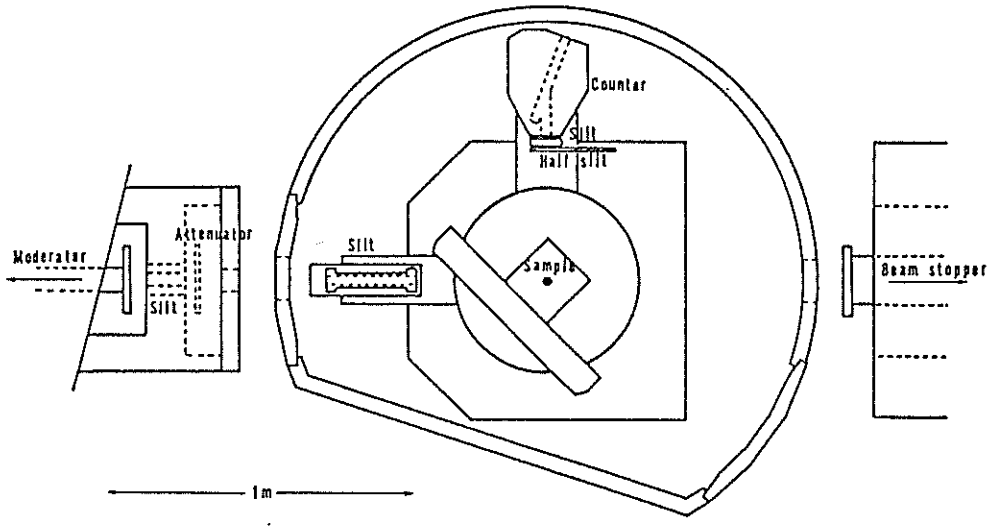

Fig. 1. Schematic drawing of FOX

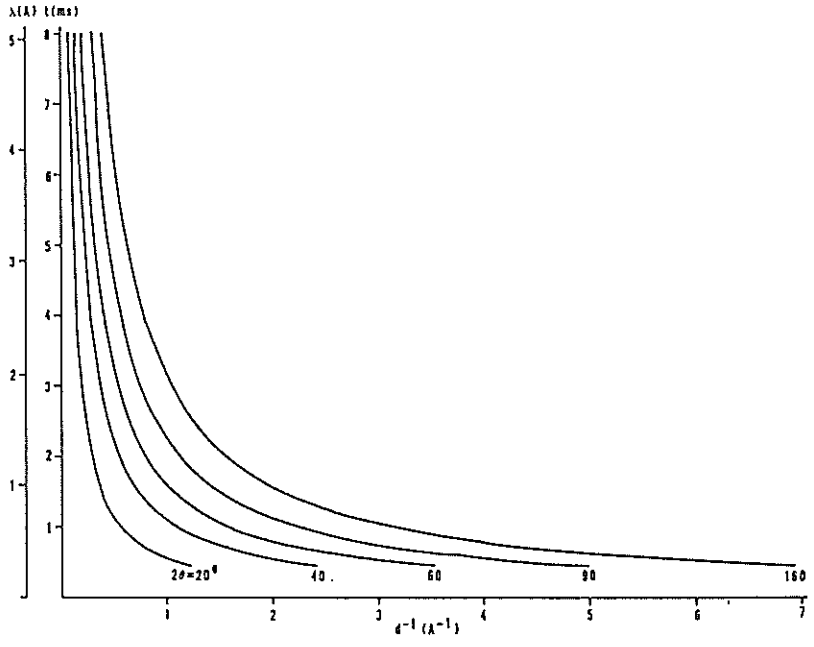

Fig. 2. Measurable range of wave length vs. reciprocal distance at each 2θ.

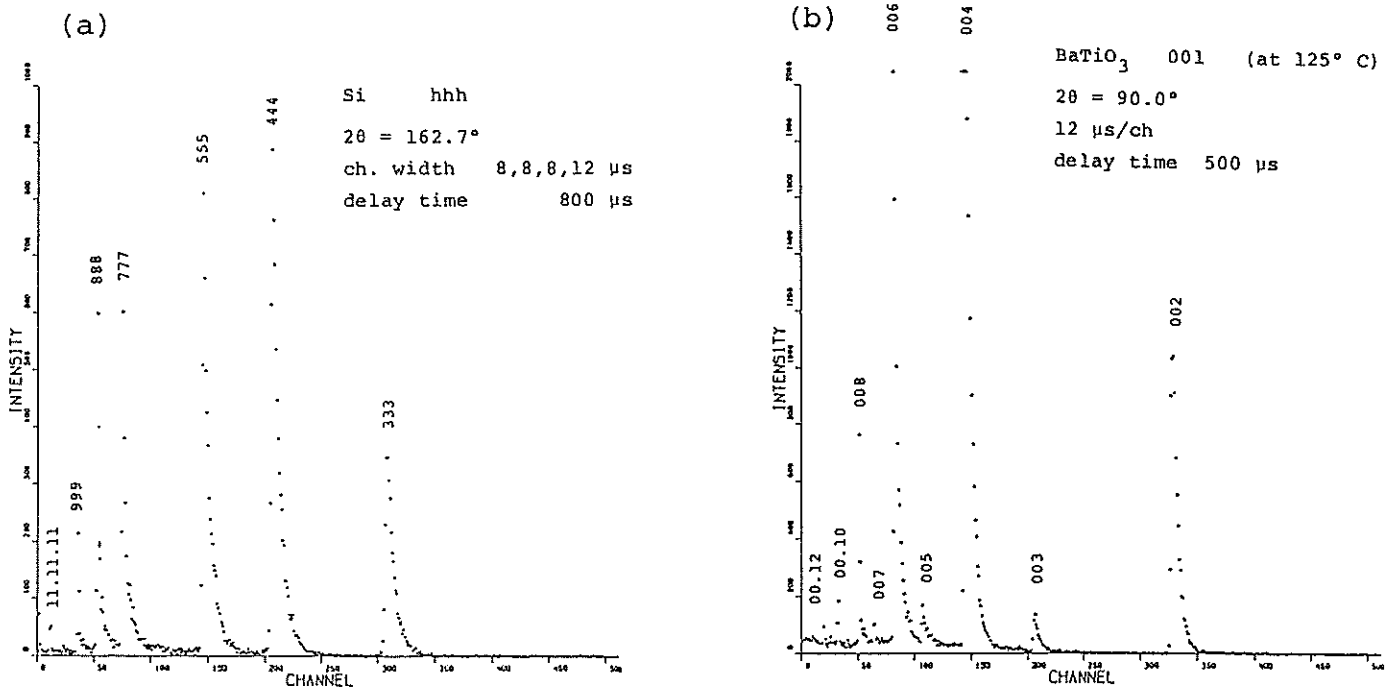

Fig. 3. Diffraction pattern of (a) Si hhh (b) $BaTiO_3$ 001 (at 125° C)

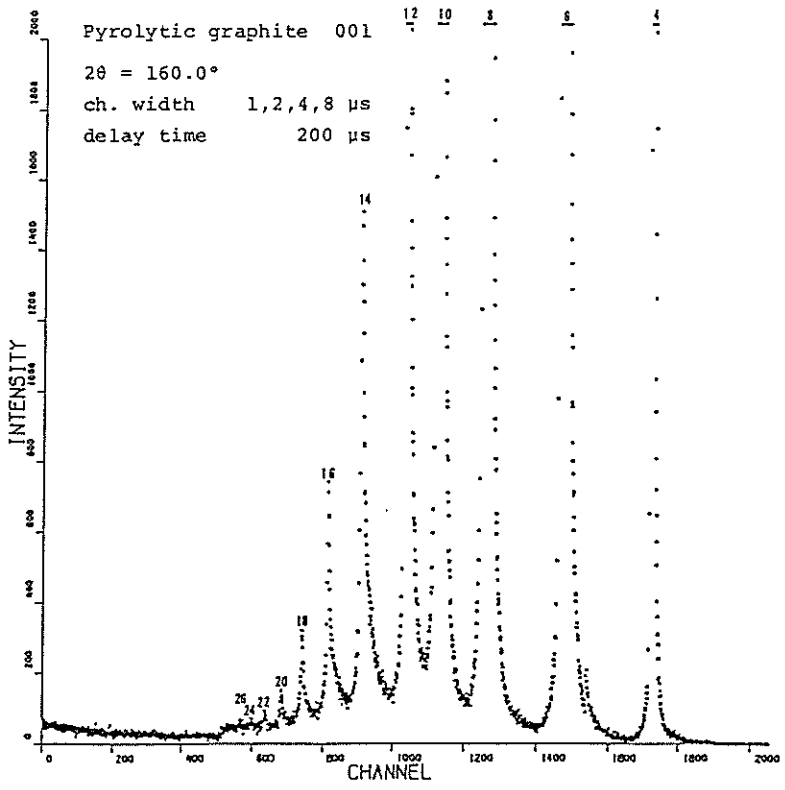

Fig. 4. Diffraction pattern of pyrolytic graphite 001

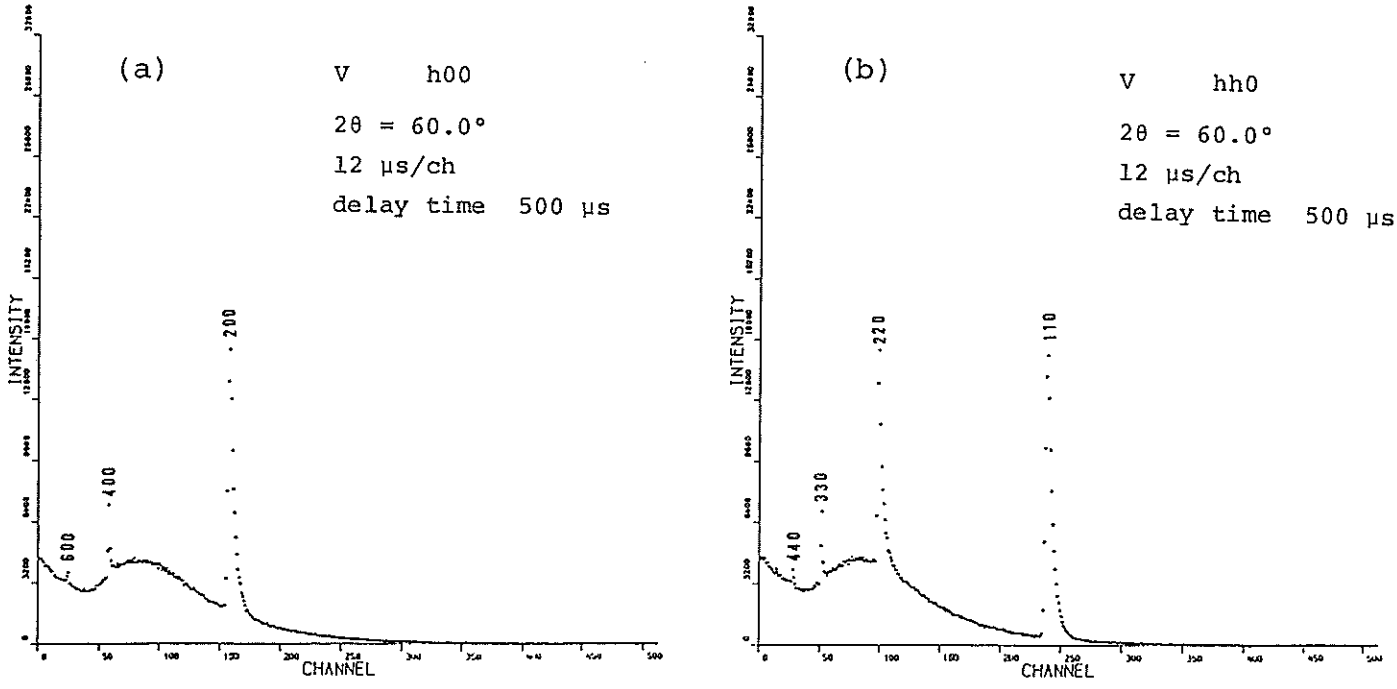

Fig. 5. Diffraction pattern of V (a) h00 (b) hh0

Tests of a Resonance Detector Spectrometer

John M. Carpenter*, Noboru Watanabe, Susumu Ikeda
Yasuhiro Masuda and Setsuo Sato

National Laboratory for High Energy Physics
Oho-machi, Tsukuba-gun, Ibaraki-ken, 305, Japan

This paper reports the results of operating a resonance detector spectrometer prototype[1] at KENS. This type of instrument will make possible spectroscopy with scattered neutron energies in the range 1 - 10 eV, with resolution in the neighborhood of 50 meV. The system uses a resonantly-absorbing material, usually in the form of a thin metal foil or plate, which captures scattered neutrons of fixed energy; a scintillation counter registeres the resulting gamma ray cascade. Time of flight disperses the energy spectrum as a function of incident neutron energy. Figure 1 illustrates the principle of the spectrometer.

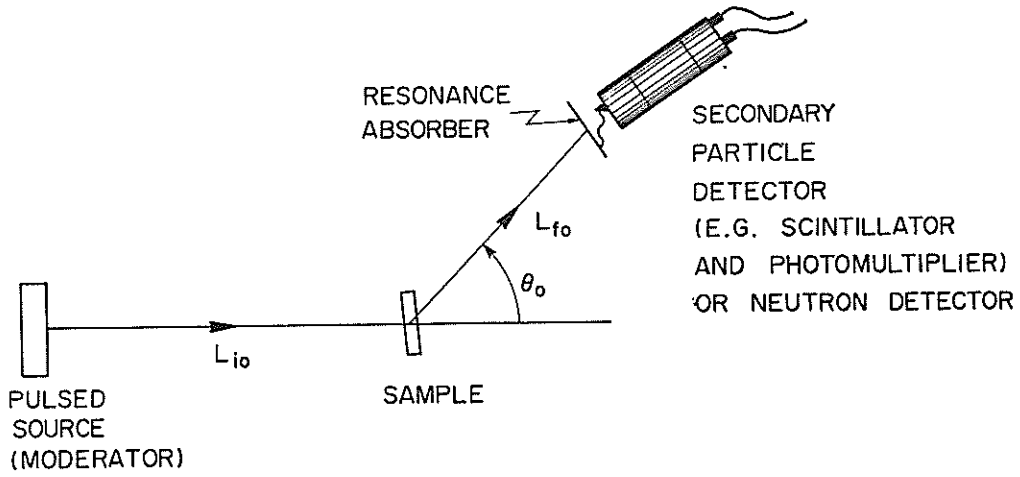

Fig. 1 Principle of Resonance Detector Spectrometer

By extensive tests to identify sources of background and find corrective measures, we arrived at some general understandings which guided our development, and some spesific principles. Both neutron and gamma ray shielding emits capture gamma rays which can be detected by the scintillator. Both may act as neutron traps, storing neutrons for several hundred microseconds. Steel and concrete structural components

---

* Permanent address: Argonne National Laboratory, Argonne, Ill. 60439 U. S. A.

capture neutrons and emit energetic gamma rays. There is the possibility that some more-or-less short-lived (10-1,000 microseconds) isomers are produced in lead shielding due to high energy neutron interactions, which decay during measuring time to produce detectable gamma rays. About 10 cm of lead is needed around the entire spectrometer to attenuate gamma rays from the surrounding concrete and steel. Outside this, about 10 cm of hydrogenous material is needed to stop neutrons from outside. Polyethylene is inappropriate because of the 150 μs decay time of thermal neutrons in this medium; The thermal neutrons emit capture gamma rays (2.2 MeV) upon capture in hydrogen, and a 7 MeV cascade when they are captured in the adjacent lead. Boron loaded resin material works well. B_4C shielding inside the spectrometer seems like a good idea. We tried configurations both with and without it, and at our levels of background, did not observe significant differences in the background. High energy neutrons accompany slow neutrons from the source, appearing in a difficult-to-stop halo around the beam. We finally found that very tight, massive material (lead, about 1 meter long, 40 cm dia.) around the incident beam is required to deal with these neutrons. With this collimation, including B_4C and hydrogenous material, we were able to operate the detector within 10 cm of center of the 4 cm wide incident beam.

We have tested various scintillators for the gamma ray detection. Scintillator materials capture neutrons both resonantly and continuously; The resulting capture and decay gammas are detected with high efficiency. The traditional NaI detector is especially bad this way. We adopted bismuth germanate scintillators, which seem quite good in this application. Plastic scintillators have rather-too-low efficiency for the energetic gamma rays we must detect. Photomultiplier photocathodes contain a small amount of antimony, which has a resonance in the neighborhood of those we want to use as monochromators. The gamma ray cascade from captures there is detected with high efficiency by the nearby scintillator, and interferes with measurements as a structured background. We found that a thin neutron shield of boron-10, between the resonance detector foil and the scintillator, reduces the background due to captures in the gamma ray detector. Important in all this, is that capture gammas appear after only about 10 % of the captures in boron, moreover, their energy is low enough that we can electronically discriminate against them. Thus we have been able to freely use boron in the shielding.

We have examined a fast and a slow electronics for this application and found that the fast system worked well, while the slow one gave serious dead time problem in the TOF spectrum due to the big resonance peaks of the scintillator materials.

We used two absorbers, one of Ta metal 12 μm thick and one prepared of 4 gm Sb metal powder bound in 1 gm epoxy resin, 50 mm square. Table summarizes the properties of these detectors.

Absorber	A,Mass Number	Density gm/cm^2	N_d, atoms/b	E_0,eV	Γ,meV	σ_0,b
^{181}Ta(100%)	180.95	16.65	6.65×10^{-5}	4.28	57	4.85×10^{4}
^{121}Sb(57.3%)	121.75	——	4.54×10^{-4}	6.24	88	4.98×10^{3}

We examined the basic resolution of the resonance detector with measurements in which the absorber foils were removed from the scintillator and placed in the sample position. Figure 2 shows the detecting probabilities measured at room temperature, which are consistent with calculations[1].

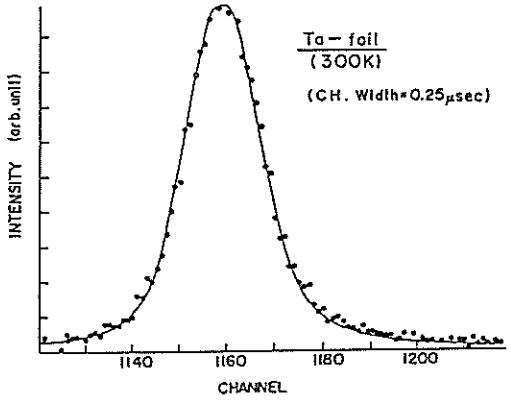

Fig. 2 Detecting probabilities measured for Ta

We have measured and understood the inelastic scattering at large wave-vector change (Q>60. A^{-1}) from graphite, vanadium, lead and bismuth; we have measured and understood the scattering at smaller wave-vector change (Q=10 A^{-1}) from graphite and hydrogen gas. Figure 3 shows typical TOF spectra measured for these sample.

Neutrons captured in the samples produce a sample-dependent capture gamma ray background in some cases. The vanadium 1/v cross section is large enough to be troublesome, which gives large constant background in TOF spectrum. The sample contains a small amount of tantalum impurity,

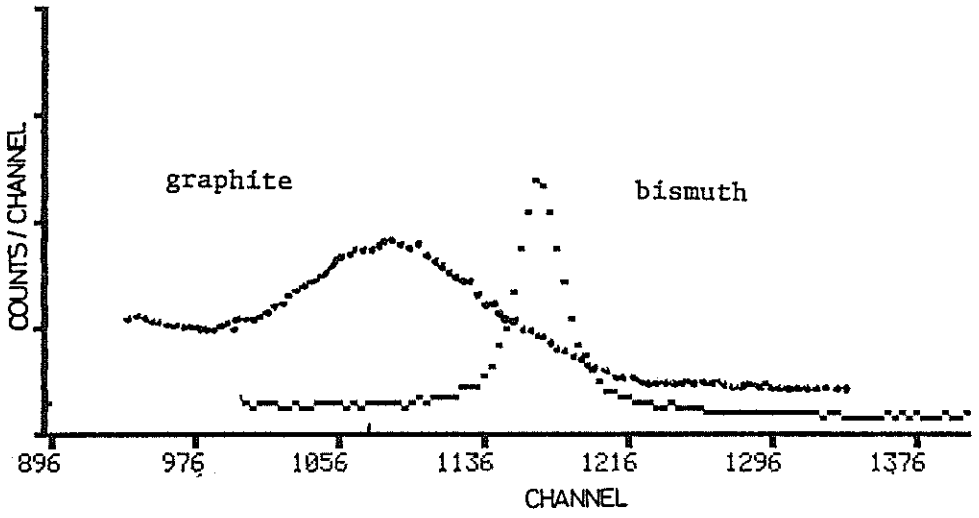

Fig. 3 Scattered neutron spectra from bismuth and graphite

even though it is some of the highest-purity, zone-refined material. Since we were using the 4.28 eV resonance of tantalum as our monochromator, this interfered with measurement of the scattering. We made an antimony absorber, with which we satisfactorily measured the scattering from vanadium. The resolution accomplished so far is only modest, around 100 meV, limited by the fact that absorbers have been subject to room-temperature Doppler broadening, as well as by the lack of a uranium-238 absorber (which has the narrowest resonance we are aware of.) Counting rates have enabled measurements to be completed in about 1/2 day. Details of the measurements and the analyses will be given in separate article[1].

We have discovered a new focussing principle which will be important in setting up higher-resolution spectrometers of this type[2]. We discovered that the spectrometer is so sensitive to small amounts of certain substances in the sample position, it might serve as a good tool for chemical and isotope analysis.

References

1) J. M. Carpenter, N. Watanabe, S. Ikeda, Y. Masuda and S. Sato, to be published in Nucl. Instrum. Methods.

2) J. M. Carpenter and N. Watanabe, to be published in Nucl. Instrum. Methods.

Production of White Polarized Neutron Beams using Longitudinally Polarized Proton Filters

J.M. Newsam, M. Ishida, S. Isagawa*, Y. Ishikawa, S. Ishimoto*, M. Kohgi, A. Masaike*, Y. Masuda*. K. Morimoto* and T. Nakajima**

Department of Physics, Tohoku University, Sendai 980

* KEK National Laboratory for High Energy Physics, Tsukuba, Ibaraki-ken

** Research Institute for Iron, Steel and Other Metals, Katahira, Sendai 980

This paper summarizes briefly the results of the experiments performed with the Pre-PEN machine. The Pre-PEN experiments represent the first stage in the construction at KENS of a spectrometer (PEN) employing a white, epithermal, polarized neutron beam. The neutron polarization was achieved by passage through a dynamically polarized proton filter (D.P.P.F.)[1]. The aim of the Pre-PEN experiments was twofold. One was to establish the technique for cooling a large area filter by liquid ^{3}He and another was to examine the geometrical dependence of the neutron polarization cross section by polarizing longitudinally the neutron beams and comparing the results with those obtained by Hiramatsu et al.[1] and Lushchikov et al.[2] where the neutrons were polarized in the transverse directions.

The general layout of the Pre-PEN machine is shown in Fig. 1. It consists of a horizontally mounted coaxial superconducting magnet with a ^{3}He cryostat in it[1], a Drabkin type spin flipper, a goniometer to install the Fe_8Co_{92} analyzer crystal and a detector rotating around the goniometer. Because of the testing nature of the Pre-PEN experiments, the machine was constructed by assembling the existing apparatuses which were not necessarily optimized for the present purpose. The neutron beam was tightly collimated to 15 × 15 mm^2 so that no neutrons bypassing the filter were monitored by the detector. The polarizing filter was

made with a polycrystalline sample of ethylene glycol with Cr^V complex. The filter was cooled to ca. 0.5 K in a cryostat by pumping on liquid ^3He. Since ^3He has a large neutron absorption cross section and the cryostat was mounted horizontally, a protection of neutron beam path from liquid ^3He constitutes the most difficult part of the experiment.

The protons of the filter were polarized by dynamic method at a frequency of 70 GHz in a magnetic field of 25 kG applied in the direction of the neutron beams (longitudinal polarization). The proton polarization was detected by analyzing the size of NMR signal from the filter. The neutron polarization was determined by two methods; either directly by Bragg reflection from a saturated Fe_8Co_{92} at discrete energies or indirectly by analyzing the intensity of the transmitted beams. In the former method, the direction of the neutron polarization was reversed by making use of Drabkin type spin flipper[3] which has successfully been used for the spin flipper of TOP[4]. The measured flipping efficiency (η) of the flipper was found to be 0.91(4) which was determined by employing a thin depolarizing iron shim according to

$$\eta = (I(\text{Flip on}) - I(\text{Flip off})) / 2 (I(\text{Shim}) - I(\text{Flip off})) \quad (1)$$

where $I(\alpha)$ is the neutron intensity in the α state.

Two types of filter configurations were finally adopted which are shown in Fig. 2. The case (a) was the original configuration where the filter materials were separated by thin layers of liquid ^3He 0.7 mm thick to increase the cooling efficiency. The filter proton could be polarized up to 45% and a good neutron polarization was achieved for thermal neutrons; 90% for 50 meV and 80% for 100 meV neutrons over the beam size of 15×15 mm^2. However, because of lowering of liquid He^3 level, the filter seemed to have the leakage neutrons with energies higher than 0.3 eV, which made difficult the measurement of the polarizability of epithermal neutrons. The case (b) was designed to remove the difficulty. Since the neutron beam size was significantly reduced in (b), we are obliged to reduce the thickness of the filter to 10 mm in order to increase the counting statistics and the neutron polarization was therefore reduced.

The results of polarization of the white neutron beams for the case (b) are shown in Fig. 3, where the polarization determined by Bragg reflection (open circles) are corrected for the efficiency of the spin

flipper and for the analyzer polarizability.

The neutron polarization, P_N, obtained after passage through a filter of proton polarization P_P is given by

$$P_N = \tanh (P_P \sigma_p Nt), \quad (2)$$

where σ_p is the polarization cross section ($= 1/4(\sigma_s - \sigma_t)$), N the number of protons per cm^3 and t the filter thickness. The solid line was calculated by eq. (2) using the data for σ_p of Lushchikov et al.[2], while the closed circles are the results of analysis from the transmission intensity T. The transmission T is given by

$$T/T_o = \exp(P_P^2 \sigma_1 Nt) \cosh(P_P \sigma_p Nt),^{2)} \quad (3)$$

with T_o the transmission of the unpolarized target. σ_1 which is the cross section depending on the materials is assumed to be zero for the present analysis. The overall agreement among the values of polarization estimated by three different methods was obtained.

Note that the neutron polarization determined by the transmission of the case (b) agrees well with that of Lushchikov et al. above 400 meV where σ_1 is expected to disappear. Our previous data at 80 meV with the transverselly polarized filter also fall on the solid line.

Several important conclusions could be derived from the Pre-PEN experiments which are summarized below.

(i) The epithermal neutron beam with neutron energies extending beyond 10 eV could successfully be polarized by the polarized proton filter method.

(ii) In case of (a) (t=15 mm, 45% proton polarization) an 80% polarization was achieved at typical neutron energy of 100 meV.

(iii) The longitudinal polarization has the same polarization cross section as the transverse one within the accuracy of the experiments as was anticipated by Hoshizaki et al.[5]

(iv) The downward deviation of the open circles from the closed circles in Fig. 3 in the high energy side is presumably due to the depolarization which would occur between the spin flipper and the analyzer. The distance between them was found not enough to satisfy the adiabatic condition.

(v) The upward deviation of the closed circles from the solid line can be attributed to σ_1 in eq. (3).

Further experiments would, however, be necessary before we conclude that σ_p in eq. (2) is completely the same for both LMN (Lushchikov et al.) and ethylene glycol (Pre-PEN).

In concluding, the D.P.P.F. method is promising in obtaining polarized epithermal neutron beams. Since the various factors will be optimized in designing PEN, including an effort to increase the total neutron intensity, PEN will become a powerful polarized epithermal neutron beam facility at KENS.

References

1) S. Ishimoto, Proc. ICANS - IV (1981) 630
S. Hiramatsu et al, Jour. Phys. Soc. Japan, 45 (1978) 949

2) V. I. Lushchikov, Yu. V. Taran and F. L. Shapiro, Soviet J. Nucl. Phys. 10 (1970) 669

3) G. M. Drabkin, E. I. Zabidarov, Ya. A. Kasman and A. I. Okorokov, Soviet Phys. JETP 29 (1969) 261

4) Y. Endoh, J. Mizuki, Y. Sasaki and H. Ono, Proc. ICANS - IV (1981) 609

5) N. Hoshizaki and A. Masaike, KEK Report 81 - 22 (1981)

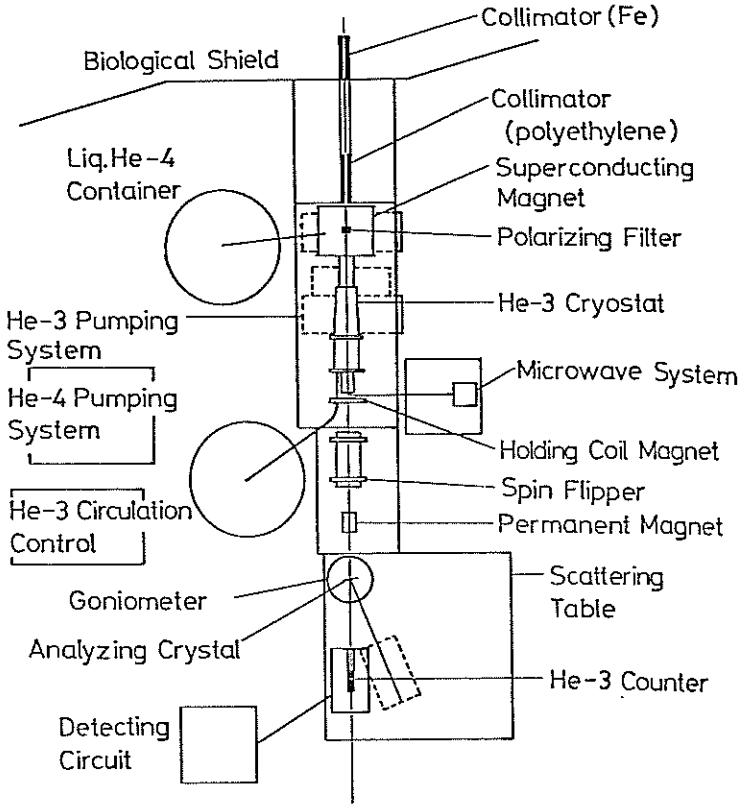

Fig. 1. Layout of Pre-PEN experiments

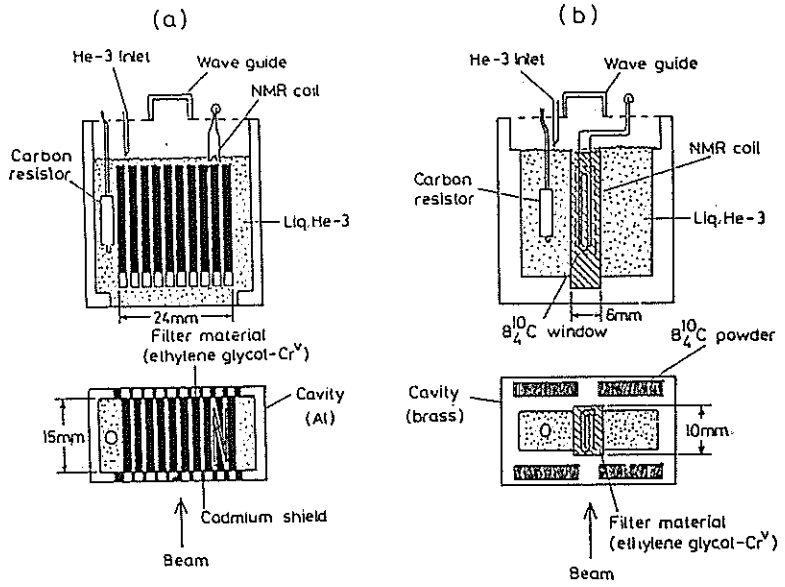

Fig. 2 Two types of filter configurations adopted in the experiment.

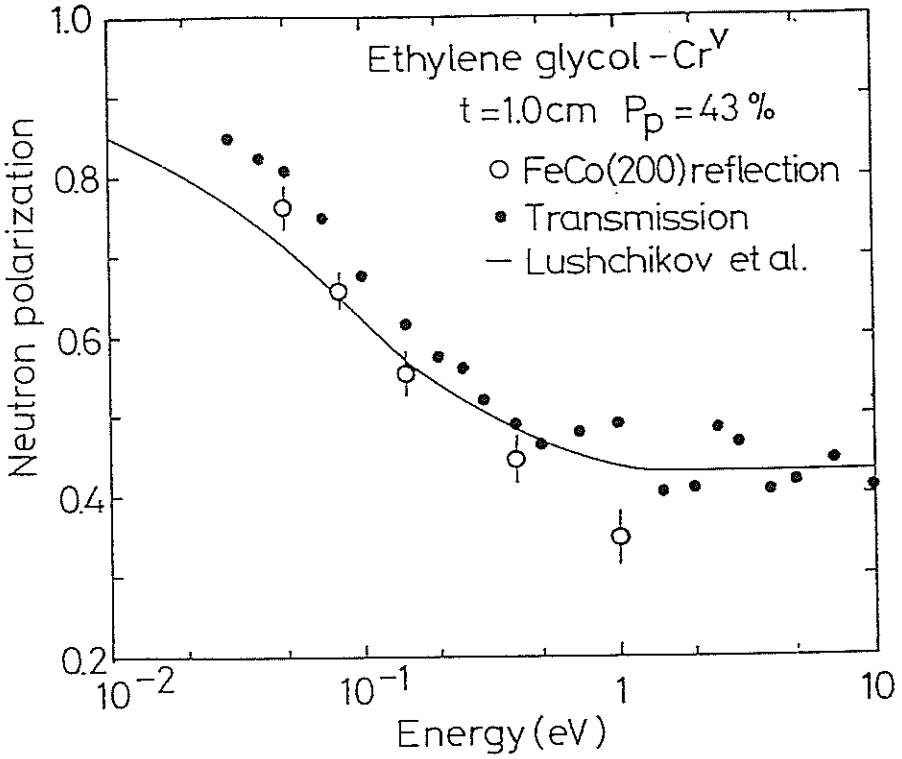

Fig. 3 Neutron polarization by D.P.P.F with the configuration (b)

Position Sensitive Neutron Detectors Using ^{6}Li Glass Scintillators

N. Niimura, K. Yamada, T. Kubota, A. Matsumoto* and S. Hoshino**

Laboratory of Nuclear Science, Faculty of Science
Tohoku University, Mikamine, Sendai 982, Japan

*Nippon Kogaku K.K., 1373 Asamizodai, Sagamihara,
Kanagawa, Japan

**Institute for Solid State Physics,
The University of Tokyo, Roppongi, Minato-ku,
Tokyo 106, Japan

The conventional gas proportional counter is often used because of its high efficiency of neutron detection, but it has one disadvantage, namely, a long dead time (i.e. several μsec). In time-of-flight measurements the dead time of detectors is a big problem, since in the TOF method the peak flux of neutrons is more important than the time-averaged flux. The dead time less tnan 100 nsec is required and a ^{6}Li-glass scintillator meets the requirement. The glass scintillator has the advantage of allowing the possibility of the large area detectors. If a proper method for defining the position of the scintillation event can be developed, it may be used in a position sensitive detector (PSD).

The PSD by the use of a fibre optic encoding method has been designed, constructed and tested. The number of ^{6}Li glass scintillator resolution elements encoded is 84 (3 × 28 arrays)and its size is 10mm × 10mm and the thinkness is 2mm. 1,600 fibres (0.25mm in diameter) are connected to the back of each element, and branched into three bundls. Each resolution element is connected by the 3 bundles of optical fibres to a unique combination of 3 photomultipliers (PM) out of a bank of 9. The photograph shows the 3 × 28 array of scintillators and the bundles of optical fibres.

The performance of the PSD was tested by the use of a KBr single crystal and a Si polycrystal. Fig. 1 shows the result of a 200 reflection of the KBr single crystal. The geometrical arrangement of the experiment is shown in the figure. The spectra in the left side and the right side show the

position and the time of flight (wavelength) of diffracted neutrons respectively. A 200 Bragg peak was observed at the expected position and wavelength by the use of the Bragg equation. The fact that there is no spurious peak shows that our encoding method works well.

Fig. 2 shows the result of 111 reflection of the silicon polycrystal. The geometrical arrangement of the experiment is the same as before. The each curved line shows the time of flight spectra at the each scintillator resolution element. Since the sample is a polycrystal, every element receives Bragg reflections, and the peak position of the time of flight shifts depending on the Bragg equation.

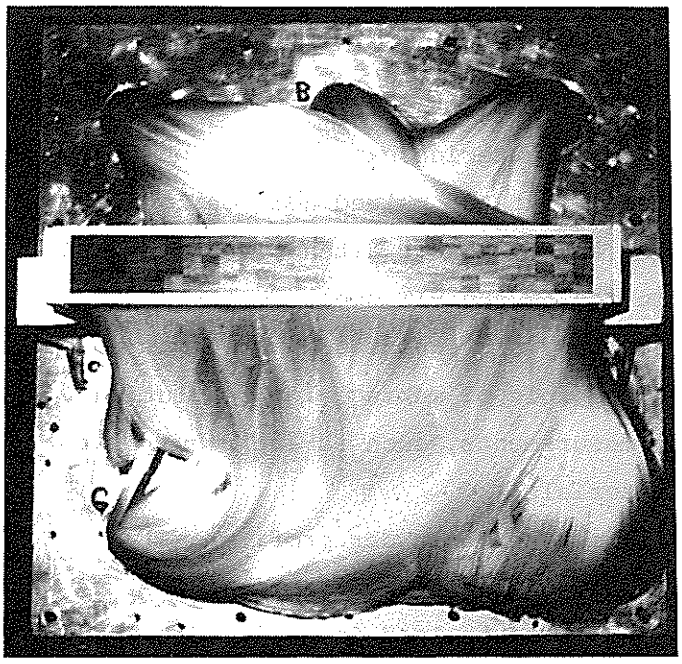

↑ Photograph: 3 × 28 array of scintillators and the bundles of optical fibres.

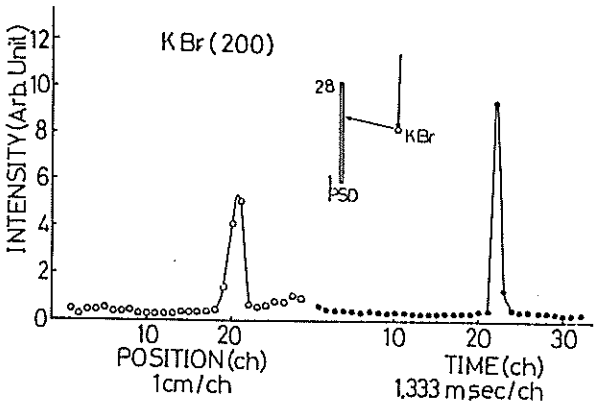

↑ Fig. 1 The 200 reflection of a KBr single crystal

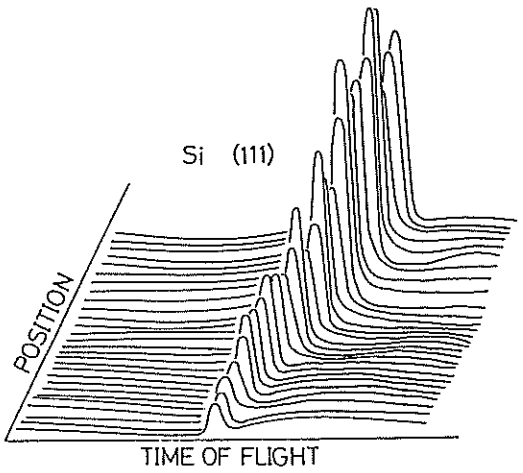

Fig. 2 The 111 reflection of a silicon polycrystal ⟶

A High Resolution Powder Diffractometer for KENS

J. M. Newsam

Department of Physics, Tohoku University, Sendai 980

Abstract:

The possibilities for and the potential of a powder diffractometer at KENS, given the present configuration of the facility, are considered. Use of a 24m flight path at the available C2 beam port would permit the construction of a diffractometer with resolution approaching 0.2 % and which would provide 2 % statistics in each of 1100 resolution elements in a count time of approximately 24 hours.

It is, perhaps arguably, in the total scattering experiments, where the entire neutron spectrum is being utilised, that the pulsed neutron facility provides the most substantial gains over the available altenatives. At KENS this feature is exploited at low resolution by the HIT spectrometer, which is already proving its potential for the study of liquids and amorphous solids. There is, however, as yet no instrument capable of making high resolution total scattering or powder diffraction mesurements, such as are required to define the structures of crystalline materials.

Recent developments in the Rietveld method of powder profile analysis (1) coupled with the resolution and range of Q that is available at spallation or electron linac neutron facilities have resulted in powder data, becoming generally competitive with single crystal diffraction data, at least in structure refinements. Indeed, the scope of the technique is well indicated in the selection of instruments chosen at other pulsed neutron facilities(2).

For the present configuration at KENS, there would appear to be three beam ports still available, H4 viewing the ambient moderator and C4 and C2 which view the cold moderator. Use of C4, however, would require joint use with LAM, with consequent aperture problems. This option is thus merely

included for completeness. The potentials of instruments at these three locations are indicated in Tables I and II.

Table I

Calculated Resolutions at E = 100 meV

Port	Δt μs	L mm	$\Delta t/t$	$\Delta d/d$
H4	15	8000	0.0082	0.0086
C4	7	17000	0.0018	0.0022
C2	7	24000	0.0013	0.0016

Table II

Approximate Counting Rates

Port	L	Neutrons S^{-1}	0.26 -2.02Å No.Res.Elements	Time for 10^4 counts channel^{-1} hours
H4	8000	2.53×10^2	215	3
C4	17000	0.56×10^2	800	40
C2	24000	$0.28 \times 10^2 \times G$*	1100	108/G

* G is a wavelength dependant gaing factor consequent on the use of the (straightened) neutron guide tube.

Planned enhancement of the KENS neutron flux will, of course, greatly reduce the required counting times. Indeed, with the anticipated increase in neutron flux, the performance of a high resolution powder diffractometer constructed on the C2 beam port would compare favourably with that currently available anywhere else in the world.

Acknowledgement

I would like to thank the Japan Society for the Promotion of Science for the award of a research fellowship.

References

1) R. B. Von Dreele, J. D. Jorgensen and C. G. Windsor: to appear

2) see, for example, Proceedings of the International Collaboration on Advanced Neutron Sources meeting IV (ICANS IV): KENS REPORT II Eds. Y. Ishikawa, N. Watanabe, Y.Endoh, N.Niimura and J. M. Newsam (1981)

SUBJECT CONTENTS

A. Instrument

B. Disordered Systems

C. Magnetic Structures & Excitations

D. Polymer & Biological Materials